INVESTIGATING THE ROLE OF PHOSPHATIDYLSERINE IN MEDIATING THE ENTRY AND RELEASE OF CHIKUNGUNYA VIRUS

by

JUDITH MARY REYES BALLISTA

(Under the Direction of Melinda A. Brindley)

ABSTRACT

Chikungunya virus (CHIKV) is an arbovirus from the *Togaviridae* family and alphavirus genus. CHIKV is transmitted by the bites of infectious *Aedes* mosquitoes, and its genome is composed of a positive-sense single-stranded RNA. In order to spread, CHIKV needs to successfully infect a variety of cell types in both the insect vector and the vertebrate host. As an enveloped virus, the lipids present in the viral envelope are essential for mediating many steps of the viral replication cycle including entry and release. Phospholipids, such as phosphatidylserine (PS), are abundant at the plasma membrane and can be incorporated into viral envelopes at the site of budding. Phosphatidylserine receptors (PSR), including the T-cell immunoglobulin and mucin domain (TIM) proteins, interact with enveloped viruses playing a role in multiple stages of their replication cycle. PS in enveloped viral particles can mediate the attachment to host cells by binding to PSR on the surface of the cells during entry and release. Despite the identification of multiple factors mediating CHIKV entry, no essential receptor has been determined. In an effort to characterize the role of PS in the viral replication cycle of CHIKV we aimed to 1) evaluate CHIKV's use of phospholipids during

viral entry and their influence on viral infectivity using a panel of mammalian and mosquito cell lines, and 2) determine the ability of PS receptors to impede the efficient release of CHIKV particles and identify viral counteracting mechanisms. We used recombinant viral particles tagged with a luminescence reporter gene, nano-luciferase, in a separate open-reading frame or directly attached to the envelope protein E2 to facilitate quantification. We found that CHIKV's use of attachment factors for mediating entry was highly cell line dependent. The production of viral particles high in envelope PS increases CHIKV's infectivity in Vero cells but not in cells lacking PSR. In contrast, the presence of PS receptors on the surface of the infected cells significantly reduced CHIKV's release efficiency. Altogether, this study highlights the importance of PS and PSR as modulators of CHIKV's entry and release providing insight into the molecular mechanisms enabling optimal infection.

INDEX WORDS: Chikungunya virus, phosphatidylserine, entry, viral release, alphavirus, TIM-1, receptors, apoptotic mimicry

INVESTIGATING THE ROLE OF PHOSPHATIDYLSERINE IN MEDIATING THE ENTRY AND RELEASE OF CHIKUNGUNYA VIRUS

by

JUDITH M. REYES BALLISTA

B.S., University of Puerto Rico – Rio Piedras Campus, 2019

A Dissertation Submitted to the Graduate Faculty of The University of Georgia in Partial Fulfillment of the Requirements for the Degree

DOCTOR OF PHILOSOPHY

ATHENS, GEORGIA

2024

INVESTIGATING THE ROLE OF PHOSPHATIDYLSERINE IN MEDIATING THE ENTRY AND RELEASE OF CHIKUNGUNYA VIRUS

by

JUDITH MARY REYES BALLISTA

Major Professor: Melinda Brindley
Committee: Maricarmen García
Biao He
Eric Lafontaine
Daniela De Souza Rajão

Electronic Version Approved:

Ron Walcott
Vice Provost for Graduate Education and Dean of the Graduate School
The University of Georgia
August 2024

DEDICATION

Para mi madre, quien sacrificó mucho de su vida por mí y me inspiró cada día a cumplir mis sueños. Todos mis logros son para ti, ningún sacrificio fue en vano. Gracias por creer en mí, te amo.

ACKNOWLEDGEMENTS

I want to express my sincerest gratitude and appreciation to everyone who supported me through every step of this journey.

To my family: Thank you to my parents, my siblings, and my extended family. Thank you for your continuous support, for loving me, and for believing in me. Even though I am far away, each of you is ever present in my mind and heart. What I do, I do for all of you.

To Hunter, Phoebe, and Juno: Thank you for being my daily care and support. I would have not been able to get to this point without you. Thank you for being patient, loving, and understanding. I do not have enough words to express how happy I am to have all of you.

To my friends: Thank you for your company and encouragement. Thank you, Amanda, who accompanied me through this journey from undergraduate to doctorate. Thank you for being thoughtful, kind, and empathetic. Thank you to Neely, Meghan, and Lexi. We saw each other grow from day one in Athens; thank you for never leaving my side and for flourishing with me. Thank you, Cristina and Aaron, who more than my friends became my mentors. Thank you for helping me overcome every obstacle in this process and celebrating every win.

To my lab mates: Thank you for making every day a little bit more fun. Thank you to all past Brindley lab members, Blanka, Kerri, and Marissa for serving as role models during my Ph.D. Thank you to Joseph, Breanna and Michael for your company, for your

moral support, and for enjoying every day of this journey with me. I appreciate every moment we spent in the lab and will forever cherish it.

To my undergraduate mentees: I am so grateful to have had the brightest young minds to help me through this process. To Antonio, Ashley, Sarah, Sydney, Ami, Grace Ann, and many other undergraduates who kept my mind fresh, arrived with the best attitude, and reminded me of the importance of what we do. I am so incredibly proud to have been part of your journey and it is a privilege to now also call you my friends and colleagues. I wish each of you all the best and I am infinitely thankful for your help and patience.

To my committee: Biao He, Eric LaFontaine, Daniela de Souza Rajão and Maricarmen García. Thank you each so very much for your helpful input, your advice, and your encouragement. You have been an integral part of my Ph.D. and I am greatly appreciative of your time and knowledge.

To my advisor, Melinda Brindley: Thank you for guiding me through this process. You laid the path for me to achieve this goal. Thank you for always having your door open for me. I would not have been able to get here if it were not for your continuous availability, guidance, and knowledge throughout this process. I really appreciate all you have done for me.

To everyone else I have not been able to mention, know that you also have been a substantial part of this process. I am beyond grateful to have had an immense network of support and people who believe in me. I am very lucky to have you.

TABLE OF CONTENTS

LIST OF TABLES

Page

LIST OF FIGURES

Page

CHAPTER 1

DISSERTATION OVERVIEW

Arthritogenic alphaviruses like chikungunya (CHIKV) are characterized by their symptoms causing debilitating joint pain that can develop into long-lasting rheumatic diseases (1). CHIKV, an alphavirus, contains a genome constituted by a positive-sense single-stranded RNA. One open reading frame encodes for four non-structural proteins and a subgenomic RNA encodes for the structural and accessory proteins (2). Each viral particle contains an icosahedral nucleocapsid and a lipid envelope that is studded with 80 glycoprotein heterodimers (3, 4). Both the E2/E1 glycoproteins and the capsid are the main mediators of CHIKV's entry and release from host cells (4–6).

Multiple entry receptors and attachment factors have been evidenced to be important for CHIKV's infection and pathogenesis in host cells. For instance, matrix remodeling-associated protein 8 (MXRA8) is a receptor highly associated with the development of disease symptoms like joint swelling (7–9). Glycosaminoglycans (GAGs) are ubiquitously expressed carbohydrates present on the surface of cells and mediate the proximity and attachment of CHIKV to the cell surface (10–12). Phosphatidylserine-binding receptors (PSR) can also mediate the binding of CHIKV particles to mammalian cells in a process referred to as apoptotic mimicry (13–15). Despite the undeniable importance of these and other factors in mediating the entry of CHIKV into host cells, no cellular receptor is denoted as an indispensable requirement for CHIKV in both mammalian and mosquito cells. The ability of CHIKV to infect and

spread in a broad range of tissues highlights the importance of further understanding its adaptability and the spectrum of entry requirements mediating tropism.

The binding between viral envelope phosphatidylserine and PSR on the surface of the cells can be highly beneficial for enhancing and initiating viral infections. Yet, recent studies have demonstrated a more novel role of PSR during viral release. For the human immunodeficiency virus (HIV) and Japanese Encephalitis virus (JEV), the presence of PSR on the surface of the cells can tether budding virions and prevent their release and consequently their spread (16, 17). HIV and JEV counteract this inhibition by either internalizing the surface receptors following entry or prompting its degradation (17, 18). Studies investigating this particular function of PSR are limited, nonetheless, this phenotype could be general for many other enveloped viruses.

Multiple studies have investigated the viral protein interactions that are needed for the efficient assembly and budding of CHIKV. For instance, the interaction between the cytoplasmic tail in the E2 glycoprotein and a hydrophobic pocket located in the capsid protein is crucial for the appropriate assembly of viral particles at the plasma membrane (6, 19, 20). However, host factors that can inhibit efficient CHIKV egress are less characterized. The membrane protein, tetherin/BST-2, has been the main factor shown to inhibit the efficient release of alphaviruses (21, 22). Identification of other inhibitory host factors could aid in identifying possible targets for the development of antiviral therapeutics.

To further characterize the role of PSR in mediating the entry, infectivity, and release of CHIKV we established the following aims:

AIM 1: Evaluate the importance of phosphatidylserine-binding receptors among other chikungunya entry factors using a panel of mammalian and mosquito cells. We hypothesized that the use of entry factors would be cell type dependent allowing interaction with multiple attachment factors; supporting CHIKV's ability to infect a broad spectrum of cell types in its host.

AIM 2: To assess the ability of phosphatidylserine-binding receptors to prevent the efficient release of chikungunya viral particles from the surface of infected cells. Given the ability of phosphatidylserine to mediate attachment of chikungunya during entry, we hypothesized that budding viral particles could reattach to these receptors on the cell surface preventing their release.

References

1. Caglioti C, Lalle E, Castilletti C, Carletti F, Capobianchi MR, Bordi L. 2013. Chikungunya virus infection: an overview. New Microbiol 36:211–227.

2. Rupp JC, Sokoloski KJ, Gebhart NN, Hardy RW. 2015. Alphavirus RNA synthesis and non-structural protein functions. J Gen Virol 96:2483–2500.

3. Voss JE, Vaney MC, Duquerroy S, Vonrhein C, Girard-Blanc C, Crublet E, Thompson A, Bricogne G, Rey FA. 2010. Glycoprotein organization of Chikungunya virus particles revealed by X-ray crystallography. Nature 468:709–12.

4. Chmielewski D, Schmid MF, Simmons G, Jin J, Chiu W. 2022. Chikungunya virus assembly and budding visualized in situ using cryogenic electron tomography. Nat Microbiol 7:1270–1279.

5. Smith TJ, Cheng RH, Olson NH, Peterson P, Chase E, Kuhn RJ, Baker TS. 1995. Putative receptor binding sites on alphaviruses as visualized by cryoelectron microscopy. Proc Natl Acad Sci U S A 92:10648–10652.

6. Jose J, Przybyla L, Edwards TJ, Perera R, Burgner JW, Kuhn RJ. 2012. Interactions of the cytoplasmic domain of Sindbis virus E2 with nucleocapsid cores promote alphavirus budding. J Virol 86:2585–2599.

7. Zhang R, Kim AS, Fox JM, Nair S, Basore K, Klimstra WB, Rimkunas R, Fong RH, Lin H, Poddar S, Crowe JE, Doranz BJ, Fremont DH, Diamond MS. 2018. Mxra8 is a receptor for multiple arthritogenic alphaviruses. Nature 557:570–574.

8. Zhang R, Earnest JT, Kim AS, Winkler ES, Desai P, Adams LJ, Hu G, Bullock C, Gold B, Cherry S, Diamond MS. 2019. Expression of the Mxra8 Receptor Promotes Alphavirus Infection and Pathogenesis in Mice and Drosophila. Cell Rep 28:2647-2658 e5.

9. Song H, Zhao Z, Chai Y, Jin X, Li C, Yuan F, Liu S, Gao Z, Wang H, Song J, Vazquez L, Zhang Y, Tan S, Morel CM, Yan J, Shi Y, Qi J, Gao F, Gao GF. 2019. Molecular Basis of Arthritogenic Alphavirus Receptor MXRA8 Binding to Chikungunya Virus Envelope Protein. Cell 177:1714-1724 e12.

10. McAllister N, Liu Y, Silva LM, Lentscher AJ, Chai W, Wu N, Griswold KA, Raghunathan K, Vang L, Alexander J, Warfield KL, Diamond MS, Feizi T, Silva LA, Dermody TS. 2020. Chikungunya Virus Strains from Each Genetic Clade Bind Sulfated Glycosaminoglycans as Attachment Factors. J Virol 94.

11. Silva LA, Khomandiak S, Ashbrook AW, Weller R, Heise MT, Morrison TE, Dermody TS. 2014. A single-amino-acid polymorphism in Chikungunya virus E2 glycoprotein influences glycosaminoglycan utilization. J Virol 88:2385–97.

12. Höök M, Kjellén L, Johansson S, Robinson J. 1984. CELL-SURFACE GLYCOSAMINOGLYCANS. Annu Rev Biochem 53:847–869.

13. Kirui J, Abidine Y, Lenman A, Islam K, Gwon YD, Lasswitz L, Evander M, Bally M, Gerold G. 2021. The Phosphatidylserine Receptor TIM-1 Enhances Authentic Chikungunya Virus Cell Entry. Cells 10.

14. Carnec X, Meertens L, Dejarnac O, Perera-Lecoin M, Hafirassou ML, Kitaura J, Ramdasi R, Schwartz O, Amara A. 2016. The Phosphatidylserine and Phosphatidylethanolamine Receptor CD300a Binds Dengue Virus and Enhances Infection. J Virol 90:92–102.

15. Jemielity S, Wang JJ, Chan YK, Ahmed AA, Li W, Monahan S, Bu X, Farzan M, Freeman GJ, Umetsu DT, Dekruyff RH, Choe H. 2013. TIM-family proteins promote infection of multiple enveloped viruses through virion-associated phosphatidylserine. PLoS Pathog 9:e1003232.

16. Li M, Ablan SD, Miao C, Zheng Y-M, Fuller MS, Rennert PD, Maury W, Johnson MC, Freed EO, Liu S-L. 2014. TIM-family proteins inhibit HIV-1 release. Proc Natl Acad Sci USA 111.

17. Xie S, Liang Z, Yang X, Pan J, Yu D, Li T, Cao R. 2021. Japanese Encephalitis Virus NS2B-3 Protein Complex Promotes Cell Apoptosis and Viral Particle Release by Down-Regulating the Expression of AXL. Virol Sin 36:1503–1519.

18. Li M, Waheed AA, Yu J, Zeng C, Chen H-Y, Zheng Y-M, Feizpour A, Reinhard BM, Gummuluru S, Lin S, Freed EO, Liu S-L. 2019. TIM-mediated inhibition of HIV-1 release is antagonized by Nef but potentiated by SERINC proteins. Proc Natl Acad Sci USA 116:5705–5714.

19. Owen KE, Kuhn RJ. 1997. Alphavirus Budding Is Dependent on the Interaction between the Nucleocapsid and Hydrophobic Amino Acids on the Cytoplasmic Domain of the E2 Envelope Glycoprotein. Virology 230:187–196.

20. Suomalainen M, Liljeström P, Garoff H. 1992. Spike protein-nucleocapsid interactions drive the budding of alphaviruses. J Virol 66:4737–4747.

21. Jones PH, Maric M, Madison MN, Maury W, Roller RJ, Okeoma CM. 2013. BST-2/tetherin-mediated restriction of chikungunya (CHIKV) VLP budding is counteracted by CHIKV non-structural protein 1 (nsP1). Virology 438:37–49.

22. Ooi Y, Dubé M, Kielian M. 2015. BST2/Tetherin Inhibition of Alphavirus Exit. Viruses 7:2147–2167.

CHAPTER 2

LITERATURE REVIEW: CHIKUNGUNYA VIRUS

History and prevalence

Chikungunya virus (CHIKV) is an enveloped Old World alphavirus from the *Togaviridae* family transmitted by the bites of infectious mosquitoes. The first description of CHIKV was documented in Tanzania in 1952 where 60-80% of each village developed symptoms (1). The virus was first isolated from a patient in Thailand in 1958 (2). Since the 1950s until the 2000s, CHIKV outbreaks have been sporadically documented in multiple countries in Africa and Asia (3). Often misdiagnosed as Dengue due to their similar symptoms, CHIKV quickly reemerged in 2004 causing multiple outbreaks in the Indian Ocean islands (4–6). The most severe outbreak arose in the island of La Réunion with ~250,000 suspected cases in a total population of ~750,000 habitants (7, 8).

CHIKV began spreading in the Americas after a major outbreak was documented on the island of Saint Martin in December 2013 (9, 10). More than a million suspected cases were reported across the American continent in less than 10 years (10). To date, more than 100 countries have at some point reported cases of chikungunya disease. According to the Centers for Disease Control (CDC), 19 countries in the Americas have reported evidence of chikungunya transmission in the last five years (11).

As outbreaks have occurred across the world, CHIKV strains have been divided into three different lineages. Each CHIKV lineage is categorized according to the

location where it originated and its genetic variability. The first is known as the West African lineage and was first isolated from enzootic cases in eastern Senegal (3, 12). The east-central-south African (ECSA) lineage originated in coastal Kenya and is responsible for the outbreak on the island of La Réunion (7, 10, 13). However, the coastal Kenya and La Réunion isolates differ in one amino acid within the E1 glycoprotein. This mutation is suspected to be responsible for CHIKV's ability to expand from being primarily transmitted by *Ae. aegypti* (Kenya) to also being spread by *Ae. albopictus* (La Réunion) (14). Finally, the Asian lineage is thought to have emerged from an African strain and was found to be the genotype responsible for the outbreaks in St. Martin and the Caribbean (15, 16).

Transmission

Chikungunya virus is an arthropod-borne virus transmitted by the bites of infectious mosquitoes from the *Aedes* genus such as *Aedes albopictus* and *Aedes aegypti* (17). As a vector-borne disease, chikungunya requires the ability to infect both mammalian and mosquito cells. Female mosquitoes need the iron and nutrients present in the blood in order to produce their eggs (18, 19). Transmission of the virus starts when an uninfected female mosquito takes a bloodmeal from an infected mammalian host. In the mosquito, the virus first infects the cells in the midgut where it eventually bypasses the midgut barrier and enters the insect's circulatory system (20). From the hemocoel, the virus eventually reaches the salivary glands. The virus replicates in the salivary glands and will be present in the saliva, where it is ready to continue the cycle of infection. Once the infectious mosquito takes a subsequent bloodmeal from an uninfected susceptible host, the virions first infect the fibroblasts in the skin (21, 22).

CHIKV can then disseminate to a wide variety of tissues in the mammalian host including but not limited to the liver, joints, lymph nodes, muscles, and the brain (23).

Chikungunya virus transmission is categorized into two cycles depending on the hosts and geographic sites of infection: sylvatic and urban cycles. The sylvatic cycle is suspected to be the originating mode of transmission where non-human primates are the major reservoir host (24). Sylvatic transmission is characterized by infection cases primarily localized in forests or savannahs. In contrast, the urban cycle primarily describes infections occurring in humans and other vertebrates and is more characterized by its transmission through the *Aedes aegypti* and *Aedes albopictus* mosquitoes (25).

Disease symptoms and prevention

Chikungunya's name originates from the African Makonde language which translates to "bent over in pain". The most common symptoms of the disease include fever and joint pain and many patients report chronic effects, such as arthralgia, polyarthritis, and morning joint stiffness (17). The arthritic symptoms caused by CHIKV have been evidenced to last from 6 months to 3 years after infection (26, 27).

In 1986, the U.S. Army Medical Research Institute of Infectious Diseases (USAMRIID) reported the development of a live-attenuated vaccine strain commonly referred to as CHIKV 181/25 (28). This vaccine strain was derived from a viral isolate of a patient in Thailand during the outbreak in 1962 (*i.e.,* strain 15561) (28). Levitt *et al.*, serially passaged the virus for eighteen times using a human embryonic lung cell line, MRC-5 (28). Despite displaying high immunogenicity in humans during clinical trials, ~8% of patients developed mild arthralgia symptoms (29). These mild side effects

paired with a shortage of funding prevented this vaccine candidate from advancing to efficacy testing (30, 31). Later studies identified two amino acid mutations present in the E2 glycoprotein responsible for the viral attenuation displayed by CHIKV 181/25 (32). This vaccine has now become an effective way to study this BSL-3 pathogen under BSL-2 laboratory conditions.

In November 2023, the U.S. Food and Drug Administration (FDA) approved the first chikungunya vaccine for medical use in the United States (33). This CHIKV vaccine, Ixchiq, is also a live-attenuated vaccine produced by the company Valneva Austria GmbH. Ixchiq (VLA1553) was attenuated by deleting a portion of the chikungunya virus genome and is administered as a single intramuscular injection (34). The safety of this vaccine was assessed in two clinical trials in North America with a total of over 3,000 participants. The administration of this vaccine includes an information warning indicating that patients might experience prolonged chikungunya-like symptoms given that 1.6% of recipients during testing experienced severe adverse reactions (33). A post-marketing study will be completed to determine the severity of these side effects in the population.

Additional treatment typically involves targeting the symptoms with non-steroidal anti-inflammatory drugs (NSAIDs). It is recommended to avoid the use of aspirin to treat CHIKV symptoms as it might increase the risk of bleeding (27). Complementary prevention techniques such as mosquito reproduction control and prevention of mosquito bites are recommended as it is one of the most effective ways to prevent transmission.

Structure and molecular composition

Chikungunya is a small, icosahedral, enveloped virus of about 70nm in size (T=4 symmetry). Its genetic material is composed of a positive-sense single-stranded RNA genome of 12kb that encodes for four nonstructural proteins and six structural and accessory proteins. While nonstructural proteins are expressed as a polyprotein from the (+)ssRNA genome, alphavirus' structural proteins are encoded within a subgenomic mRNA produced from the negative sense RNA replication intermediate (35) **(Figure 1)**. The viral genome is protected by a 5' cap and a 3' polyadenylated tail.

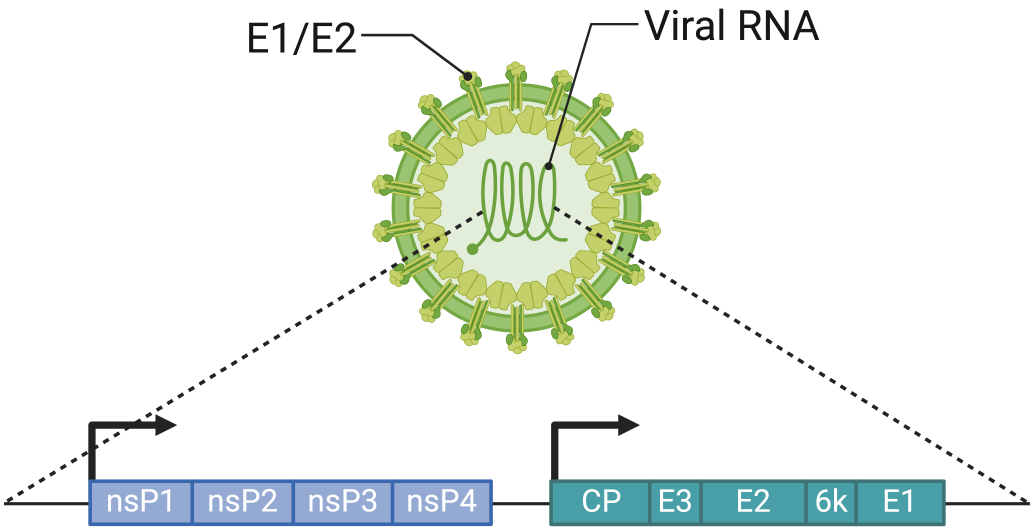

Figure 1. Schematic representation of the alphavirus genome. The first open reading frame of CHIKV's genome encodes for four nonstructural proteins. A subgenomic RNA encodes for the structural and accessory proteins. Diagram was created in biorender.com

The viral structural proteins and accessory proteins are comprised of the capsid, E3, E2, 6K, TF, and E1 proteins. These proteins are important in mediating the attachment, fusion, assembly, and release of alphaviruses. During viral entry, CHIKV E1 and E2 glycoprotein spikes mediate the steps of attachment and fusion. E1 and E2

assemble in 80 trimeric heterodimers through a non-covalent bond on the surface of the viral particles (36). The viral protein E2 can come in contact with receptors on the surface of host cells to mediate endocytosis (37–40). Next, the fusion peptide within the E1 protein, a class 2 fusion protein, is exposed after experiencing low pH conditions in the endosomal compartments leading to viral fusion and release of the viral genome (37).

In the cellular cytoplasm, the nonstructural polyprotein is cleaved into four independent viral proteins: nsP1, nsP2, nsP3, and nsP4. Each of these proteins plays an important role in the formation of replication complexes and evasion of the immune system. The nonstructural protein 1 (nsP1) is 535 amino acids in length and is the main anchor of replication complexes to the plasma membrane, the site of alphavirus replication (41). NsP1 displays methyltransferase (MTase) and guanylyltransferase (GTase) activity that allows it to cap nascent RNAs and protects double-stranded RNA intermediates against cellular recognition (42–44). Coupled with the palmitoylation of cysteine residues in nsP1, this monotopic membrane protein anchors to the inner phospholipid leaflet of the plasma membrane (45–47). NsP1 assembles into a characteristic crown structure and forms the invaginations where RNA synthesis occurs, known as spherules (41, 44).

The nonstructural protein 2 (nsP2) contains multiple domains that provide its roles during infection: protease, helicase, nucleoside-triphosphatase (NTPase), RNA-dependent triphosphatase (RTPase), and MTase-like domains (48–52). The most essential role of nsP2 involves its cysteine protease activity site (localized in the amino acid 478) (49). As a protease, it mediates the cleavage of the viral nonstructural

polyprotein in the cytoplasm and allows the start of viral replication (49, 50). The helicase activity of nsP2 coupled with the NTPase and RTPase domains enables it to unravel double-stranded nucleic acids to facilitate replication (51, 53). The NTPase and RTPase activity source the energy needed for the translocation of the viral helicase across the RNA and aid in the 5' capping activity (52, 54).

NsP2 also plays an important role in inducing cytopathic effects in host cells and mediating the evasion of immune responses (48, 55). Aside from its function in the cytoplasm, nsP2 translocates to the nucleus of infected cells where it can trigger the shutoff of cellular transcription and translation. This viral protein is able to induce the degradation of the required DNA-dependent RNA polymerase II subunit RPB1 (RPB1) through polyubiquitination (56). A short variable peptide loop (VLoop) found in the MTase-like domain of nsP2 provides transcriptional inhibitory functions independent of its role in the formation of replication complexes (48, 57). Mutations in this VLoop have also shown depletion of cytopathic effect and trigger type I IFN responses (48).

The non-structural protein 3 (nsP3) is involved in the synthesis of negative-sense single-stranded RNA to continue production of viral genomes. NsP3 is a phosphoprotein that displays affinity for ADP-ribose, DNA and RNA molecules (58, 59). Although it plays an essential role during virus replication, its specific role in genome replication remains mostly unknown (60, 61).

Alphavirus non-structural protein 4 (nsP4) is a key viral protein as it encodes for the RNA-dependent RNA polymerase (RdRp) (62, 63). NsP4 is only produced 10% of the time during translation of the nonstructural polyprotein when the formation of an RNA loop allows for suppression of the stop codon at the end of the nsP3 peptide (64).

This protein displays putative terminal adenylyl transferase activity that grants it the ability to repair and maintain the poly-A tail at the 3' end (65).

Once new genomes have been synthesized, capsid, E glycoproteins, and the accessory proteins mediate the assembly and egress of viral particles. Capsid protein is composed of 261 amino acids that encompass the viral nucleocapsid core to protect the genomic RNA within the particles (66). Capsid contains an N-terminal RNA binding domain that interacts with the genomic material and a C-terminal serine protease domain that allows it to self-cleave from the structural polyprotein (67, 68). Similar to nsP2, CHIKV's capsid has been shown to encode a signal that allows for nuclear-cytoplasm translocation and trigger transcriptional shutoff during with New World alphaviruses (69, 70). During assembly, capsid accumulates in the cytoplasm and oligomerizes forming particles ready to bud at the plasma membrane (66).

The exterior of the CHIK virions is covered in 80 mature viral spikes made up of E1-E2 heterodimers. The E3-E2, also referred to as p62, is a spike intermediate produced from the structural polyprotein. The accessory protein E3 serves as a leader peptide for E2, is required for the proper folding and assembly of the glycoprotein, and protects the fusion peptide of E1 during assembly (37, 71, 72). The immature p62-heterodimers trimerize to form the viral spikes (37). During transport to the cell surface, an exposed furin site in p62 is cleaved at the trans-Golgi giving rise to the mature glycoprotein (37, 73).

The E1 glycoprotein is coupled with the accessory protein 6K, named after its molecular weight (6kDa). 6K is a hydrophobic protein composed of two transmembrane alpha helices (74). The C-terminal alpha helix contains the signal peptidase site to

cleave E1 and the translocation signal for E1 to be shuttled to the cell surface (74). The accessory protein TF (TransFrame) is produced as a result of a ribosomal frameshift that only occurs about 10-18% of the time from a slippery codon motif in 6K (75). Both 6K and TF are incorporated into the viral particles in different amounts (76, 77). Palmitoylation of TF and the putative ion channel activity of 6K and TF have been evidenced to play an important role in enhancing viral particle release (77–82).

Viral entry

The entry of chikungunya virus initiates at the surface of the host cells, where E2 binds to host receptors and attachment factors (83). This initial attachment triggers clathrin-mediated endocytosis (84). In some alphaviruses, such as Sindbis virus, there is evidence of fusion at the plasma membrane (85, 86). For CHIKV infection, endocytosis is dependent on the activity of dynamin which mediates the pinching of endocytic vesicles from the cell surface (84, 87). Following internalization, the virions enter the early endosome where mildly acidic pH triggers a conformational change of the CHIKV glycoprotein spike and facilitates membrane fusion between the viral envelope and the endocytic vesicle (88). This releases the viral genetic material into the cytoplasm of the host cell in a receptor-independent manner (89). The positive-sense RNA genome is then translated, initiating infection.

CHIKV displays a wide cellular tropism, able to infect a broad range of cell types in both the mosquito and the mammalian host (23). Many studies have attempted to identify one ubiquitously expressed receptor that mediates the attachment to host cells. However, each tissue culture cell line can display a variety of receptors and attachment

molecules in the surface. This heterogeneity should be taken in consideration during studies evaluating the role of each attachment factor.

In 2012, prohibitin 1 (PHB1) was suggested to be the first identified CHIKV receptor (90). Despite being a molecule widely present among a variety of cell types and displaying an ability to bind to CHIKV particles, cell lines expressing PHB1 (e.g., U937) were unable to exhibit a productive infection (90, 91). These results lead to believe that although PHB1 might be an effective attachment factor, other entry receptors might be required.

Matrix remodeling associated 8 protein (MXRA8) is recognized as an important CHIKV receptor associated with the development of pathogenic symptoms (92, 93). MXRA8 binds in the interface between two E glycoproteins within the spike (92, 94). Interference between CHIKV spike and MXRA8 during *in vivo* studies resulted in a significant reduction of foot swelling in mice (92). Although it is undeniably important in mediating entry, cells lacking MXRA8 are still permissive to CHIKV infection. Mice lacking MXRA8 get infected with CHIKV and produce viremia, but lack of joint swelling lead authors to suggest MXRA8 plays an important role in pathogenesis (92). Since MXRA8 is not an essential receptor for CHIKV, other factors might also play a role in mediating attachment to host cells.

Another important attachment factor identified for CHIKV are glycosaminoglycans (GAGs), particularly Heparan Sulfate (HS) (40, 95). GAGs are complex carbohydrates widely expressed in the cell surface of mammalian and mosquito cells making them a great candidate for mediating attachment across multiple cell types (96, 97). Interaction with GAGs such as HS serve as a tethering element, increasing the proximity of viral

particles to cellular receptors. However, multiple studies have seen an association between serial passaging of viruses in cell culture and dependency on HS binding for entry (98, 99). Therefore, the role of GAGs in entry might not be essential in natural transmission.

Role of lipids in viral entry

Phospholipids can also play an essential role in the entry of multiple enveloped viruses including CHIKV, in a process known as apoptotic mimicry. Phosphatidylserine (PS) is one of the most abundant negatively charged phospholipids in the plasma membrane of mammalian cells (100, 101). In healthy cells, anionic phospholipids like phosphatidylethanolamine (PE) and PS are normally maintained in the inner leaflet of the plasma membrane to maintain membrane asymmetry (102). When cells undergo apoptosis, PS is exposed to the outer leaflet to trigger phagocytosis (102, 103). Apoptotic mimicry is described as the ability of enveloped viruses to manipulate the composition of their viral envelope, incorporating higher levels of PS that can mediate the attachment to PS receptors (PSR) and mimic apoptotic bodies (104). The process of apoptotic mimicry was first described for the entry of vaccinia virus to host cells (105). To date, many other enveloped viruses have been shown to display increased entry in the presence of PS receptors (106–113).

PS binding receptors can be categorized into two main families: T-cell Immunoglobin and Mucin domain (TIM) or Tyro, Axl, Mertk (TAM) family receptors. TIM receptors are expressed in a wide variety of cell types including immune and epithelial cells such as keratinocytes (114–117). TIM receptors play a role in the regulation of the immune response, stimulate the activation of T helper cells (Th2), and enhance their

proliferation (114). The immunoglobin-like variable domain (IgV) in the TIM family receptors forms a pocket that serves as the PS binding domain, attaching to PS in the envelope of viral particles (107, 108, 111, 118). Although the IgV serves as the binding site, the length and structure of the mucin-like domain in TIM receptors are also important for efficient binding of viral particles (119).

Members of the TAM family require the presence of a protein ligand like the growth arrest-specific protein 6 (Gas6) or the vitamin K-dependent protein S (ProS1) in order to bind to phosphatidylserine (120–123). This family of receptors is characterized by its receptor tyrosine kinase activity, where the protein ligands allow the dimerization of receptors and activate the kinase domain for effective intracellular communication (120, 124). Similar to the TIM family, TAM receptors play an important role in the regulation of the immune system by suppressing inflammatory responses (125, 126).

CHIKV, similar to other enveloped viruses, can utilize PS receptors, including TIM-1 and Axl, to mediate entry into host cells (110, 111, 127). Cells overexpressing TIM-1 on its surface, display increased levels of entry and transduction of particles (110, 111). Infection of PSR-producing cells with CHIKV, Zika, and Ebola can be inhibited by the addition of PS-containing liposomes (112, 127). Also, another aminophospholipid binding receptor, CD300a, has been evidenced to mediate the entry of CHIKV by attaching primarily to PE and to a lesser extent PS (128).

Beyond the role of envelope PS mediating the attachment to host cells during virus entry, lipids also play a role in the fusion of alphaviruses. The presence of cholesterol and sphingomyelin in the membrane of host cells can increase the fusion of CHIKV and other closely related alphaviruses like Semliki Forest virus (SFV) and

Sindbis virus (SINV) (84, 89, 129–136). The role of lipids during viral fusion is well characterized for SFV. It is estimated that one cholesterol molecule per two phospholipid molecules is needed for SFV fusion, mirroring the levels of these lipids in the plasma membrane of eukaryotic cells (131). Although sphingolipids are not suggested to play a structural role during fusion, it has been suggested that low levels are required to stabilize the interaction between E1 and the cellular membrane (129, 133, 134). Efficient fusion was observed with multiple members of the sphingolipid family including sphingomyelin, hexosylceramides, and as a minimum, ceramides (134).

Viral release

Alphavirus egress takes place at the plasma membrane of infected cells (66, 137). Chikungunya's virions are composed of a lipid bilayer acquired from the site of budding and studded with the viral glycoproteins which surrounds a nucleocapsid core (37, 66). The release of new viral particles starts in the cytoplasm during assembly, where the capsid proteins oligomerize to form the nucleocapsid cores (66). The glycoproteins are first synthesized in the endoplasmic reticulum and transported through the Golgi via the secretory pathway where they incorporate post-translational modifications (138–140). Following furin cleavage, the newly assembled spikes are positioned at the plasma membrane to be incorporated during egress (140, 141).

Assembled nucleocapsid colocalize with the glycoprotein spikes at the site of budding (137, 142, 143). To avoid premature fusion activity, the E1 fusion loop needs to be protected by the p62 intermediate (144). The p62-E1 intermediate displays resistance to dissociation in the presence of acidic buffers, in contrast to the mature E2-E1 heterodimer (144). The interaction between the nucleocapsid and viral spikes is

mediated through a motif in the cytoplasmic tail of the E2 protein and the hydrophobic pocket of capsid (142, 145–147). This leads to the proper organization of outer viral spikes and nucleocapsid core and the release of an icosahedral viral particle (66). Previous studies have demonstrated that budding-inhibitory antibodies produce wider inter-spike gaps and prevent lateral interactions between glycoproteins, further highlighting the importance of efficient coordination during this process (66, 148, 149).

The accessory proteins 6K and TF have been suggested to play a role in viral egress of alphaviruses, but the mechanism is still unclear. When the 6K protein was first characterized in 1980, there was no knowledge that a ribosomal frameshift could result in the production of a second accessory protein now referred to as TF (150). During this time, multiple studies suggested the role of 6K during viral egress and possible incorporation into the viral particles (76, 79, 151). In 2008, a study revealed the production of TF from a 9-nucleotide slippery sequence which caused a need to differentiate previously reported findings between the two proteins (75).

Despite sharing a common N-terminus sequence, 6K and TF seem to play different roles during viral exit. Deletion of both 6K and TF shows a significant decrease in virus particle production (79, 151, 152). The function of 6K appears to be limited to the host cell and it is only incorporated into viral particles at low levels (76, 152). The ion channel activity displayed by 6K in SINV is essential for proper trafficking of glycoprotein heterodimers and formation of cytopathic vacuoles during viral egress (78). Wildtype budding phenotype was observed when complementing mutated SINV lacking 6K with another viral protein with ion channel activity, HIV's Vpu (78). However, in the case of SFV, hampering 6K production did not affect proper spike assembly or

transportation to the plasma membrane (151). A working hypothesis is that 6K serves as a spacer for proper positioning of spikes at the plasma membrane and enhances the E2-Capsid interactions to produce a fully assembled viral particle (76, 153). In contrast to 6k, TF is predominantly incorporated into viral particles (75, 152). Although TF also displays ion channel activity, its specific function during viral egress is unclear. The position and characteristics of TF within the viral genome have been a barrier for proper assessment of its function in the absence of 6K (153).

Despite alphavirus egress being characterized by budding at the plasma membrane, studies suggest direct cell-to-cell transmission and alternate sites of budding in mosquito cells (137, 154–156). Development of intercellular extensions emulating filopodia has been visualized for multiple alphaviruses including CHIKV and SINV in a cell-type dependent manner (137, 156, 157). Cell-to-cell spread through these extensions appears to be independent of cellular receptors (156). This transmission omitting a cell-free stage of the virus, represents a great advantage for alphavirus to efficiently evade recognition by the host's immune system (158).

Fully assembled viral particles have also been detected budding from intracellular cytopathic vacuoles in mosquito cells (154). Lower levels of glycoprotein were observed at the plasma membrane, further supporting altered localization of structural proteins in insect cells during egress (154). Previous studies suggested that a depletion or interference of 6K's activity increases the levels of cell-associated virus possibly causing an increase in intracellular budding (79, 159). Although it is not clear if this is the normal mechanism of budding in invertebrate cells, if the activity of 6K in

mosquito cells is not efficient, this could explain the distinct egress pathways between mammalian and mosquito cells (153).

Role of lipids during egress

Lipids can play many roles in the exit of alphaviruses from host cells, from lipid post-translational modifications (PTM) to lipid composition and distribution within the viral envelope. Among PTMs, palmitoylation of viral structural proteins is particularly important for the efficient egress of alphaviruses. The proteins E1, E2, and TF all get palmitoylated and hindering this PTM's results in a decrease in viral particle production (77, 81, 82, 160). Previous studies postulated that an association between palmitoylation and ion channel activity might help explain the role of TF during viral egress, however, more studies are necessary to evaluate this hypothesis (153, 161, 162). Alternatively, palmitoylation of these viral proteins could be important for the efficient trafficking and attachments to the plasma membrane (77, 160).

As viruses bud from the cell surface, the composition of the plasma membrane can be crucial for their efficient release. For example, the presence of cholesterol at the site of budding is crucial for SFV particle production (163, 164). Despite cholesterol being important for the fusion and replication of CHIKV, to date, no studies have evaluated its role during budding (165). Modulation of other lipids in the leaflet of the plasma membrane could also affect the fluidity and trigger membrane curvatures, consequently affecting budding (166).

References

1. Robinson MC. 1955. An epidemic of virus disease in Southern Province, Tanganyika territory, in 1952–1953. Transactions of the Royal Society of Tropical Medicine and Hygiene 49:28–32.

2. Hammon WMcD, Rundnick A, Sather GE. 1960. Viruses Associated with Epidemic Hemorrhagic Fevers of the Philippines and Thailand. Science 131:1102–1103.

3. Weaver SC, Forrester NL. 2015. Chikungunya: Evolutionary history and recent epidemic spread. Antiviral Research 120:32–39.

4. Ross RW. 1956. The Newala epidemic: III. The virus: isolation, pathogenic properties and relationship to the epidemic. J Hyg 54:177–191.

5. Cordel H, Quatresous I, Paquet C, Couturier E. 2006. Imported cases of chikungunya in metropolitan France, April 2005 - February 2006. Weekly releases (1997–2007) 11.

6. Carey DE. 1971. Chikungunya and dengue: A Case of Mistaken Identity? J Hist Med Allied Sci XXVI:243–262.

7. Bessaud M, Peyrefitte CN, Pastorino BAM, Tock F, Merle O, Colpart J-J, Dehecq J-S, Girod R, Jaffar-Bandjee M-C, Glass PJ, Parker M, Tolou HJ, Grandadam M. 2006. Chikungunya virus strains, Reunion Island outbreak. Emerg Infect Dis 12:1604–1606.

8. Zeller H, Van Bortel W, Sudre B. 2016. Chikungunya: Its History in Africa and Asia and Its Spread to New Regions in 2013–2014. J Infect Dis 214:S436–S440.

9. Cassadou S, Boucau S, Petit-Sinturel M, Huc P, Leparc-Goffart I, Ledrans M. 2014. Emergence of chikungunya fever on the French side of Saint Martin island, October to December 2013. Euro Surveill 19:20752.

10. Morrison TE. 2014. Reemergence of chikungunya virus. J Virol 88:11644–11647.

11. Areas at Risk for Chikungunya. Center for Disease Control and Prevention - Chikungunya virus. https://www.cdc.gov/chikungunya/geo/index.html.

12. Volk SM, Chen R, Tsetsarkin KA, Adams AP, Garcia TI, Sall AA, Nasar F, Schuh AJ, Holmes EC, Higgs S, Maharaj PD, Brault AC, Weaver SC. 2010. Genome-scale phylogenetic analyses of chikungunya virus reveal independent emergences of recent epidemics and various evolutionary rates. J Virol 84:6497–504.

13. Schuffenecker I, Iteman I, Michault A, Murri S, Frangeul L, Vaney M-C, Lavenir R, Pardigon N, Reynes J-M, Pettinelli F, Biscornet L, Diancourt L, Michel S, Duquerroy S, Guigon G, Frenkiel M-P, Bréhin A-C, Cubito N, Desprès P, Kunst F, Rey FA, Zeller H, Brisse S. 2006. Genome microevolution of chikungunya viruses causing the Indian Ocean outbreak. PLoS Med 3:e263.

14. Tsetsarkin KA, Vanlandingham DL, McGee CE, Higgs S. 2007. A single mutation in chikungunya virus affects vector specificity and epidemic potential. PLoS Pathog 3:e201.

15. Leparc-Goffart I, Nougairede A, Cassadou S, Prat C, De Lamballerie X. 2014. Chikungunya in the Americas. The Lancet 383:514.

16. Powers AM, Brault AC, Tesh RB, Weaver SC. 2000. Re-emergence of Chikungunya and O'nyong-nyong viruses: evidence for distinct geographical lineages and distant evolutionary relationships. J Gen Virol 81:471–9.

17. Caglioti C, Lalle E, Castilletti C, Carletti F, Capobianchi MR, Bordi L. 2013. Chikungunya virus infection: an overview. New Microbiol 36:211–227.

18. Rivera-Pérez C, Clifton ME, Noriega FG. 2017. How micronutrients influence the physiology of mosquitoes. Current Opinion in Insect Science 23:112–117.

19. Zhou G, Kohlhepp P, Geiser D, Frasquillo MDC, Vazquez-Moreno L, Winzerling JJ. 2007. Fate of blood meal iron in mosquitoes. Journal of Insect Physiology 53:1169–1178.

20. Monteiro VVS, Navegantes-Lima KC, de Lemos AB, da Silva GL, de Souza Gomes R, Reis JF, Rodrigues Junior LC, da Silva OS, Romão PRT, Monteiro MC. 2019. Aedes-Chikungunya Virus Interaction: Key Role of Vector Midguts Microbiota and Its Saliva in the Host Infection. Front Microbiol 10:492.

21. Couderc T, Chrétien F, Schilte C, Disson O, Brigitte M, Guivel-Benhassine F, Touret Y, Barau G, Cayet N, Schuffenecker I, Desprès P, Arenzana-Seisdedos F, Michault A, Albert ML, Lecuit M. 2008. A mouse model for Chikungunya: young age and inefficient type-I interferon signaling are risk factors for severe disease. PLoS Pathog 4:e29.

22. Wichit S, Diop F, Hamel R, Talignani L, Ferraris P, Cornelie S, Liegeois F, Thomas F, Yssel H, Missé D. 2017. Aedes Aegypti saliva enhances chikungunya virus replication in human skin fibroblasts via inhibition of the type I interferon signaling pathway. Infect Genet Evol 55:68–70.

23. Matusali G, Colavita F, Bordi L, Lalle E, Ippolito G, Capobianchi MR, Castilletti C. 2019. Tropism of the Chikungunya Virus. Viruses 11:E175.

24. Tsetsarkin KA, Chen R, Weaver SC. 2016. Interspecies transmission and chikungunya virus emergence. Curr Opin Virol 16:143–150.

25. Tsetsarkin KA, Chen R, Sherman MB, Weaver SC. 2011. Chikungunya virus: evolution and genetic determinants of emergence. Current Opinion in Virology 1:310–317.

26. Ganu MA, Ganu AS. 2011. Post-chikungunya chronic arthritis--our experience with DMARDs over two year follow up. J Assoc Physicians India 59:83–86.

27. Suhrbier A, Jaffar-Bandjee M-C, Gasque P. 2012. Arthritogenic alphaviruses—an overview. Nat Rev Rheumatol 8:420–429.

28. Levitt NH, Ramsburg HH, Hasty SE, Repik PM, Cole FE, Lupton HW. 1986. Development of an attenuated strain of chikungunya virus for use in vaccine production. Vaccine 4:157–162.

29. Edelman R, Tacket CO, Wasserman SS, Bodison SA, Perry JG, Mangiafico JA. 2000. Phase II safety and immunogenicity study of live chikungunya virus vaccine TSI-GSD-218. Am J Trop Med Hyg 62:681–685.

30. Rezza G. 2015. Do we need a vaccine against chikungunya? Pathog Glob Health 109:170–173.

31. Hoke CH, Pace-Templeton J, Pittman P, Malinoski FJ, Gibbs P, Ulderich T, Mathers M, Fogtman B, Glass P, Vaughn DW. 2012. US Military contributions to the global response to pandemic chikungunya. Vaccine 30:6713–6720.

32. Gorchakov R, Wang E, Leal G, Forrester NL, Plante K, Rossi SL, Partidos CD, Adams AP, Seymour RL, Weger J, Borland EM, Sherman MB, Powers AM, Osorio JE, Weaver SC. 2012. Attenuation of Chikungunya Virus Vaccine Strain 181/Clone 25 Is Determined by Two Amino Acid Substitutions in the E2 Envelope Glycoprotein. J Virol 86:6084–6096.

33. 2023. FDA Approves First Vaccine to Prevent Disease Caused by Chikungunya Virus. FDA US Food and Drug Administration. https://www.fda.gov/news-events/press-announcements/fda-approves-first-vaccine-prevent-disease-caused-chikungunya-virus.

34. Chikungunya – VLA1553. Valneva. https://valneva.com/research-development/chikungunya/.

35. Rupp JC, Sokoloski KJ, Gebhart NN, Hardy RW. 2015. Alphavirus RNA synthesis and non-structural protein functions. J Gen Virol 96:2483–2500.

36. Zhou QF, Fox JM, Earnest JT, Ng T-S, Kim AS, Fibriansah G, Kostyuchenko VA, Shi J, Shu B, Diamond MS, Lok S-M. 2020. Structural basis of Chikungunya virus inhibition by monoclonal antibodies. Proc Natl Acad Sci U S A 117:27637–27645.

37. Voss JE, Vaney MC, Duquerroy S, Vonrhein C, Girard-Blanc C, Crublet E, Thompson A, Bricogne G, Rey FA. 2010. Glycoprotein organization of Chikungunya virus particles revealed by X-ray crystallography. Nature 468:709–12.

38. Holmes AC, Basore K, Fremont DH, Diamond MS. 2020. A molecular understanding of alphavirus entry. PLoS Pathog 16:e1008876.

39. Basore K, Kim AS, Nelson CA, Zhang R, Smith BK, Uranga C, Vang L, Cheng M, Gross ML, Smith J, Diamond MS, Fremont DH. 2019. Cryo-EM Structure of Chikungunya Virus in Complex with the Mxra8 Receptor. Cell 177:1725-1737 e16.

40. Silva LA, Khomandiak S, Ashbrook AW, Weller R, Heise MT, Morrison TE, Dermody TS. 2014. A single-amino-acid polymorphism in Chikungunya virus E2 glycoprotein influences glycosaminoglycan utilization. J Virol 88:2385–97.

41. Jones R, Bragagnolo G, Arranz R, Reguera J. 2021. Capping pores of alphavirus nsP1 gate membranous viral replication factories. Nature 589:615–619.

42. Tomar S, Narwal M, Harms E, Smith JL, Kuhn RJ. 2011. Heterologous production, purification and characterization of enzymatically active Sindbis virus nonstructural protein nsP1. Protein Expr Purif 79:277–284.

43. Ahola T, Laakkonen P, Vihinen H, Kääriäinen L. 1997. Critical residues of Semliki Forest virus RNA capping enzyme involved in methyltransferase and guanylyltransferase-like activities. J Virol 71:392–397.

44. Zhang K, Law Y-S, Law MCY, Tan YB, Wirawan M, Luo D. 2021. Structural insights into viral RNA capping and plasma membrane targeting by Chikungunya virus nonstructural protein 1. Cell Host & Microbe 29:757-764.e3.

45. Grimley PM, Berezesky IK, Friedman RM. 1968. Cytoplasmic Structures Associated with an Arbovirus Infection: Loci of Viral Ribonucleic Acid Synthesis. J Virol 2:1326–1338.

46. Froshauer S, Kartenbeck J, Helenius A. 1988. Alphavirus RNA replicase is located on the cytoplasmic surface of endosomes and lysosomes. The Journal of cell biology 107:2075–2086.

47. Zhang N, Zhao H, Zhang L. 2019. Fatty Acid Synthase Promotes the Palmitoylation of Chikungunya Virus nsP1. J Virol 93:e01747-18.

48. Akhrymuk I, Lukash T, Frolov I, Frolova EI. 2019. Novel Mutations in nsP2 Abolish Chikungunya Virus-Induced Transcriptional Shutoff and Make the Virus Less Cytopathic without Affecting Its Replication Rates. J Virol 93:e02062-18.

49. Pastorino BAM, Peyrefitte CN, Almeras L, Grandadam M, Rolland D, Tolou HJ, Bessaud M. 2008. Expression and biochemical characterization of nsP2 cysteine protease of Chikungunya virus. Virus Res 131:293–298.

50. Vasiljeva L, Valmu L, Kääriäinen L, Merits A. 2001. Site-specific protease activity of the carboxyl-terminal domain of Semliki Forest virus replicase protein nsP2. J Biol Chem 276:30786–30793.

51. Gomez de Cedrón M, Ehsani N, Mikkola ML, García JA, Kääriäinen L. 1999. RNA helicase activity of Semliki Forest virus replicase protein NSP2. FEBS Lett 448:19–22.

52. Karpe YA, Aher PP, Lole KS. 2011. NTPase and 5'-RNA triphosphatase activities of Chikungunya virus nsP2 protein. PLoS One 6:e22336.

53. Das PK, Merits A, Lulla A. 2014. Functional cross-talk between distant domains of chikungunya virus non-structural protein 2 is decisive for its RNA-modulating activity. J Biol Chem 289:5635–5653.

54. Vasiljeva L, Merits A, Auvinen P, Kääriäinen L. 2000. Identification of a novel function of the alphavirus capping apparatus. RNA 5'-triphosphatase activity of Nsp2. J Biol Chem 275:17281–17287.

55. Göertz GP, McNally KL, Robertson SJ, Best SM, Pijlman GP, Fros JJ. 2018. The Methyltransferase-Like Domain of Chikungunya Virus nsP2 Inhibits the Interferon Response by Promoting the Nuclear Export of STAT1. J Virol 92:e01008-18.

56. Akhrymuk I, Kulemzin SV, Frolova EI. 2012. Evasion of the innate immune response: the Old World alphavirus nsP2 protein induces rapid degradation of Rpb1, a catalytic subunit of RNA polymerase II. J Virol 86:7180–7191.

57. Meshram CD, Lukash T, Phillips AT, Akhrymuk I, Frolova EI, Frolov I. 2019. Lack of nsP2-specific nuclear functions attenuates chikungunya virus replication both in vitro and in vivo. Virology 534:14–24.

58. Malet H, Coutard B, Jamal S, Dutartre H, Papageorgiou N, Neuvonen M, Ahola T, Forrester N, Gould EA, Lafitte D, Ferron F, Lescar J, Gorbalenya AE, de Lamballerie X, Canard B. 2009. The crystal structures of Chikungunya and Venezuelan equine encephalitis virus nsP3 macro domains define a conserved adenosine binding pocket. J Virol 83:6534–6545.

59. Peranen J, Takkinen K, Kalkkinen N, Kaariainen L. 1988. Semliki Forest Virus-specific Non-structural Protein nsP3 Is a Phosphoprotein. Journal of General Virology 69:2165–2178.

60. McPherson RL, Abraham R, Sreekumar E, Ong S-E, Cheng S-J, Baxter VK, Kistemaker HAV, Filippov DV, Griffin DE, Leung AKL. 2017. ADP-ribosylhydrolase activity of Chikungunya virus macrodomain is critical for virus replication and virulence. Proc Natl Acad Sci USA 114:1666–1671.

61. Gao Y, Goonawardane N, Ward J, Tuplin A, Harris M. 2019. Multiple roles of the non-structural protein 3 (nsP3) alphavirus unique domain (AUD) during Chikungunya virus genome replication and transcription. PLoS Pathog 15:e1007239.

62. Chen MW, Tan YB, Zheng J, Zhao Y, Lim BT, Cornvik T, Lescar J, Ng LFP, Luo D. 2017. Chikungunya virus nsP4 RNA-dependent RNA polymerase core domain

displays detergent-sensitive primer extension and terminal adenylyltransferase activities. Antiviral Res 143:38–47.

63. Rubach JK, Wasik BR, Rupp JC, Kuhn RJ, Hardy RW, Smith JL. 2009. Characterization of purified Sindbis virus nsP4 RNA-dependent RNA polymerase activity in vitro. Virology 384:201–208.

64. De Groot RJ, Rümenapf T, Kuhn RJ, Strauss EG, Strauss JH. 1991. Sindbis virus RNA polymerase is degraded by the N-end rule pathway. Proc Natl Acad Sci USA 88:8967–8971.

65. Tomar S, Hardy RW, Smith JL, Kuhn RJ. 2006. Catalytic Core of Alphavirus Nonstructural Protein nsP4 Possesses Terminal Adenylyltransferase Activity. J Virol 80:9962–9969.

66. Chmielewski D, Schmid MF, Simmons G, Jin J, Chiu W. 2022. Chikungunya virus assembly and budding visualized in situ using cryogenic electron tomography. Nat Microbiol 7:1270–1279.

67. Aggarwal M, Sharma R, Kumar P, Parida M, Tomar S. 2015. Kinetic characterization of trans-proteolytic activity of Chikungunya virus capsid protease and development of a FRET-based HTS assay. Sci Rep 5:14753.

68. Perera R, Owen KE, Tellinghuisen TL, Gorbalenya AE, Kuhn RJ. 2001. Alphavirus nucleocapsid protein contains a putative coiled coil alpha-helix important for core assembly. J Virol 75:1–10.

69. Thomas S, Rai J, John L, Schaefer S, Pützer BM, Herchenröder O. 2013. Chikungunya virus capsid protein contains nuclear import and export signals. Virol J 10:269.

70. Garmashova N, Gorchakov R, Volkova E, Paessler S, Frolova E, Frolov I. 2007. The Old World and New World alphaviruses use different virus-specific proteins for induction of transcriptional shutoff. J Virol 81:2472–2484.

71. Lobigs M, Zhao HX, Garoff H. 1990. Function of Semliki Forest virus E3 peptide in virus assembly: replacement of E3 with an artificial signal peptide abolishes spike heterodimerization and surface expression of E1. J Virol 64:4346–4355.

72. Zhang X, Kielian M. 2004. Mutations that promote furin-independent growth of Semliki Forest virus affect p62-E1 interactions and membrane fusion. Virology 327:287–296.

73. Zhang X, Fugère M, Day R, Kielian M. 2003. Furin processing and proteolytic activation of Semliki Forest virus. J Virol 77:2981–2989.

74. Liljeström P, Garoff H. 1991. Internally located cleavable signal sequences direct the formation of Semliki Forest virus membrane proteins from a polyprotein precursor. J Virol 65:147–154.

75. Firth AE, Chung BY, Fleeton MN, Atkins JF. 2008. Discovery of frameshifting in Alphavirus 6K resolves a 20-year enigma. Virol J 5:108.

76. Gaedigk-Nitschko K, Schlesinger MJ. 1990. The sindbis virus 6K protein can be detected in virions and is acylated with fatty acids. Virology 175:274–281.

77. Ramsey J, Renzi EC, Arnold RJ, Trinidad JC, Mukhopadhyay S. 2017. Palmitoylation of Sindbis Virus TF Protein Regulates Its Plasma Membrane Localization and Subsequent Incorporation into Virions. J Virol 91:e02000-16.

78. Elmasri Z, Negi V, Kuhn RJ, Jose J. 2022. Requirement of a functional ion channel for Sindbis virus glycoprotein transport, CPV-II formation, and efficient virus budding. PLoS Pathog 18:e1010892.

79. Loewy A, Smyth J, Von Bonsdorff CH, Liljeström P, Schlesinger MJ. 1995. The 6-kilodalton membrane protein of Semliki Forest virus is involved in the budding process. J Virol 69:469–475.

80. Melton JV, Ewart GD, Weir RC, Board PG, Lee E, Gage PW. 2002. Alphavirus 6K Proteins Form Ion Channels. Journal of Biological Chemistry 277:46923–46931.

81. Schmidt M, Schmidt MF, Rott R. 1988. Chemical identification of cysteine as palmitoylation site in a transmembrane protein (Semliki Forest virus E1). J Biol Chem 263:18635–18639.

82. Ivanova L, Schlesinger MJ. 1993. Site-directed mutations in the Sindbis virus E2 glycoprotein identify palmitoylation sites and affect virus budding. J Virol 67:2546–2551.

83. Smith TJ, Cheng RH, Olson NH, Peterson P, Chase E, Kuhn RJ, Baker TS. 1995. Putative receptor binding sites on alphaviruses as visualized by cryoelectron microscopy. Proc Natl Acad Sci U S A 92:10648–10652.

84. Hoornweg TE, Van Duijl-Richter MKS, Ayala Nuñez NV, Albulescu IC, Van Hemert MJ, Smit JM. 2016. Dynamics of Chikungunya Virus Cell Entry Unraveled by Single-Virus Tracking in Living Cells. J Virol 90:4745–4756.

85. Vancini R, Wang G, Ferreira D, Hernandez R, Brown DT. 2013. Alphavirus genome delivery occurs directly at the plasma membrane in a time- and temperature-dependent process. J Virol 87:4352–4359.

86. Paredes AM, Ferreira D, Horton M, Saad A, Tsuruta H, Johnston R, Klimstra W, Ryman K, Hernandez R, Chiu W, Brown DT. 2004. Conformational changes in Sindbis virions resulting from exposure to low pH and interactions with cells suggest that cell penetration may occur at the cell surface in the absence of membrane fusion. Virology 324:373–386.

87. Sourisseau M, Schilte C, Casartelli N, Trouillet C, Guivel-Benhassine F, Rudnicka D, Sol-Foulon N, Le Roux K, Prevost MC, Fsihi H, Frenkiel MP, Blanchet F, Afonso PV, Ceccaldi PE, Ozden S, Gessain A, Schuffenecker I, Verhasselt B, Zamborlini A, Saib A, Rey FA, Arenzana-Seisdedos F, Despres P, Michault A, Albert ML, Schwartz O. 2007. Characterization of reemerging chikungunya virus. PLoS Pathog 3:e89.

88. Bernard E, Solignat M, Gay B, Chazal N, Higgs S, Devaux C, Briant L. 2010. Endocytosis of Chikungunya Virus into Mammalian Cells: Role of Clathrin and Early Endosomal Compartments. PLoS ONE 5:e11479.

89. van Duijl-Richter MKS, Blijleven JS, van Oijen AM, Smit JM. 2015. Chikungunya virus fusion properties elucidated by single-particle and bulk approaches. J Gen Virol 96:2122–2132.

90. Wintachai P, Wikan N, Kuadkitkan A, Jaimipuk T, Ubol S, Pulmanausahakul R, Auewarakul P, Kasinrerk W, Weng WY, Panyasrivanit M, Paemanee A, Kittisenachai S, Roytrakul S, Smith DR. 2012. Identification of prohibitin as a Chikungunya virus receptor protein. J Med Virol 84:1757–70.

91. Wikan N, Sakoonwatanyoo P, Ubol S, Yoksan S, Smith DR. 2012. Chikungunya Virus Infection of Cell Lines: Analysis of the East, Central and South African Lineage. PLoS ONE 7:e31102.

92. Zhang R, Kim AS, Fox JM, Nair S, Basore K, Klimstra WB, Rimkunas R, Fong RH, Lin H, Poddar S, Crowe JE, Doranz BJ, Fremont DH, Diamond MS. 2018. Mxra8 is a receptor for multiple arthritogenic alphaviruses. Nature 557:570–574.

93. Feng F, Bouma EM, Hu G, Zhu Y, Yu Y, Smit JM, Diamond MS, Zhang R. 2023. Colocalization of Chikungunya Virus with Its Receptor MXRA8 during Cell Attachment, Internalization, and Membrane Fusion. J Virol 97:e0155722.

94. Song H, Zhao Z, Chai Y, Jin X, Li C, Yuan F, Liu S, Gao Z, Wang H, Song J, Vazquez L, Zhang Y, Tan S, Morel CM, Yan J, Shi Y, Qi J, Gao F, Gao GF. 2019.

Molecular Basis of Arthritogenic Alphavirus Receptor MXRA8 Binding to Chikungunya Virus Envelope Protein. Cell 177:1714-1724 e12.

95. McAllister N, Liu Y, Silva LM, Lentscher AJ, Chai W, Wu N, Griswold KA, Raghunathan K, Vang L, Alexander J, Warfield KL, Diamond MS, Feizi T, Silva LA, Dermody TS. 2020. Chikungunya Virus Strains from Each Genetic Clade Bind Sulfated Glycosaminoglycans as Attachment Factors. J Virol 94.

96. Ciano KA, Saredy JJ, Bowers DF. 2014. Heparan sulfate proteoglycan: an arbovirus attachment factor integral to mosquito salivary gland ducts. Viruses 6:5182–5197.

97. Esko JD, Kimata K, Lindahl U. 2009. Proteoglycans and Sulfated Glycosaminoglycans, p. . *In* Varki, A, Cummings, RD, Esko, JD, Freeze, HH, Stanley, P, Bertozzi, CR, Hart, GW, Etzler, ME (eds.), Essentials of Glycobiology, 2nd ed. Cold Spring Harbor Laboratory Press, Cold Spring Harbor (NY).

98. Klimstra WB, Ryman KD, Johnston RE. 1998. Adaptation of Sindbis virus to BHK cells selects for use of heparan sulfate as an attachment receptor. J Virol 72:7357–7366.

99. Gardner CL, Hritz J, Sun C, Vanlandingham DL, Song TY, Ghedin E, Higgs S, Klimstra WB, Ryman KD. 2014. Deliberate attenuation of chikungunya virus by adaptation to heparan sulfate-dependent infectivity: a model for rational arboviral vaccine design. PLoS Negl Trop Dis 8:e2719.

100. Kay JG, Fairn GD. 2019. Distribution, dynamics and functional roles of phosphatidylserine within the cell. Cell Commun Signal 17:126.

101. Leventis PA, Grinstein S. 2010. The Distribution and Function of Phosphatidylserine in Cellular Membranes. Annu Rev Biophys 39:407–427.

102. Balasubramanian K, Schroit AJ. 2003. Aminophospholipid Asymmetry: A Matter of Life and Death. Annu Rev Physiol 65:701–734.

103. Segawa K, Nagata S. 2015. An Apoptotic 'Eat Me' Signal: Phosphatidylserine Exposure. Trends in Cell Biology 25:639–650.

104. Amara A, Mercer J. 2015. Viral apoptotic mimicry. Nat Rev Microbiol 13:461–9.

105. Mercer J, Helenius A. 2008. Vaccinia virus uses macropinocytosis and apoptotic mimicry to enter host cells. Science 320:531–535.

106. Brouillette RB, Phillips EK, Patel R, Mahauad-Fernandez W, Moller-Tank S, Rogers KJ, Dillard JA, Cooney AL, Martinez-Sobrido L, Okeoma C, Maury W. 2018. TIM-1 Mediates Dystroglycan-Independent Entry of Lassa Virus. J Virol 92.

107. Richard AS, Zhang A, Park SJ, Farzan M, Zong M, Choe H. 2015. Virion-associated phosphatidylethanolamine promotes TIM1-mediated infection by Ebola, dengue, and West Nile viruses. Proc Natl Acad Sci U S A 112:14682–7.

108. Moller-Tank S, Kondratowicz AS, Davey RA, Rennert PD, Maury W. 2013. Role of the phosphatidylserine receptor TIM-1 in enveloped-virus entry. J Virol 87:8327–41.

109. Meertens L, Carnec X, Lecoin MP, Ramdasi R, Guivel-Benhassine F, Lew E, Lemke G, Schwartz O, Amara A. 2012. The TIM and TAM families of phosphatidylserine receptors mediate dengue virus entry. Cell Host Microbe 12:544–57.

110. Kirui J, Abidine Y, Lenman A, Islam K, Gwon YD, Lasswitz L, Evander M, Bally M, Gerold G. 2021. The Phosphatidylserine Receptor TIM-1 Enhances Authentic Chikungunya Virus Cell Entry. Cells 10.

111. Jemielity S, Wang JJ, Chan YK, Ahmed AA, Li W, Monahan S, Bu X, Farzan M, Freeman GJ, Umetsu DT, Dekruyff RH, Choe H. 2013. TIM-family proteins promote infection of multiple enveloped viruses through virion-associated phosphatidylserine. PLoS Pathog 9:e1003232.

112. Zhang L, Richard AS, Jackson CB, Ojha A, Choe H. 2020. Phosphatidylethanolamine and Phosphatidylserine Synergize To Enhance GAS6/AXL-Mediated Virus Infection and Efferocytosis. J Virol 95.

113. Moller-Tank S, Maury W. 2014. Phosphatidylserine receptors: Enhancers of enveloped virus entry and infection. Virology 468–470:565–580.

114. Umetsu SE, Lee W-L, McIntire JJ, Downey L, Sanjanwala B, Akbari O, Berry GJ, Nagumo H, Freeman GJ, Umetsu DT, DeKruyff RH. 2005. TIM-1 induces T cell activation and inhibits the development of peripheral tolerance. Nat Immunol 6:447–454.

115. Kondratowicz AS, Lennemann NJ, Sinn PL, Davey RA, Hunt CL, Moller-Tank S, Meyerholz DK, Rennert P, Mullins RF, Brindley M, Sandersfeld LM, Quinn K, Weller M, McCray PB, Chiorini J, Maury W. 2011. T-cell immunoglobulin and mucin domain 1 (TIM-1) is a receptor for Zaire Ebolavirus and Lake Victoria Marburgvirus. Proc Natl Acad Sci U S A 108:8426–31.

116. Kobayashi N, Karisola P, Peña-Cruz V, Dorfman DM, Jinushi M, Umetsu SE, Butte MJ, Nagumo H, Chernova I, Zhu B, Sharpe AH, Ito S, Dranoff G, Kaplan GG, Casasnovas JM, Umetsu DT, Dekruyff RH, Freeman GJ. 2007. TIM-1 and TIM-4 glycoproteins bind phosphatidylserine and mediate uptake of apoptotic cells. Immunity 27:927–940.

117. Bernard E, Hamel R, Neyret A, Ekchariyawat P, Moles JP, Simmons G, Chazal N, Despres P, Misse D, Briant L. 2015. Human keratinocytes restrict chikungunya virus replication at a post-fusion step. Virology 476:1–10.

118. Santiago C, Ballesteros A, Martínez-Muñoz L, Mellado M, Kaplan GG, Freeman GJ, Casasnovas JM. 2007. Structures of T cell immunoglobulin mucin protein 4 show a metal-Ion-dependent ligand binding site where phosphatidylserine binds. Immunity 27:941–951.

119. Moller-Tank S, Albritton LM, Rennert PD, Maury W. 2014. Characterizing Functional Domains for TIM-Mediated Enveloped Virus Entry. J Virol 88:6702–6713.

120. Lemke G. 2013. Biology of the TAM receptors. Cold Spring Harb Perspect Biol 5:a009076.

121. Stitt TN, Conn G, Gore M, Lai C, Bruno J, Radziejewski C, Mattsson K, Fisher J, Gies DR, Jones PF. 1995. The anticoagulation factor protein S and its relative, Gas6, are ligands for the Tyro 3/Axl family of receptor tyrosine kinases. Cell 80:661–670.

122. Nagata K, Ohashi K, Nakano T, Arita H, Zong C, Hanafusa H, Mizuno K. 1996. Identification of the product of growth arrest-specific gene 6 as a common ligand for Axl, Sky, and Mer receptor tyrosine kinases. J Biol Chem 271:30022–30027.

123. Morizono K, Xie Y, Olafsen T, Lee B, Dasgupta A, Wu AM, Chen ISY. 2011. The Soluble Serum Protein Gas6 Bridges Virion Envelope Phosphatidylserine to the TAM Receptor Tyrosine Kinase Axl to Mediate Viral Entry. Cell Host & Microbe 9:286–298.

124. Linger RMA, Keating AK, Earp HS, Graham DK. 2008. TAM receptor tyrosine kinases: biologic functions, signaling, and potential therapeutic targeting in human cancer. Adv Cancer Res 100:35–83.

125. Scott RS, McMahon EJ, Pop SM, Reap EA, Caricchio R, Cohen PL, Earp HS, Matsushima GK. 2001. Phagocytosis and clearance of apoptotic cells is mediated by MER. Nature 411:207–211.

126. Graham DK, DeRyckere D, Davies KD, Earp HS. 2014. The TAM family: phosphatidylserine-sensing receptor tyrosine kinases gone awry in cancer. Nat Rev Cancer 14:769–785.

127. Groß R, Reßin H, Von Maltitz P, Albers D, Schneider L, Bley H, Hoffmann M, Cortese M, Gupta D, Deniz M, Choi J-Y, Jansen J, Preußer C, Seehafer K, Pöhlmann S, Voelker DR, Goffinet C, Pogge-von Strandmann E, Bunz U, Bartenschlager R, El Andaloussi S, Sparrer KMJ, Herker E, Becker S, Kirchhoff F, Münch J, Müller JA. 2024. Phosphatidylserine-exposing extracellular vesicles in body fluids are an innate defence against apoptotic mimicry viral pathogens. Nat Microbiol 9:905–921.

128. Carnec X, Meertens L, Dejarnac O, Perera-Lecoin M, Hafirassou ML, Kitaura J, Ramdasi R, Schwartz O, Amara A. 2016. The Phosphatidylserine and Phosphatidylethanolamine Receptor CD300a Binds Dengue Virus and Enhances Infection. J Virol 90:92–102.

129. van Duijl-Richter MKS, Hoornweg TE, Rodenhuis-Zybert IA, Smit JM. 2015. Early Events in Chikungunya Virus Infection-From Virus Cell Binding to Membrane Fusion. Viruses 7:3647–3674.

130. Kuo S-C, Chen Y-J, Wang Y-M, Tsui P-Y, Kuo M-D, Wu T-Y, Lo SJ. 2012. Cell-based analysis of Chikungunya virus E1 protein in membrane fusion. J Biomed Sci 19:44.

131. Kielian M, Chanel-Vos C, Liao M. 2010. Alphavirus Entry and Membrane Fusion. Viruses 2:796–825.

132. Kielian M, Chatterjee PK, Gibbons DL, Lu YE. 2002. Specific Roles for Lipids in Virus Fusion and Exit Examples from the Alphaviruses, p. 409–455. *In* Hilderson, H, Fuller, S (eds.), Fusion of Biological Membranes and Related Problems. Springer US, Boston, MA.

133. Umashankar M, Sánchez-San Martín C, Liao M, Reilly B, Guo A, Taylor G, Kielian M. 2008. Differential cholesterol binding by class II fusion proteins determines membrane fusion properties. J Virol 82:9245–9253.

134. Nieva JL, Bron R, Corver J, Wilschut J. 1994. Membrane fusion of Semliki Forest virus requires sphingolipids in the target membrane. EMBO J 13:2797–2804.

135. Kielian MC, Helenius A. 1984. Role of cholesterol in fusion of Semliki Forest virus with membranes. J Virol 52:281–283.

136. Mooney JJ, Dalrymple JM, Alving CR, Russell PK. 1975. Interaction of Sindbis virus with liposomal model membranes. J Virol 15:225–231.

137. Martinez MG, Snapp E-L, Perumal GS, Macaluso FP, Kielian M. 2014. Imaging the alphavirus exit pathway. J Virol 88:6922–6933.

138. Griffiths G, Quinn P, Warren G. 1983. Dissection of the Golgi complex. I. Monensin inhibits the transport of viral membrane proteins from medial to trans

Golgi cisternae in baby hamster kidney cells infected with Semliki Forest virus. J Cell Biol 96:835–850.

139. Mulvey M, Brown DT. 1996. Assembly of the Sindbis virus spike protein complex. Virology 219:125–132.

140. De Curtis I, Simons K. 1988. Dissection of Semliki Forest virus glycoprotein delivery from the trans-Golgi network to the cell surface in permeabilized BHK cells. Proc Natl Acad Sci USA 85:8052–8056.

141. Yap ML, Klose T, Urakami A, Hasan SS, Akahata W, Rossmann MG. 2017. Structural studies of Chikungunya virus maturation. Proc Natl Acad Sci USA 114:13703–13707.

142. Suomalainen M, Liljeström P, Garoff H. 1992. Spike protein-nucleocapsid interactions drive the budding of alphaviruses. J Virol 66:4737–4747.

143. Zheng Y, Kielian M. 2013. Imaging of the alphavirus capsid protein during virus replication. J Virol 87:9579–9589.

144. Wahlberg JM, Boere WA, Garoff H. 1989. The heterodimeric association between the membrane proteins of Semliki Forest virus changes its sensitivity to low pH during virus maturation. J Virol 63:4991–4997.

145. Jose J, Przybyla L, Edwards TJ, Perera R, Burgner JW, Kuhn RJ. 2012. Interactions of the cytoplasmic domain of Sindbis virus E2 with nucleocapsid cores promote alphavirus budding. J Virol 86:2585–2599.

146. Skoging U, Vihinen M, Nilsson L, Liljeström P. 1996. Aromatic interactions define the binding of the alphavirus spike to its nucleocapsid. Structure 4:519–529.

147. Lee S, Owen KE, Choi HK, Lee H, Lu G, Wengler G, Brown DT, Rossmann MG, Kuhn RJ. 1996. Identification of a protein binding site on the surface of the alphavirus nucleocapsid and its implication in virus assembly. Structure 4:531–541.

148. Jin J, Liss NM, Chen D-H, Liao M, Fox JM, Shimak RM, Fong RH, Chafets D, Bakkour S, Keating S, Fomin ME, Muench MO, Sherman MB, Doranz BJ, Diamond MS, Simmons G. 2015. Neutralizing Monoclonal Antibodies Block Chikungunya Virus Entry and Release by Targeting an Epitope Critical to Viral Pathogenesis. Cell Rep 13:2553–2564.

149. Jin J, Galaz-Montoya JG, Sherman MB, Sun SY, Goldsmith CS, O'Toole ET, Ackerman L, Carlson L-A, Weaver SC, Chiu W, Simmons G. 2018. Neutralizing Antibodies Inhibit Chikungunya Virus Budding at the Plasma Membrane. Cell Host Microbe 24:417-428.e5.

150. Welch WJ, Sefton BM. 1980. Characterization of a small, nonstructural viral polypeptide present late during infection of BHK cells by Semliki Forest virus. J Virol 33:230–237.

151. Liljeström P, Lusa S, Huylebroeck D, Garoff H. 1991. In vitro mutagenesis of a full-length cDNA clone of Semliki Forest virus: the small 6,000-molecular-weight membrane protein modulates virus release. J Virol 65:4107–4113.

152. Snyder JE, Kulcsar KA, Schultz KLW, Riley CP, Neary JT, Marr S, Jose J, Griffin DE, Kuhn RJ. 2013. Functional characterization of the alphavirus TF protein. J Virol 87:8511–8523.

153. Ramsey J, Mukhopadhyay S. 2017. Disentangling the Frames, the State of Research on the Alphavirus 6K and TF Proteins. Viruses 9:228.

154. Jose J, Taylor AB, Kuhn RJ. 2017. Spatial and Temporal Analysis of Alphavirus Replication and Assembly in Mammalian and Mosquito Cells. mBio 8:e02294-16.

155. Hahon N, Zimmerman WD. 1970. Chikungunya Virus Infection of Cell Monolayers by Cell-to-Cell and Extracellular Transmission. Appl Microbiol 19:389–391.

156. Martinez MG, Kielian M. 2016. Intercellular Extensions Are Induced by the Alphavirus Structural Proteins and Mediate Virus Transmission. PLoS Pathog 12:e1006061.

157. Jose J, Tang J, Taylor AB, Baker TS, Kuhn RJ. 2015. Fluorescent Protein-Tagged Sindbis Virus E2 Glycoprotein Allows Single Particle Analysis of Virus Budding from Live Cells. Viruses 7:6182–6199.

158. Brown R, Wan J, Kielian M. 2018. The Alphavirus Exit Pathway: What We Know and What We Wish We Knew. Viruses 10:89.

159. Schlesinger MJ, London SD, Ryan C. 1993. An in-frame insertion into the Sindbis virus 6K gene leads to defective proteolytic processing of the virus glycoproteins, a

trans-dominant negative inhibition of normal virus formation, and interference in virus shut off of host-cell protein synthesis. Virology 193:424–432.

160. Ryan C, Ivanova L, Schlesinger MJ. 1998. Effects of site-directed mutations of transmembrane cysteines in sindbis virus E1 and E2 glycoproteins on palmitylation and virus replication. Virology 249:62–67.

161. Shipston MJ. 2011. Ion Channel Regulation by Protein Palmitoylation. Journal of Biological Chemistry 286:8709–8716.

162. Veit M. 2012. Palmitoylation of virus proteins. Biol Cell 104:493–515.

163. Marquardt MT, Phalen T, Kielian M. 1993. Cholesterol is required in the exit pathway of Semliki Forest virus. J Cell Biol 123:57–65.

164. Lu YE, Kielian M. 2000. Semliki forest virus budding: assay, mechanisms, and cholesterol requirement. J Virol 74:7708–19.

165. Sousa IP, Carvalho CAM, Gomes AMO. 2020. Current Understanding of the Role of Cholesterol in the Life Cycle of Alphaviruses. Viruses 13:35.

166. Graham TR, Kozlov MM. 2010. Interplay of proteins and lipids in generating membrane curvature. Current Opinion in Cell Biology 22:430–436.

CHAPTER 3

CHIKUNGUNYA VIRUS ENTRY AND INFECTIVITY IS PRIMARILY FACILITATED THROUGH CELL DEPENDENT ATTACHMENT FACTORS IN MAMMALIAN AND MOSQUITO CELLS[1]

[1]Reyes Ballista, J.M.*; Miazgowicz, K.L.*; Acciani, M.D.; Jimenez, A.R.; Belloli, R.S.; Havranek, K.E.; Brindley, M.A. Chikungunya virus entry and infectivity is primarily facilitated through cell line dependent attachment factors in mammalian and mosquito cells. *Frontiers in Cell and Developmental Biology* 2023, 11:1085913. Reprinted here with permission of publisher. *Authors contributed equally to this work and share first authorship.

Abstract

Chikungunya virus (CHIKV) is the causative agent of the human disease chikungunya fever, characterized by debilitating acute and chronic arthralgia. No licensed vaccines or antivirals are currently available for CHIKV. Therefore, the prevention of attachment of viral particles to host cells is a potential intervention strategy. As an arbovirus, CHIKV infects a wide variety of cells in both its mammalian and mosquito host. This broad cell tropism might stem from CHIKV's ability to bind to a variety of entry factors in the host cell including phosphatidylserine receptors (PSRs), glycosaminoglycans (GAGs), and the proteinaceous receptor Mxra8, among others. In this study, we aimed to determine the relevance of each attachment factor during CHIKV entry into a panel of mammalian and mosquito cells. Our data suggest that the importance of particular binding factors during CHIKV infection is highly cell line dependent. Entry into mammalian Vero cells was mediated through attachment to PSRs, mainly T-cell immunoglobulin mucin domain-1 (TIM-1). Conversely, CHIKV infection into HAP1 and NIH3T3 was predominantly mediated by heparan sulfate (HS) and Mxra8, respectively. Entry into mosquito cells was independent of PSRs, HS, and Mxra8. Although entry into mosquito cells remains unclear, our data denotes the importance of careful evaluation of reagents used to identify receptor use in invertebrate cells. While PSRs, GAGs, and Mxra8 all enhance entry in a cell line dependent manner, none of these factors are necessary for CHIKV entry, suggesting additional host factors are involved.

Introduction

Chikungunya virus (CHIKV) is a mosquito-borne alphavirus that can cause debilitating arthralgia and joint pain. Outbreaks of CHIKV were originally limited to Africa or Asia (1,2), but recent emergence introduced it throughout the Americas and Europe (3–6). The expansion of mosquito vectors (*i.e., Aedes albopictus*) to temperate regions increases the likelihood of future outbreaks (5,7–9). Since we lack both vaccines and antivirals for this arbovirus, currently vector control remains the most effective strategy to limit spread. Therefore, developing interventions that interrupt transmission is essential to mitigating the global health burden of CHIKV.

CHIKV, in the *Togaviridae* family, has a positive-sense single-stranded RNA genome (10,11). Its virions are enveloped, icosahedral particles, studded with 80 glycoprotein spikes comprised of trimeric E1/E2 heterodimers (12,13). The trimeric E1/E2 spikes mediate cellular attachment (11) and fusion of viral-cellular membranes initiating infection (11,14). Both cellular binding and fusion efficiently occur in mammalian and mosquito cells, suggesting that the virus must rely on highly conserved pathways or can exploit multiple pathways to enter both vertebrate and invertebrate cells. CHIKV particles interact with and productively infect a wide variety of cells, from mosquito midgut cells to human macrophages **(Figure 2)** (15,16). Matrix remodeling associated 8 (Mxra8) (17), glycosaminoglycans (GAGs) (18–21), C-type lectins (22,23) and phosphatidylserine receptors (PSRs) (24–26) have all been implicated in promoting CHIKV entry into mammalian cells. The CHIKV-Mxra8 interaction has been linked to pathogenesis (17,27). While Mxra8-deficient mice did not develop joint inflammation, infectious virus was still detected in peripheral tissues during acute infection (27),

supporting the notion that Mxra8 plays a role in pathogenesis, but alternative surface molecules are involved in mediating viral establishment and dissemination.

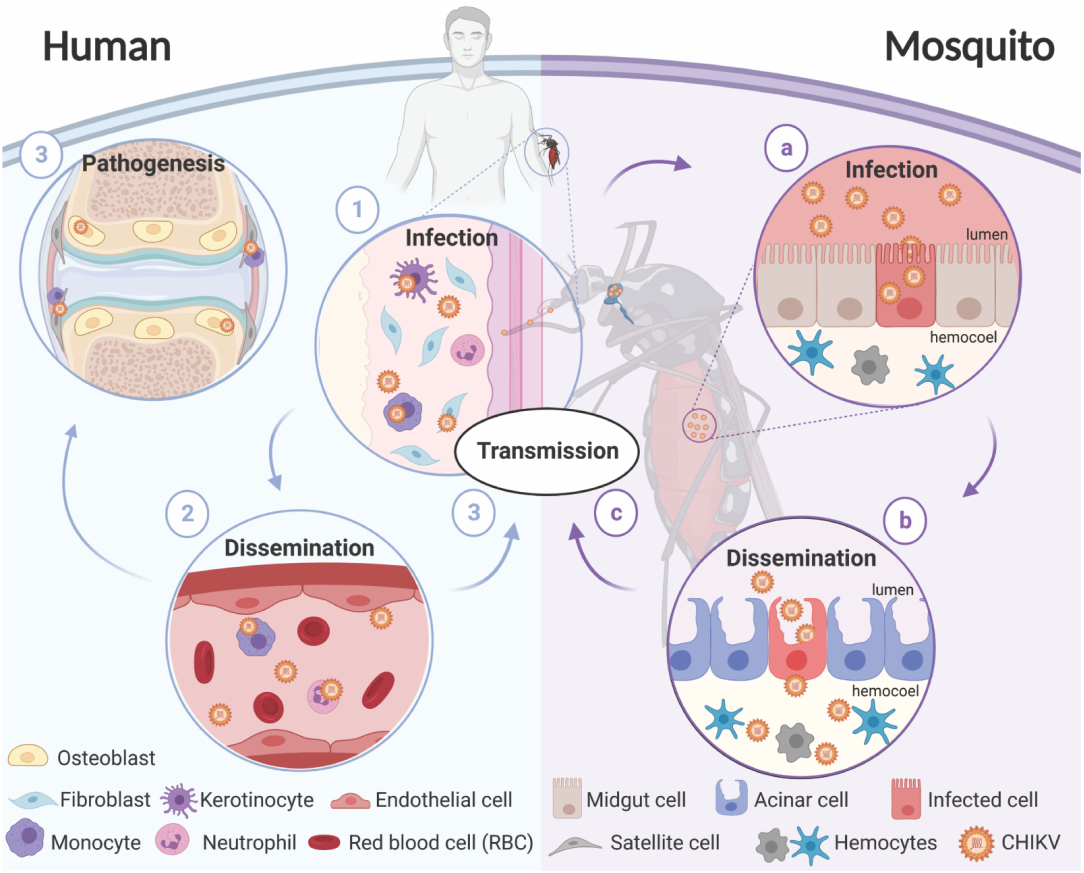

Figure 2. Schematic representation of CHIKV transmission cycle. CHIKV transmission starts when a female mosquito bites an infectious host. The virus enters through the bloodmeal and **(a)** infects the mosquito's midgut, **(b)** enters the circulatory system where it disseminates to different tissues, and **(c)** eventually reaches the salivary glands. The virions present in the salivary glands of the mosquito are transmitted to a susceptible vertebrate host when the mosquito takes a blood meal. In humans, **(1)** virions enter and replicate in the fibroblasts and **(2)** disseminate until **(3)** reaching target tissues including the liver, joints, lymph nodes, muscles, and the brain. Diagram was created by Dr. Miazgowicz in biorender.com

Glycosaminoglycans (GAGs) are repeating chains of negatively charged polysaccharides present on cell surfaces and in the extracellular matrix (28). GAGs, such as heparan sulfate (HS), are associated with common cellular processes including

mediating adhesion and growth factor signaling (29). Many viruses interact with GAGs, linking viral particles to the cell surface (30–32). Previously, both CHIKV and Sindbis, a closely related alphavirus, were shown to utilize GAGs for attachment to host cells (21,30). While tissue culture adaptation can select for increased GAG interaction, some field isolates of CHIKV are associated with HS utilization (33). Production of mucopolysaccharides is conserved among vertebrates and invertebrates including human and mosquito cells (34–37).

Phosphatidylserine receptors (PSRs) facilitate pathogen attachment to cells by binding to virion lipids (24,38–42). Viruses containing phosphatidylserine (PS) in the outer leaflet of the viral envelope can engage PSRs on host cells, mimicking apoptotic bodies and triggering internalization in a process termed apoptotic mimicry (43). The production of TIMs, TAMs, or CD300a PSRs facilitates entry of Ebola, Dengue, and CHIKV in some cell lines (25,26,38,40,42,44,45). Although the process of apoptotic mimicry in mammalian cells is well studied, the use of PSRs in mosquito cells by arboviruses is not.

Previous studies suggested that heat shock cognate 70 protein (HSC70) and ATP synthase β (ATPSβ) are important for CHIKV to enter mosquito cells (46,47), but confirmatory support is lacking. Currently, no binding partner has been identified as essential for CHIKV infection. The broad host and cellular tropism of CHIKV may stem from its ability to bind a multitude of molecules present on the cell surface as opposed to a single ubiquitous factor.

In this study, we assessed the role of proposed CHIKV binding factors in both mammalian and mosquito cells. CHIKV entry into mammalian cells was highly

conditional to the cell line examined. CHIKV attachment on mosquito cells does not rely on HS, PSRs, Mxra8, HSC70, or ATPSβ. Productive infection of CHIKV was not reliant on any one attachment factor. Overall, these data suggest that CHIKV entry requires an additional receptor yet to be identified or CHIKV entry can occur through a variety of cellular interactions that result in particle internalization.

Materials and Methods

Cell lines. Human near-haploid cells (HAP1) derived from the male chronic myelogenous leukemia cell line KBM-7 (RRID:CVCL_Y019), HAP1 flippase subunit knockout (KO) line (HAP1ΔCDC50a, HZGHC005423c007, RRID:CVCL_TS94), and HAP1 scramblase KO line (HAP1ΔXKR8, HZGHC005916c007, RRID:CVCL_TY32) were purchased from Horizon Discovery (United Kingdom). HAP1 and HAP1 KO lines were cultured in Iscove's modified Dulbecco's medium (IMDM) supplemented with 8% (v/v) fetal bovine serum (FBS). Vero-SLAM cells (VeroS) produce the human measles receptor SLAM (48). The Vero wildtype, Vero lacking T-cell immunoglobulin mucin domain-1 (VeroΔTIM), Vero lacking Axl receptor tyrosine kinase (VeroΔAxl), and Vero lacking both TIM-1 and Axl (VeroΔTIM/Axl) cells were a kind gift from Dr. Wendy Maury at the University of Iowa (41). All vervet monkey cells (VeroS, VeroSΔCDC50a, VeroSΔXKR8, Vero, VeroΔTIM, VeroΔAxl, and VeroΔTIM/Axl) were maintained with DMEM supplemented with 5% (v/v) FBS. Mouse embryo fibroblast cells (NIH3T3) were purchased from ATCC (CRL-1658, RRID:CVCL_0594) and maintained with DMEM supplemented with 10% (v/v) FBS. All mammalian cells were kept in a humidified chamber held at 37°C and with a 5% CO_2 content. Mosquito *Aedes albopictus* C6/36

cells (ATCC Cat# CRL-1660, RRID:CVCL_Z230) were maintained with Leibovitz's L-15 medium supplemented with 10% (v/v) FBS in a humidified chamber held at 28°C. *Aedes aegypti* Aag2 larval homogenate cells, a kind gift from Michael Strand at the University of Georgia, were maintained in SFX insect medium with 2% (v/v) FBS in a humidified chamber at 28°C. All cell lines were periodically tested for mycoplasma using the PlasmoTest™ - Mycoplasma Detection Kit (InvivoGen, cat. rep-pt1).

CRISPR-Cas9 mediated generation of VeroS KO cell lines. VeroS cells have a significantly higher transfection efficiency than Vero cells and were therefore chosen to produce the knockout cell lines. Three guide RNAs targeting each *Chlorocebus sabaeus* gene, XKR8 (GGCACTGCTCGACTACCACC, TGATCTACTTCCTGTGGAAC, CAGCTATGTGGCCCTGCACT) and CDC50a (TACGGCTGGCACGGTGCTAC, TCGTCGTTACGTGAAATCTC, GTGAACTGGCTTAAACCAGT), were inserted into pSpCas9(BB)-2A-GFP (pX458), which was a gift from Feng Zhang (Addgene plasmid #48138, RRID:Addgene_48138) (49) and verified using Sanger sequencing. VeroS cells were transfected with equivalent amounts of pSpCas9(BB)-2A-GFP bearing each of the three guide RNAs using GeneJuice (Sigma-Aldrich, cat. 70967). Three days post-transfection, VeroS cells were counted and distributed at a density of 0.5 cells per well into 96-well plates. Cells were monitored for 3 weeks to maintain single colony clones, and non-clonal wells were discarded. Wells corresponding to single clones were expanded to 24-well plates and assessed for CRISPR knockout. CRISPR XKR8 and CDC50a KOs were validated by extracting total DNA and PCR amplifying the guide RNA targeted regions. PCR amplicons spanning *xkr8* CRISPR regions were gel purified and submitted for Sanger sequencing to verify *xkr8* modification, which showed a 136

bp deletion in exon 2. We could not amplify *cdc50a* CRISPR regions in exons 1 and 3 but could amplify the CRISPR region targeting exon 5, indicating the presence of a large deletion spanning multiple exons in CDC50a. CRISPR CDC50a KO was also validated using a functional screen for externalized PS.

DNA transfections. Transfection efficiency and cytotoxicity varied with each cell line and gene KO. We paired different transfection reagents with different cell lines to optimize transfection efficiency and reduce cytotoxicity. HAP1 cells were transfected with JetOptimus (PolyPlus, cat. 117-07), while VeroS and 293T cells with GeneJuice (Sigma-Aldrich, cat. 70967) according to manufacturer recommendations. Expression vectors encoding a GFP-fused transmembrane hTIM-1 (a gift from Wendy Maury at the University of Iowa)(41), pCS6-L-SIGN (Transomic; cat. BC038851), pTiger-Mxra8 (Mxra8 open reading frame from Transomic; cat BC006213 was cloned into the pTiger expression vector), or pMax-GFP (Lonza) were used to assess CHIKV entry. pTiger was a gift from Garry Nolan (Addgene plasmid # 1728; http://n2t.net/addgene:1728;RRID: Addgene_1728).

Viruses. Chikungunya virus (CHIKV) strain 181 clone 25 (181/c25) was used to conduct experiments in a BSL2 laboratory environment. Reporter genes were cloned into pSinRep5-181/25c, a gift from Terence Dermody (Addgene plasmid #60078), using overlapping PCR. The reporters were added as additional transcriptional units between the nonstructural and structural genes, similar to the previously characterized viruses (50). Full-length DNA CHIKV clones containing reporter genes (*gfp, mKate, or Nluc*) were linearized and *in vitro* transcribed (Ambion, cat. AM1344) adhering to the manufacturer's protocol. Infectious CHIKV virions encoding reporter genes were

recovered after direct RNA transfection (1µg) into VeroS cells with Lipofectamine 3000 (ThermoFisher, cat. L3000001). Unless otherwise stated, viral stocks were propagated in VeroS cells, and passage 3 viral stocks were used for all experiments. The amount of infectious virus was determined by calculating the 50% tissue culture infective dose ($TCID_{50}$) units per mL through end-point dilution using the Spearman-Karber method (51). Recombinant vesicular stomatitis viruses containing the CHIKV, Ebola, or Lassa glycoproteins were generated as previously described (52). Coxsackie B5 virus was amplified in VeroS cells.

Cell surface staining. 293T, VeroS, HAP1 and Vero cells were plated at $2x10^5$ cells per well in 12-well plates 48 hrs before staining. Cells were transfected with plasmids encoding Mxra8, hTIM-1-GFP, or L-SIGN along with a plasmid encoding GFP 24 hrs before immunofluorescence staining. Transfected cells were rapidly cooled and stained in blocking solution (dPBS with 1% (v/v) bovine serum albumin (BSA)) containing anti-Mxra8 (1:100, W040-3, MBL International, RRID:AB_2801291), anti-hTIM1(1:100, AF1750, R&D Systems, RRID:AB_2116561), or anti-CLEC4M (L-SIGN/CD299) 2G1 antibody (1:100, MA5-21012, ThermoFisher, RRID:AB_2605445) at 4°C with gentle shaking for 1 hr. Cells were washed with PBS before lifting the cells with a scraper. Cells were pelleted (500xg for 5 mins), resuspended, and washed in PBS two additional times before adding secondary anti-goat Cy5 (1:2500, 072-02-13-06, KPL) or anti-mouse Alexa Fluor 647 (1:2500, A32728, Invitrogen, RRID: AB_2633277) and incubated at 4°C in the dark for 30 mins. Cells were washed with PBS three times and then analyzed via flow cytometry. Cell populations were gated using forward scatter/side scatter. The mean fluorescence intensity (MFI) of the indicated secondary

antibody (Cy5 or AF647) was recorded from a minimum of 10,000 GFP-positive cells per experiment. All experiments were completed three independent times. All cells were analyzed using a NovoCyte Quanteon (Agilent) flow cytometer.

Luminescence entry assay. Cells were plated at a density of $2.5x10^4$ cells per well in a 96-well plate, the day before infection. Cells were infected with CHIKV-Nluc, rVSVΔG-LASV-NlucP, or Coxsackie B5 at an MOI of 0.05. Two hours post-infection, cells were treated with 10 mM ammonium chloride (NH_4Cl) to inhibit subsequent rounds of replication. Eight hours after infection, cells infected with CHIKV or rVSVΔG-LASV were lysed with NanoGlo substrate, and lysates were quantified in a GloMax Explorer (Promega) according to the manufacturer's instructions. Cells infected with Coxsackie B5 were harvested 24hrs post-infection and cell viability was assessed using Cell Titer Glo and quantified in a GloMax Explorer (Promega) according to the manufacturer's instructions.

Competition assays. CHIKV-Nluc stocks were used to assess the ability of antibodies, liposomes, heparan sulfate, or sodium azide to block infection in the indicated cell lines. Cells were seeded at $5x10^4$ cells per well in a 96-well plate, one day prior to infection. For each well in the competition assay, approximately 150 CHIKV-Nluc virions were added. 24 hrs following infection, cells were lysed with NanoGlo substrate, and lysates were quantified in a GloMax Explorer (Promega) according to the manufacturer's instructions. Data is displayed as percent of control which was calculated by dividing the luminescence values at each condition with the control (mock inhibitor added).

Antibody competition to the virus: Virus was incubated with the indicated concentrations of CHIKV polyclonal antibody (IBT, cat. 04-008) or no antibody control (PBS) at room

temperature for 45 mins. After incubation, the virus-CHIKV antibody mix was added to the cells.

Antibody and Sodium Azide competition to the cells: Cells were incubated with the indicated concentrations of Mxra8 clone 9G2.D6 antibody (EMD Millipore Corp., cat. MABF2275), HSC70 monoclonal antibody (Invitrogen, cat. MA3-014, RRID:AB_325462), Mouse IgG2a K Isotype control eBM2a (eBioscience Inc., cat. 14-472481), ATP5B pAb (Abnova, cat. H00000506-D01P, H00000506-D01P), XKR8 antibody (ThermoFisher, cat. PA5-65799), human EBOV monoclonal KZ52 antibody (IBT, cat. 0260-001), Sodium Azide (Sigma-Aldrich, cat. 26628-22-8), or control (PBS). After incubation at 37°C for 20 minutes, cells were infected.

Heparan Sulfate competition: Following a protocol previously found to block CHIKV infection in CHO cells, the indicated concentration of heparan sulfate (Sigma-Aldrich, cat. H7640-1MG), or control PBS was added to cells at 37°C for 10 mins prior to infection. After the 10 min pre-treatment, virus was added.

Liposome competition: PC:PE:PS liposomes (75% PC: 20% PE: 5% PS) and PC-only liposomes (42), were sonicated for 20 minutes or 1 hr respectively. The indicated concentration of liposomes or PBS was added to cells at 37°C for 10 mins prior to infection. After the 10 min pre-treatment, virus was added.

Cell-to-cell viral spread kinetics. Cells were plated at either $7.5x10^4$ cells per well in a 48-well plate (HAP1 lines) or $5x10^4$ cells per well in a 24-well plate (Vero lines) 1 day prior to infection. Assuming the density of cells doubled overnight, cells were inoculated with CHIKV-GFP virus (MOI of 0.1). After 1 hr (T = 0 hpi) virus inoculum was removed and replaced with complete media. At the indicated time, cells were lifted in trypsin,

resuspended in PBS, and fixed in 1.85% (v/v) formaldehyde. GFP-positive cells were enumerated in a NovoCyte Quanteon (Aligent) flow cytometer. Live cells were first gated based on forward/side scatter, and cellular aggregates were removed by gating with forward scatter area to height. Uninfected cells were used to set the GFP gate. 10,000 live cells were collected and the percent infection (% GFP^+) was recorded and compared over time.

Luminescence entry kinetics assay. Vero and ΔTIM/Axl cells were seeded at $2.5x10^4$ cells per well in a 96-well plate. One day after seeding, cells were infected with CHIKV-Nluc with approximately 500 or 50 CHIKV-Nluc virions per well, as indicated. NH_4Cl at 10mM was added at the indicated time points to inhibit low pH in the endosomal compartments. 8 hrs post-infection, cells were lysed with NanoGlo substrate, and lysates were quantified in a GloMax Explorer (Promega) according to the manufacturer's instructions.

Quantification of cellular outer leaflet phosphatidylserine (PS). Cellular surface levels of PS were assessed using Promega's RealTime-Glo Annexin V Apoptosis and Necrosis Assay (Promega, cat. JA1012) according to manufacturer specifications. HAP1 or VeroS cell lines were plated in media supplemented with 0.1 M HEPES at $3.0x10^4$ or 10^4 cells per well, respectively, in a 96-well black-walled, clear bottom plate 1 day before treatment. Cells were infected with CHIKV-mKate (MOI of 1.0) or mock infected. Kit components 1-4 were added to cells 1 hr following infection and the plate was moved into a pre-warmed GloMax Explorer. Kit components 1-4 were used at 0.5x concentration in HAP1 cell lines as cytotoxicity was observed at 1x manufacturer

recommendations. Luminescence (Annexin V) measurements were collected 24 hr following infection in a GloMax Explorer (Promega) held at 37°C.

Real-time quantification PCR (RT-qPCR) of genome equivalents. CHIKV genome equivalents/mL were calculated via RT-qPCR. Viral RNA was extracted from infected cell supernatant (Zymo, cat. 11-355), eluted in nuclease-free water, and converted to cDNA with random hexamer primers (ThermoFisher, cat. 4388950) following kit protocols. RT-qPCR reactions were set up with cDNA, TaqMan Gene Master Mix (Applied Biosystems, cat. 4369016), primers, and TaqMan probe (5'-6FAMACTTGCTTTGATCGCCTTGGTGAGAMGBNFQ-3') as previously described (53) with each sample run in duplicate. A plasmid-based standard curve of a full-length CHIKV clone was used to enumerate the total number of genome equivalents per mL of the original sample. A no template control (NTC) and no amplification control (NAC) were included in each run on a StepOne platform (Applied Biosystems, cat. 4376357). The amplification profile included 1 cycle of 2 mins at 50°C, 10 mins at 95°C, followed by 40 cycles of 15 secs at 95°C and 1 min at 60°C.

Quantification of viral outer leaflet phosphatidylserine (PS). *Virus Production:* T75 flasks were seeded with wild type, ΔXKR8, and ΔCDC50a HAP1 and VeroS cells with 7.2 x 10^6 cells or 3.6 × 10^6 cells, respectively. After 24 hrs, wild-type and ΔXKR8 cells were infected with CHIKV using an MOI of 0.001, and ΔCDC50a cells were infected using an MOI of 0.01. After 12 hrs at 37°C, the inoculum was removed, cells were treated with citric acid buffer (40 mM citric acid, 10 mM KCl, 135 mM NaCl [pH 3.0]) for 1 min, rinsed, and FBS-free media was added. After incubating for an additional 36 hrs, the supernatant was collected, cleared twice using centrifugation (6,000xg), and

overlaid on a 20% sucrose cushion. Overlaid supernatants were then subjected to ultracentrifugation at (234,116xg) for 2 hrs at 4°C. Pellets were resuspended in 100 µL PBS.

Input normalization: Prior to staining, purified CHIKV samples were normalized using RT-qPCR. To ensure normalization we compared protein levels, normalized samples were denatured using SDS-urea buffer (200 mM Tris [pH 6.8], 8 M urea, 5% SDS, 0.1 mM EDTA, 0.03% bromophenol blue), run on Mini-PROTEAN TGX Stain-Free Precast Gels (Bio-Rad), and imaged with a ChemiDoc XRS digital imaging system (Bio-Rad), capsid protein was readily detected. Gels were then subjected to immunoblot analysis for CHIKV E using an anti-E antibody (1:1000, R&D Systems, MAB97792SP).

Particle surface PS staining: Similar to previous protocols (54,55), equivalent numbers of CHIKV particles were conjugated to 4-µm aldehyde/sulfate latex beads (ThermoFisher) overnight at 4°C with gentle shaking. Due to differences in viral yields between cell types, beads were bound with approximately 10^6 genome equivalents from HAP1 cell lines and 10^9 genome equivalents from VeroS cell lines.

Beads were blocked with a final concentration of 1% (v/v) bovine serum albumin (BSA) in PBS for 2 hrs while rotating at room temperature. Beads were washed 3 times with 1% (v/v) BSA in PBS and then incubated with 100 µl of AnV binding buffer containing AnV-PE conjugate for 30 mins on ice. Beads were diluted 1:4 in AnV binding buffer and analyzed using the NovoCyte Quanteon flow cytometer (Agilent). Bead-only samples were included as a mock control.

Specific infectivity. We used the ratio of infectious viral particles to genome equivalents to assess particle infectivity. This ratio represents the number of infectious

particles in a viral stock. A value close to 1 indicates a virus stock is more infectious, or each particle has a higher probability of starting an infection. Particle number was determined by quantifying the number of genome equivalents in the virus preparation using qRT-PCR described above. When comparing various cell lines, infectivity was determined by $TCID_{50}$ units per mL, instead of the traditional plaque forming units (PFUs) as not all our cell lines tolerated forming a confluent monolayer under an agar.

PNGase F and Heparinase digestion. Ultracentrifuge-concentrated CHIKV-Nluc virions were treated with PNGase F (New England Biolabs, cat. P0704S) or Heparinase II from *Flavobacterium heparinum* (Sigma-Aldrich, cat. H6512) in a 37°C water bath for 18 hrs following manufacturer's non-denaturing protocol. An aliquot of treated virions was denatured and analyzed through SDS-PAGE using an anti-CHIKV E1 antibody (1:1000, R&D Systems, MAB97792SP). To assess the effect of treatment on infection, cells were plated at $2.5x10^4$ cells per well in a 96-well plate. Cells were infected at an MOI of 0.05 for 24 hrs, lysed with NanoGlo substrate, and quantified in a GloMax Explorer (Promega) according to the manufacturer's instructions.

Sodium Azide cell viability assays. Cells were seeded at $5x10^4$ cells per well in a 96-well plate, one day prior to infection. Sodium Azide (Sigma-Aldrich, cat. 26628-22-8), or control (PBS) was added to each well and incubated at 37°C for 20 minutes. Following incubation, approximately 150 CHIKV-Nluc virions were added to each well. 24 hrs following infection, cells were lysed with Cell Titer Glo or RealTime-Glo MT (Promega), and lysates were quantified in a GloMax Explorer (Promega) according to the manufacturer's instructions. Data is displayed as percent of control which was

calculated by dividing the luminescence values at each condition with the control (mock inhibitor added).

Flow Cytometry entry assay. Cells were plated at $2.5x10^5$ cells per well in a 24-well plate, 1 day prior to infection. CHIKV-GFP virus inoculum was prepared using DMEM FBS-free media and 250μL was added to each cell line. After 2 hr, the virus inoculum was removed and replaced with complete media containing NH_4Cl (10mM). 18hpi, cells were lifted, resuspended in PBS, and fixed in 1.85% (v/v) formaldehyde. GFP-positive cells were enumerated in a NovoCyte Quanteon (Aligent) flow cytometer. Live cells were first gated based on forward/side scatter, and cellular aggregates were removed by gating with forward scatter area to height. Uninfected cells were used to set the GFP gate. At least 10,000 live cells were collected and the percent infection (% GFP^+) was recorded.

Statistical analysis. Data were visualized and analyzed using GraphPad Prism software (v9.4.0, macOS). An unpaired parametric Student T-test assuming equal variance was used to test for statistical significance for data on a linear scale (*e.g.,* percent GFP^+). An unpaired parametric Student T-test using a Welch's correction was used to test for statistical significance for normalized data (*e.g.*, percent of control, normalized MFI). Logarithmic data were natural log (ln) transformed and then assessed with an unpaired parametric Student T-test assuming equal variance (*e.g.*, titer, luminescence). When comparing all cell lines, ANOVA with Tukey's multiple comparisons test was used.

Results

Exogenously expressed attachment factors differentially enhance CHIKV infection.

Previous studies demonstrate that CHIKV infection can be enhanced by the addition of proteins including Mxra8, C-type lectins (*i.e.,* L-SIGN), and PSRs (*i.e.* TIM-1 and Axl) in 293T cells (24,25,39). Human 293T cells are an epithelial-like cell isolated from a fetal kidney (56). While 293T are permissive for CHIKV infection, they are poorly susceptible, and the addition of various attachment factors enhances entry (24,25,39). First, we confirmed previous findings in 293T cells and expanded the evaluation to include HAP1 and VeroS cells (21,26,57). HAP1 cells, a human haploid cell line derived from chronic myeloid leukemia KBM7 cells, have been used to understand CHIKV interactions with GAGs (18,21). Vero cells are a vervet monkey kidney cell line that is commonly used to amplify viral stocks (58). VeroS cells are Vero cells engineered to produce the measles virus receptor SLAM. VeroS cells are readily transfected whereas Vero cells are not, therefore in experiments requiring transfection, VeroS cells were used. Antibody staining and flow cytometry was used to establish the presence or absence of endogenous surface TIM-1, Mxra8, or L-SIGN in the cell lines **(Figure 3)**. Aligned with published data, 293T and HAP1 cells lack the endogenous surface presentation of TIM-1 (25,38,39,59), Mxra8 (17,21), and L-SIGN (60), while endogenous TIM-1 and Mxra8 are present on the surface of VeroS cells **(Figure 3)**.

To determine if the over-expression of TIM-1, Mxra8, and/or L-SIGN can enhance CHIKV infection, cells were transfected with plasmids encoding each entry factor either fused to GFP or along with a plasmid encoding GFP. Plasmid transfection

effectively produced the entry factors on the cell surface **(Figure 3)**. In 293T cells, exogenous Mxra8, TIM-1, and L-SIGN all similarly enhanced CHIKV infection, while only Mxra8 promoted infection in HAP1 cells **(Figure 4A)**. Over-expression of Mxra8 and TIM-1 or introducing L-SIGN in VeroS cells did not enhance CHIKV entry.

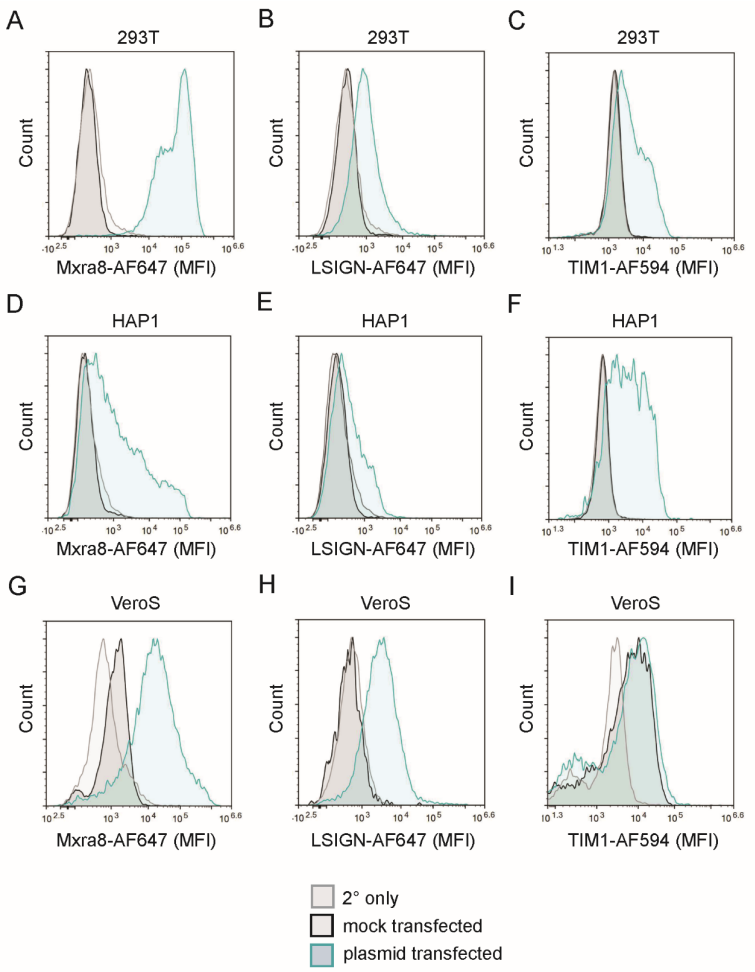

Figure 3. Endogenous and exogenous expression of Mxra8, L-SIGN, and TIM-1 in 293T, HAP1 and VeroS cells. Surface presentation of known CHIKV attachment factors (Mxra8, L-SIGN, or TIM-1) was assessed before and after transfection via flow cytometry in **(A-C)** 293T, **(D-F)** HAP1, or **(G-I)** VeroS.

To confirm that the infection enhancements were specific to CHIKV, we infected cells producing exogenous entry factors with recombinant vesicular stomatitis virus (rVSV) containing the Lassa virus (rVSVΔG-LASV) **(Figure 4B)** or Ebola virus

(rVSVΔG-EBOV) **(Figure 4C)** glycoproteins (52). Both 293T and HAP1 cells produce properly glycosylated alpha-dystroglycan, the high-affinity receptor for Lassa virus (61,62), whereas VeroS cells do not (41,63). As expected, the overproduction of TIM-1, Mxra8, or L-SIGN did not significantly increase rVSVΔG-LASV infection in either 293T, HAP1, or VeroS cells **(Figure 4B)**.

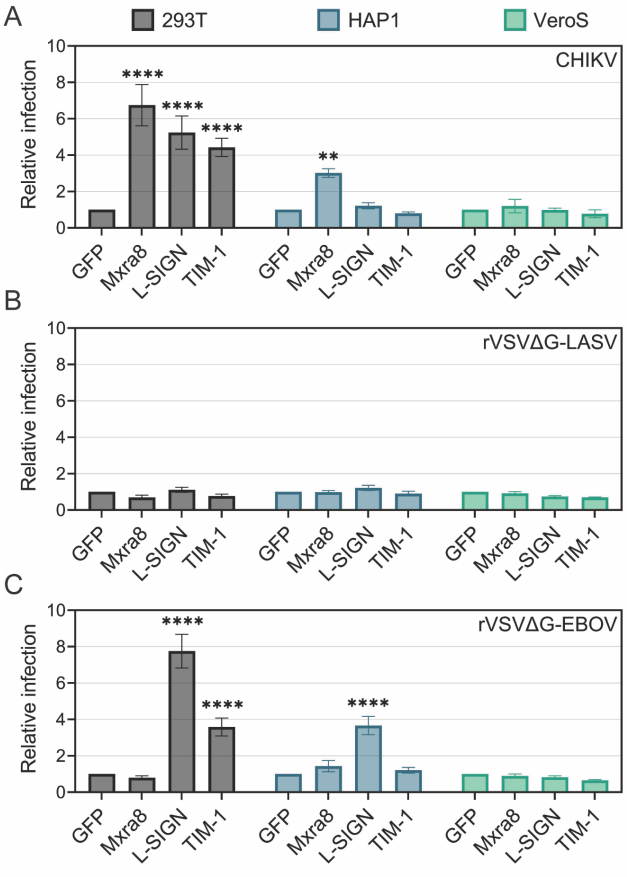

Figure 4. Mxra8, L-SIGN, and TIM-1 enhance CHIKV infection in 293T cells. 293T, HAP1, and VeroS cells were transfected with either TIM-1-GFP, Mxra8 and GFP, L-SIGN and GFP, or GFP alone. 24 hrs post-transfection, cells were inoculated with either mKate-expressing **(A)** CHIKV strain 181/c25, **(B)** recombinant vesicular stomatitis virus containing the Lassa virus glycoprotein (rVSVΔG-LASV), or **(C)** rVSV containing the Ebola virus glycoprotein (rVSVΔG-EBOV) for 1 hr. 12 hrs following infection the cells were enumerated in a flow cytometer. Relative infection was calculated as the proportion of infected cells ($mKate^+$) among transfected cells (GFP^+) normalized to infection levels in a GFP-only control. Data are presented as the mean ± SEM from three independent experiments. Data were compared with a two-way ANOVA with multiple comparisons, comparing row effects (receptors produced) to the GFP only control: **, $p < 0.01$; ****, $p < 0.0001$.

Entry of rVSVΔG-EBOV is enhanced by PSRs (24,39) and L-SIGN (64,65), but not by Mxra8. As expected, rVSVΔG-EBOV infection was enhanced in TIM-1$^+$ 293T cells but Mxra8 did not enhance infection in any of the cell lines **(Figure 4C)**. L-SIGN enhanced rVSVΔG/EBOV infection by 8-fold in 293T cells and 3.5-fold in HAP1 cells but had no effect in VeroS cells **(Figure 4C)**. Together, these data suggest the various attachment factors can all enhance CHIKV entry, but in specific cell lines.

CHIKV exhibits a cell type-dependent use of entry factors in mammalian cells.

To compare the CHIKV entry pathways in mammalian cells without over-expressing entry factors, we focused on three cell lines: 1) NIH3T3 cells, a mouse fibroblast cell line that was used to identify Mxra8 as a CHIKV receptor (17); 2) HAP1 cells, and 3) Vero cells. First, CHIKV viral stocks were titrated on the three cell lines. We observed that HAP1 and Vero cells were the most susceptible and permissive, displaying titers 10-fold higher than the NIH3T3 cells **(Figure 5A)**. We also monitored reporter activity produced after a single round of infection with CHIKV-Nluc. Luciferase activity mirrored the titer data, with both HAP1 and Vero cells produced more than 10-fold higher signals than NIH3T3 cells **(Figure 5B)**. These differences suggest that the entry and/or replication efficiency of CHIKV varies among different cell lines.

To determine the relevance of GAGs, PSRs, and Mxra8 in facilitating CHIKV infection in HAP1, NIH3T3 and Vero cells, we performed competitive inhibition assays. First, to demonstrate CHIKV entry could be blocked in all cell lines, we used a neutralizing CHIKV antibody to inhibit infection. As expected, the luciferase signal produced by CHIKV-Nluc infection was reduced in a dose-dependent manner with the addition of increasing concentrations of CHIKV antibody **(Figure 5C)**. However,

increasing amounts of Mxra8 antibody only inhibited CHIKV infection in NIH3T3 cells but did not affect entry into HAP1 nor Vero cells **(Figure 5D)**. The role of GAGs in CHIKV infection was evaluated by adding heparan sulfate (HS) to compete for entry. Soluble HS can compete with HS on the cells, blocking CHIKV entry (21,33). High concentrations of soluble HS significantly inhibited CHIKV infection in HAP1 cells but did not negatively impact entry into Vero cells at any concentration **(Figure 5E)**. HS modestly inhibited infection into NIH3T3 cells at the highest concentration, but the reduction was not statistically significant **(Figure 5E)**.

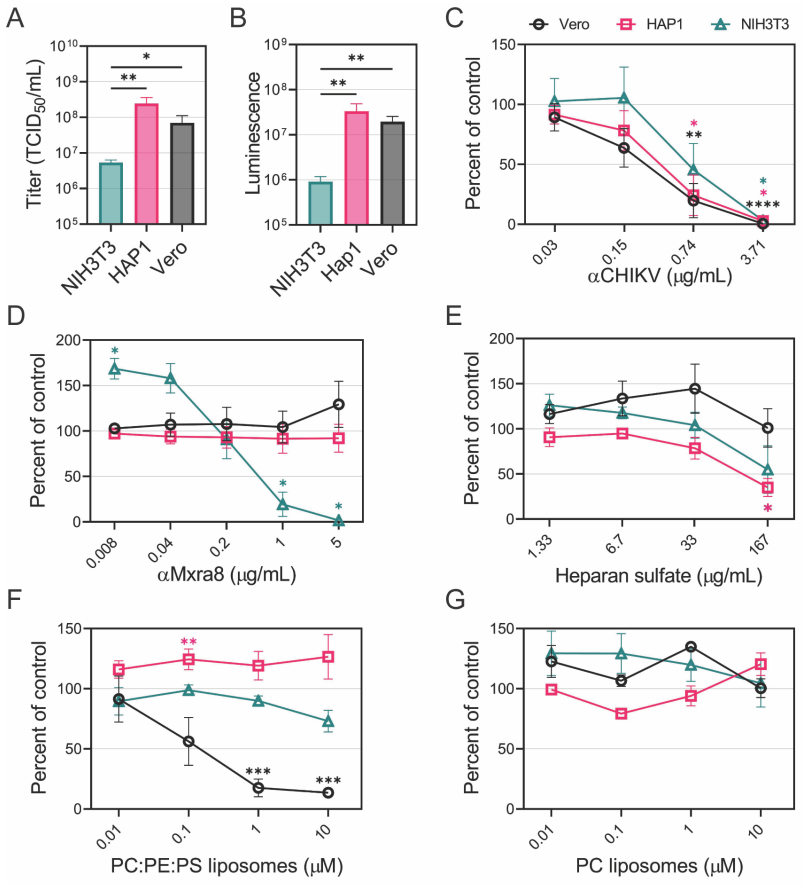

Figure 5. CHIKV viral apoptotic mimicry is cell-type dependent in mammalian cells. (A) CHIKV stock titers NIH3T3, HAP1, and Vero cells. **(B)** Luminescence levels produced by CHIKV-Nluc in NIH3T3, HAP1, and Vero cells after one round of replication. CHIKV-Nluc stocks were used to assess the ability of **(C)** CHIKV antibody, **(D)** Mxra8 antibody, **(E)** heparan sulfate, **(F)** PS-containing liposomes (75% PC: 20%

PE: 5% PS), and **(G)** PC-only liposomes, to block infections into either NIH3T3 (△), HAP1 (□), or Vero (◯) mammalian cells at the indicated concentrations. Data are presented as the mean percent of control ± SEM from at least three independent experiments performed in duplicate or triplicate. For each treatment, the level of Nluc was measured and compared to the no inhibitor added control to determine percent of control. **(A-B)** Unpaired parametric Student's T-test was performed to determine statistical significance among cell lines, **(C-E)** with unequal variance (Welch's correction) compared to a no-treatment control, or **(F-G)** comparing between PC:PE:PS vs PC liposomes. *, $p < 0.05$; **, $p < 0.01$; ***, $p < 0.001$; ****, $p < 0.0001$.

To prevent interaction with PSRs, we added liposomes containing the anionic phospholipids PS and phosphatidylethanolamine (PE) dispersed in neutral phosphatidylcholine (PC), previously demonstrated to efficiently bind PSRs (42). PC:PE:PS liposomes did not inhibit CHIKV infection in HAP1 and NIH3T3 cells **(Figure 5F)**. Conversely, Vero cells exhibited dose-dependent inhibition, where a ~90% reduction in infection was achieved by competing with 10 μM PC:PE:PS liposomes **(Figure 5F)**. PC-only liposomes did not inhibit CHIKV infection in any of the cell lines **(Figure 5G)**, confirming the PS/PE-dependent inhibition in Vero cells. These data support the hypothesis that CHIKV entry can occur through several different entry pathways, but specific pathways may mediate the majority of CHIKV entry into a given cell line: Mxra8 in NIH3T3 cells, HS in HAP1 cells, and PSRs in Vero cells.

CHIKV entry into Vero cells is driven mainly through PS receptors.

CHIKV entry into Vero cells was greatly reduced in the presence of anionic phospholipid liposomes suggesting PS receptors may play a role in mediating CHIKV entry into Vero cells. Vero cells produce both TIM-1 and Axl which bind to and internalize PS-containing cargo (41). To further evaluate CHIKV entry into Vero cells, we compared CHIKV-*Nluc* infection in Vero cells lacking TIM-1 (ΔTIM), Axl (ΔAxl), or both TIM-1 and Axl (ΔTIM/Axl). Similar to our VeroS cells, Vero cells present

endogenous TIM-1 and Mxra8 **(Figure 6)**. Entry of rVSVΔG-LASV in Vero cells relies mainly on TIM-1 production, but lack of Axl expression can modestly decrease susceptibility to infection (41). We observed that CHIKV infection closely mirrors LASV entry **(Figure 7A)**. Cells lacking Axl displayed reduced infection (~50%), but entry into ΔTIM-1 or ΔTIM/Axl cells was substantially inhibited (>95%). To demonstrate that the cells retain susceptibility to other viruses, we used Coxsackie B virus (CoxB), a naked virus that enters through the Coxsackie and adenovirus receptor (CAR) (66). CoxB was able to infect all four Vero lines at similar efficiencies **(Figure 7A)**.

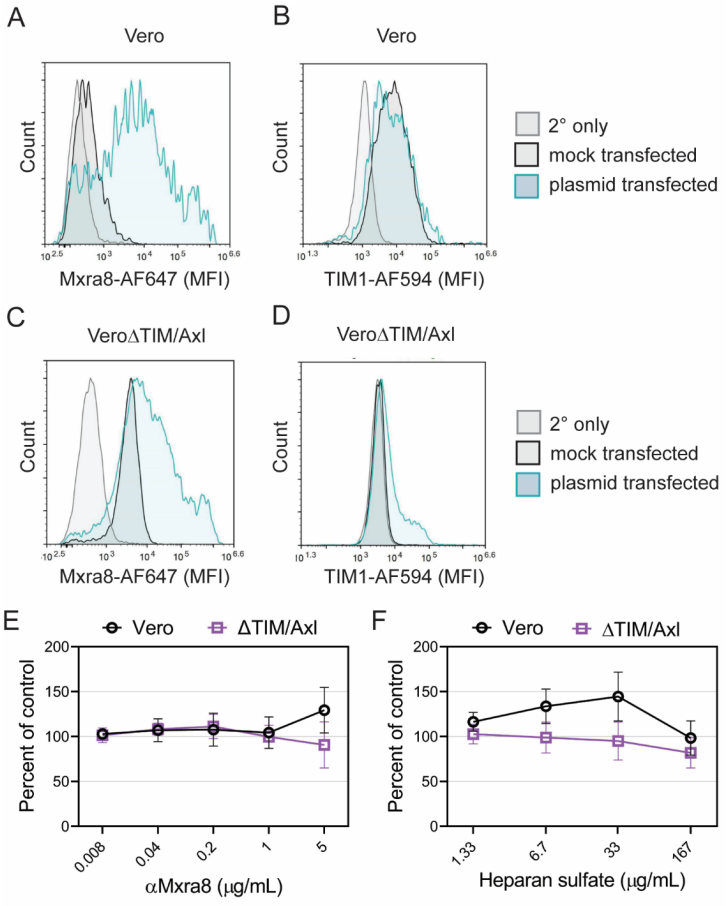

Figure 6. CHIKV entry into VeroΔTIM/Axl is not inhibited by Mxra8 antibodies or HS. Surface staining of attachment factors, Mxra8 and TIM-1, in Vero **(A-B)** and VeroΔTIM/Axl **(C-D)** cells before and after transfection using flow cytometry. The ability of **(E)** Mxra8 antibody and **(F)** heparan sulfate to block CHIKV infection into VeroΔTIM/Axl cells was assessed at the indicated concentrations. Vero inhibition assay

data shown in Figure 3 are presented again for comparison as VeroΔTIM/Axl cells were included as a treatment group during the experiment. Data are presented as the mean ± SEM from three independent experiments performed in triplicate. Unpaired parametric Student's T-test was performed to determine statistical significance **(E-F)** with unequal variance (Welch's correction) compared to a no-treatment control. ***, $p < 0.001$.

When multi-cycle CHIKV infection was examined, we observed that, despite a delay, CHIKV eventually spreads and infects ΔTIM/Axl cells **(Figure 7B)**. To monitor how quickly the particles are internalized in the cells and escape from the low pH cellular compartment, we blocked endosomal escape with ammonium chloride (NH_4Cl) at multiple time points throughout infection. While the ΔTIM/Axl cells produced lower luciferase levels, the time of endosomal escape appeared similar to Vero cells **(Figure 7C)**. To adjust for the total level of virus entering the ΔTIM/Axl cells, we added 1/10th of the virus to the parental Vero cells. This amount of virus resulted in a similar level of infection in both Vero and ΔTIM/Axl cells **(Figure 7D)**. CHIKV appeared to escape from the endosome at the same rate in both cell lines, suggesting the lack of TIM-1 and Axl decreases particle binding or internalization efficiency, but once endocytosis is initiated, the viral particles are trafficked to a low-pH compartment at a similar rate.

To explore how CHIKV infection proceeds in Vero cells lacking TIM-1 and Axl, we assessed the role of Mxra8 antibody, heparan sulfate, or liposomes to block CHIKV infection through competition assays **(Figures 6E-F and 7E-F)**. We did not observe significant virus inhibition in the ΔTIM/Axl cells by any treatment, suggesting CHIKV is utilizing an additional minor entry pathway in Vero cells in the absence of the PSRs TIM-1 and Axl.

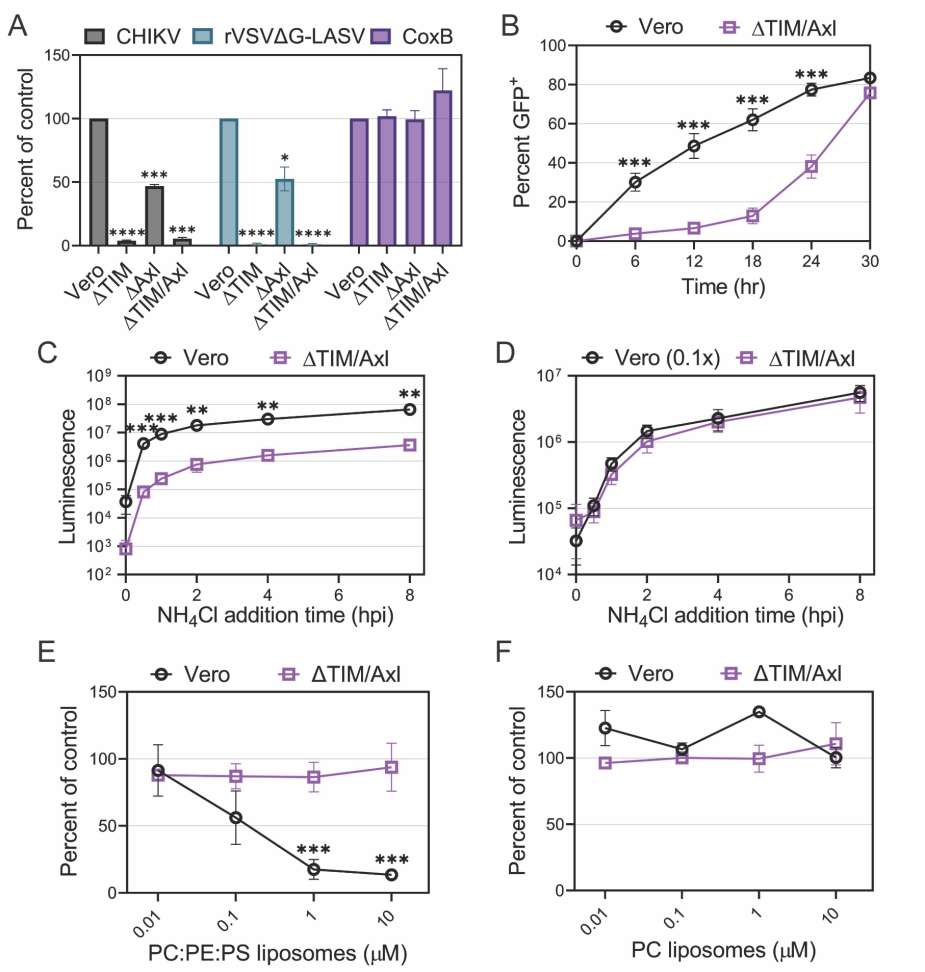

Figure 7. Entry of CHIKV into Vero cells is mediated mainly through TIM-1. (A) Entry of CHIKV-Nluc, rVSVΔG-LASV-Nluc, and CoxB into Vero, VeroΔTIM, VeroΔAxl, and VeroΔTIM/Axl after one round of replication was assessed by luciferase assays or cell viability (CoxB). **(B)** Luminescence values from the knockout cells was compared to the values observed in the parental Vero to determine the percent of control. CHIKV-GFP cellular spread kinetics were quantified by flow cytometry and the percent of GFP^+ cells over time in Vero and VeroΔTIM/Axl cells. Kinetics of endosomal escape of CHIKV was determined by infecting Vero and VeroΔTIM/Axl cells with **(C)** equal amounts of virus or **(D)** 10-fold less virus in Vero cells. Cells were treated with NH_4Cl at the indicated time points and luminescence was measured 8 hours post-infection. The ability of **(E)** PS-containing liposomes (75% PC: 20% PE: 5% PS) and **(F)** PC-only liposomes, to block CHIKV infection into VeroΔTIM/Axl, cells was assessed at the indicated concentrations. The data for each respective panel were generated at the same time and in the same way as the data displayed in Figure 3. We present the Vero data from Figure 3 again to allow for easy visual comparison to the VeroΔTIM/Axl data. Unpaired parametric Student's T-test was performed to determine statistical significance with unequal variance comparing PC:PE:PS to PC liposomes. Data are presented as the mean percent of control ± SEM from three independent experiments performed in triplicate. *, $p < 0.05$; **, $p < 0.01$; ***, $p < 0.001$; ****, $p < 0.0001$.

Increased levels of exposed viral envelope PS increase CHIKV infectivity in Vero cells.

To further evaluate the role of PS and PSRs in CHIKV infection, we produced CHIKV particles with either high or low levels of PS in the outer leaflet of the virion membrane. Cells maintain PS asymmetry with flippases that constitutively move PS from the outer to inner leaflet of the plasma membrane (67,68). During cell death, which is triggered during CHIKV infection, flippases become inactive and scramblases are activated, increasing PS levels in the outer leaflet (67). By producing virus in cells with modified PS translocation dynamics, we can produce particles with either high or low levels of PS (54). Knocking out the scramblase XKR8 in HAP1 cells (HAP1ΔXKR8) prevents apoptosis-induced scramblase activity, resulting in cells with low outer leaflet PS even during CHIKV infection **(Figure 8A)** (54). In contrast, knocking out the flippase subunit CDC50a in HAP1 cells (HAP1ΔCDC50a) eliminates P4-ATPase flippase activity, resulting in cells with relatively high PS levels in the outer leaflet of the plasma membrane **(Figure 8A)**. Particles produced in ΔXKR8 were low in PS compared to particles produced in ΔCDC50a, which were PS-high **(Figures 8B-D)**. Since CHIKV infection induces apoptosis, we were not surprised to find that particles produced in infected HAP1 cells to have PS levels at only moderately lower levels than our PS-high particles produced in HAP1ΔCDC50a cells **(Figure 8D)**.

We infected a panel of mammalian cell lines with the PS-high and PS-low CHIKV virions to determine if the envelope PS levels altered infectivity. Genome equivalents were calculated for each viral inoculum and compared to the titer based on tissue culture infectious dose 50 value ($TCID_{50}$) to calculate the specific infectivity on each cell

type. The levels of PS on the particle correlated positively with specific infectivity when infecting Vero and VeroS cells **(Figure 8E)**. This correlation was not observed in VeroΔTIM/Axl, NIH3T3, nor HAP1 cells **(Figure 8E)**. Similar data was obtained when CHIKV particles were produced in VeroS cells lacking CDC50a or XKR8, except that wild-type VeroS produced particles had a PS profile more akin to particles produced in VeroSΔXKR8 cells due to weak scramblase activity **(Figure 9)**. This further suggests that CHIKV entry into Vero cells is driven primarily by apoptotic mimicry, while it occurs through alternative pathways in the other tested mammalian cell lines.

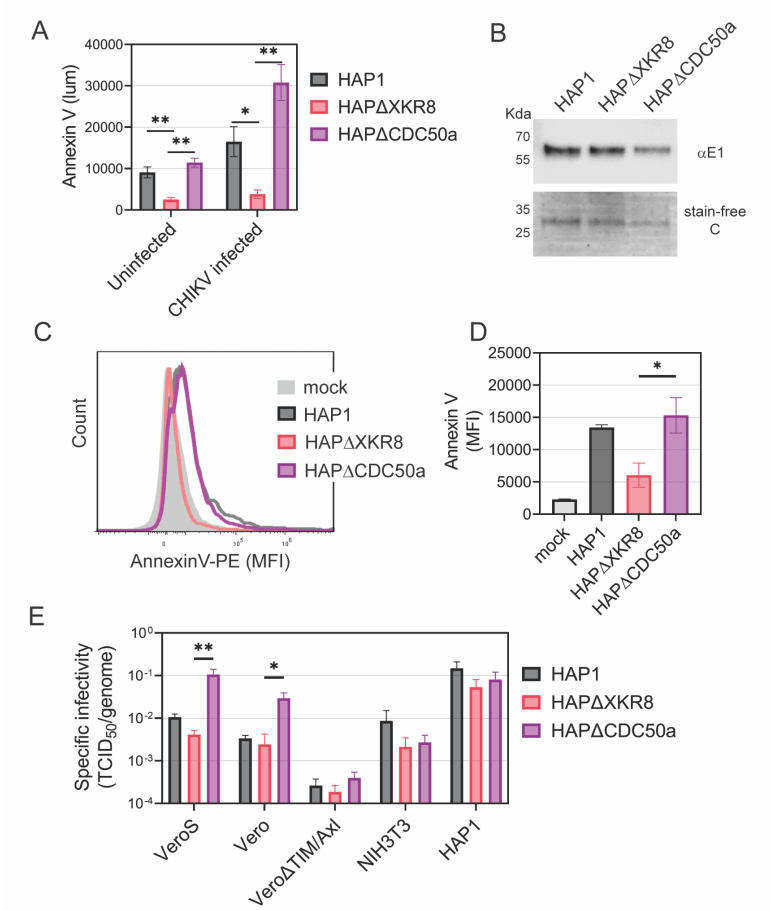

Figure 8. CHIKV virion PS levels correlate with specific infectivity in Vero cells. **(A)** HAP1 cell lines were monitored for Annexin V binding (luminescence) at 24 hrs using a GloMax Explorer microplate reader. Parental, ΔXKR8, and ΔCDC50a cells were either untreated or infected with CHIKV (strain 181/c25, MOI 1). **(B)** CHIKV was

propagated in HAP1 cells and HAP1 cell lines knocked out for scramblases (ΔXKR8) and flippase subunits (ΔCDC50a). Particles were normalized to genome equivalents and examined with immunoblot using a CHIKV E1 antibody and assessed for purity using a stain-free gel. **(C-D)** Annexin V conjugated to PE was used to stain normalized amounts of virus-bound beads and quantified via flow cytometry. A bead-only control (mock) was used to establish a baseline signal. MFI values from three independent trials were normalized to parental values (HAP1) with the mean and ±SEM displayed. An unpaired parametric T-test with Welch's correction was used test for statistical significance between ΔXKR8 and ΔCDC50a conditions. **(E)** The ratio of $TCID_{50}$ to genome copy equivalents for each sample was used to assess the infectivity of particles produced from HAP1 cell lines on a panel of commonly used mammalian cell types (monkey Vero, mouse NIH3T3, and human HAP1). Data are presented as the mean ± SEM from three independent experiments performed in duplicate or triplicates. Infectivity values were natural log (ln) transformed before performing an unpaired parametric student T-test between ΔXKR8 and ΔCDC50a conditions. *, $p < 0.05$; **, $p < 0.01$.

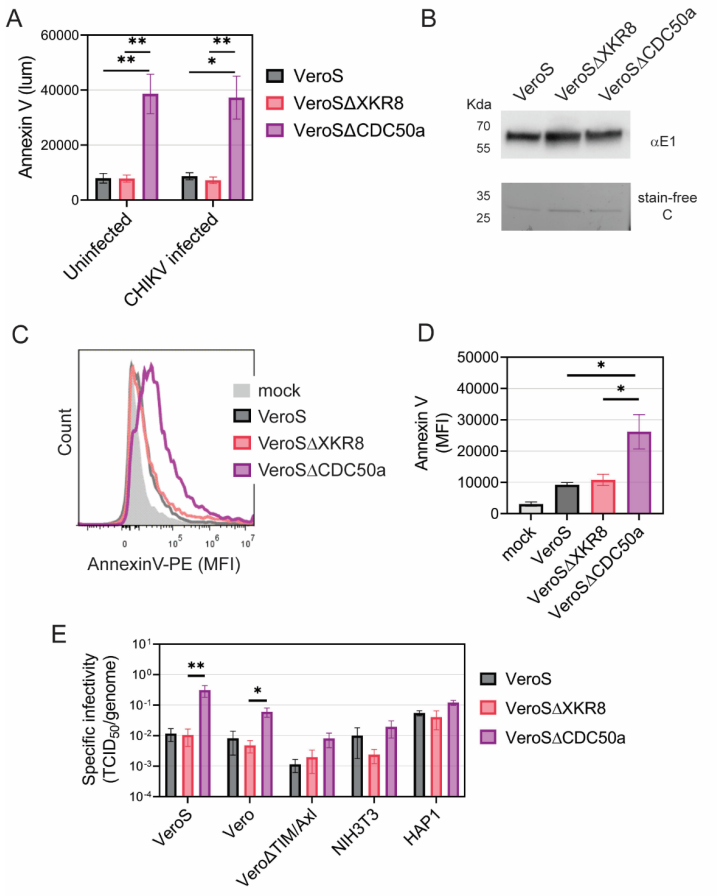

Figure 9. Altering PS levels in CHIKV virion envelope produced in Vero knockout cells recapitulates phenotypes observed with HAP1 cell lines. (A) VeroS cell lines were monitored for Annexin V binding (luminescence) at 24 hrs using a GloMax Explorer microplate reader. Parental, ΔXKR8, and ΔCDC50a cells were either untreated

or infected with CHIKV (strain 181/c25, MOI 1.0). At least three independent replicates were conducted with bars representing the mean and error (±SEM). To quantify levels of externalized PS on the CHIKV viral particle, CHIKV was propagated through the VeroS knockout cell lines. **(B)** Viral inputs were immunoblotted with a CHIKV antibody and assessed for purity using a stain-free gel. **(C-D)** Annexin V conjugated to PE was used to stain normalized amounts of virus-bound beads and quantified via FACs analysis. A bead-only control (mock) was used to establish a baseline signal. MFI values from three independent trials were normalized to parental values (VeroS) with the mean and ±SEM displayed. An unpaired parametric T-test with Welch's correction was used test for statistical significance. **(E)** The ratio of $TCID_{50}$ to particle (genome copy equivalents) for each sample was used to assess the infectivity of particles produced from VeroS cell lines on a panel of mammalian cells (Vero, VeroΔTIM/Axl, NIH3T3, and HAP1). Infectivity values were natural log (ln) transformed prior to performing an unpaired parametric student T-test. At least three independent replicates were conducted with bars representing the mean and error (±SEM).

CHIKV infection of mosquito cell lines is not mediated through PS receptors or heparan sulfate.

The attachment factors promoting CHIKV entry into insect cells are poorly defined. We first evaluated CHIKV infectivity in mosquito cells in the presence of competitors that reduced entry into mammalian cell lines. Mosquitoes do not have a Mxra8 orthologue (17,27), therefore, we did not assess that antibody competition. As anticipated, CHIKV-neutralizing antibodies blocked replication in *Ae. albopictus* (C6/36) and *Ae. aegypti* (Aag2) cells **(Figure 10A)**. Addition of heparan sulfate did not affect CHIKV infection in C6/36 cells but, interestingly, caused an increase in infection in Aag2 cells **(Figure 10B)**. Neither PS-containing nor PC-only liposomes altered CHIKV infection in mosquito cells **(Figures 10C and D)**, and modulation of viral envelope PS levels did not significantly affect particle infectivity **(Figure 10E, Figure 11)**. Together, these data suggest CHIKV infection in mosquito cells does not occur through PSRs or heparan sulfate.

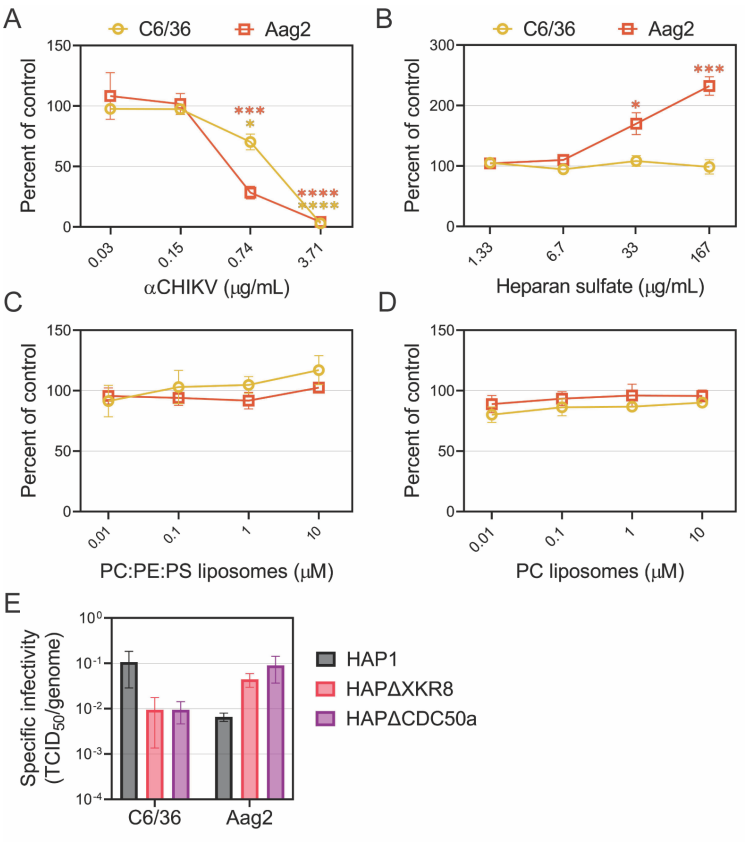

Figure 10. CHIKV infection in mosquito cells is not inhibited by the addition of heparan sulfate or liposomes. CHIKV stocks were used to assess the ability of **(A)** CHIKV antibody **(B)** heparan sulfate, **(C)** PS-containing liposomes (75% PC: 20% PE: 5% PS) and **(D)** PC-only liposomes to block infections into either C6/36 or Aag2 mosquito cells at the indicated concentrations. **(E)** The ratio of $TCID_{50}$ to genome copy equivalents for each sample was used to assess the infectivity of particles produced from HAP1 cell lines on mosquito C6/36 and Aag2 cells. Infectivity values were natural log (ln) transformed prior to performing an unpaired parametric student T-test between ΔXKR8 and ΔCDC50a conditions. Data are presented as the mean ± SEM from at least three independent experiments performed in triplicate. *, $p < 0.05$; ***, $p < 0.001$; ****, $p < 0.0001$.

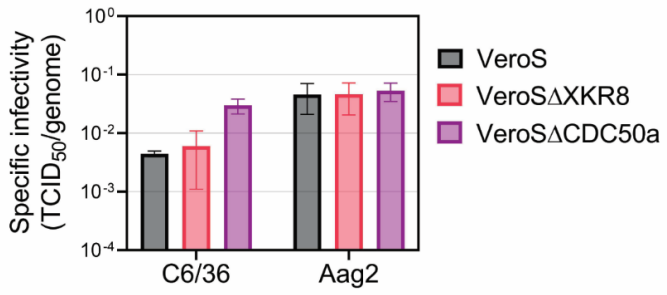

Figure 11. Modulation of viral envelope PS levels does not alter the infectivity of CHIKV in mosquito cells. The ratio of $TCID_{50}$ to particle (genome copy equivalents) for

each sample was used to assess the infectivity of particles produced from VeroS cell lines on a panel of mosquito cells (C6/36 and Aag2). Infectivity values were natural log (ln) transformed prior to performing an unpaired parametric student T-test. At least three independent replicates were conducted with bars representing the mean and error (±SEM).

To determine if carbohydrates on the viral particle influence CHIKV infection, we treated CHIKV particles with either PNGase F, an enzyme that cleaves N-linked glycosylations, or heparinase II which cleaves heparin and heparan sulfate. Treatment with PNGase F resulted in approximately half of the E1 protein migrating faster on the SDS-PAGE gel, suggesting removal of some of the N-linked glycans **(Figure 12A)**. Heparinase II treatment did not result in an observable shift in E1 migration, but because only the terminal sugar moieties would have been removed it was not predicted to significantly alter gel migration. We observed a slight increase (~45%) in infection of PNGase-treated particles into C6/36 cells (p=0.052) but it did not significantly alter infectivity in Vero, HAP1, or Aag2 cells **(Figure 12B)**. Treatment with heparinase did not affect infection of CHIKV in any of the cell lines **(Figure 12B)**.

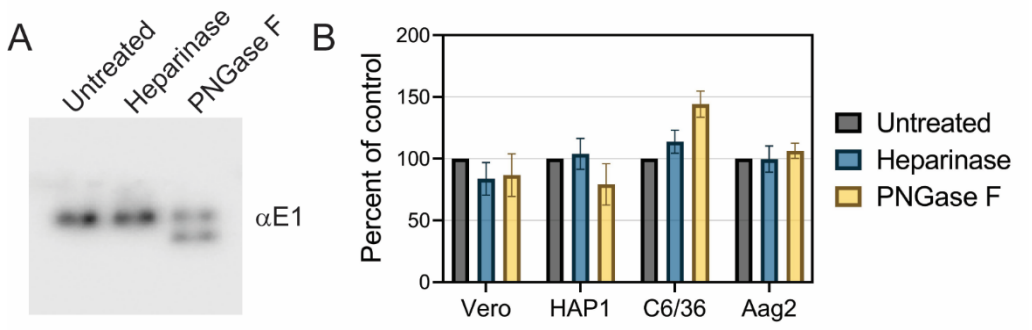

Figure 12. CHIKV infection of mosquito cells is not affected by the loss of N-linked glycans or glycosaminoglycans. CHIKV-Nluc virions were treated with either PNGase F, Heparinase, or untreated. Treated and untreated virions were **(A)** immunoblotted with an antibody against CHIKV E1 glycoprotein or **(B)** used for infection of Vero, HAP1, C6/36, and Aag2. At 24hpi cells were lysed with NanoGlo substrate and lysates were quantified with a GloMax Explorer. Data are presented as the mean ± SEM

from three independent experiments performed in triplicate. Unpaired parametric Student's T-test with unequal variance (Welch's correction) was performed to determine statistical significance compared to a no-treatment control.

Mosquito cells are sensitive to sodium azide causing inhibition of virus infection.

Previous studies suggested CHIKV entry into mosquito cell lines is mediated through heat shock cognate 70 protein (HSC70) and ATP synthase β (ATPSβ) (46,47). To confirm these findings, we performed competition assays with antibodies against these proteins in C6/36, Aag2, and Vero cells. The addition of an HSC70 antibody inhibited CHIKV infection in C6/36 and Aag2 cells in a dose-dependent manner but did not alter infection in Vero cells **(Figure 13A)**. However, competition with several negative control antibodies that were either nonspecific (IgG2a) or random (XKR8), also decreased CHIKV infection in mosquito cells **(Figures 13B and Figure 14A)**. We did not observe inhibition with addition of antibodies targeting ATPSβ **(Figure 13C)**. Upon careful inspection of the composition of the antibodies utilized, we observed a correlation between the amount of sodium azide (NaN_3) preservative and the degree of CHIKV inhibition **(Table 1)**. The highest level of NaN_3 was present in the IgG2a antibody while the ATPSβ antibody did not contain any NaN_3. To determine if the inhibition previously observed was due to the level of NaN_3 present during infection, we performed additional experiments adding either only NaN_3 or an additional negative control antibody that lacks NaN_3 (αEBOV) **(Figures 13D and Figure 14B)**. Congruent with the αATPSβ lacking NaN_3, we did not see any inhibition of CHIKV infection in the presence of the EBOV antibody. In contrast, the addition of NaN_3 alone, at concentrations reflective of its use as an antibody preservative, inhibited CHIKV infection in mosquito cells but not in Vero cells **(Figure 13D)**. We assesses the effect of

the same concentration s of sodium azide in the cell viability of C6/36 and Aag2 cells by measuring the ATP levels **(Figure 13E)** or the reducing potential of the cells **(Figure 13F).** We observed a decreased in cell viability at high concentrations of NaN_3. These data suggest that the inhibition previously observed in C6/36 and Aag2 cells was due to the presence of NaN_3 preservative in commercially available antibodies.

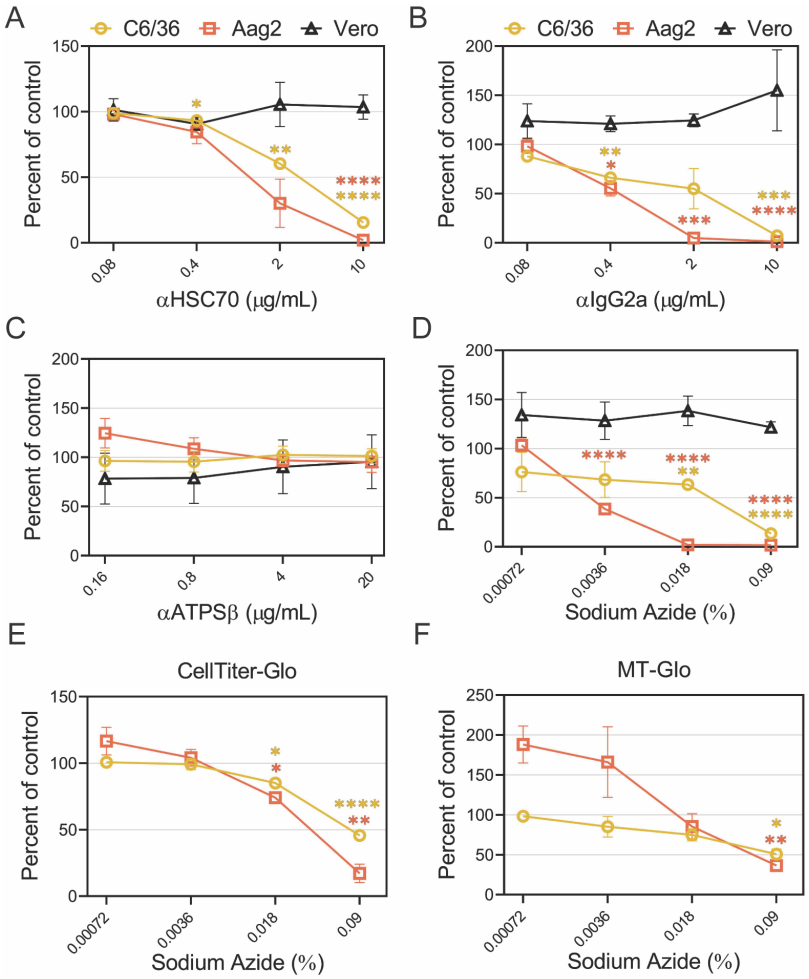

Figure 13. Sodium azide preservatives cause inhibition of CHIKV production in mosquito cells. CHIKV-Nluc stocks were used to assess the ability of **(A)** HSC70, **(B)** IgG2a, **(C)** ATPSβ, or (**D**) sodium azide only to block infections into either C6/36, Aag2, or Vero cells at the indicated concentrations. Twenty-four hours following infection the cells were lysed with NanoGlo substrate and lysates were quantified with a GloMax Explorer. Cell viability of infected C6/36 and Aag2 cells was determined after treatment with sodium azide or PBS as control by measuring ATP levels **(E)** or reducing potential of the cells **(F)**. Twenty-four hours following infection the cells were lysed with Cell Titer Glo or RealTime-Glo MT, respectively, and quantified with a GloMax Explorer. Data are

presented as the mean ± SEM from at least three independent experiments performed in duplicate. Unpaired parametric Student's T-test with Welch's correction was performed to determine statistical significance compared to a no-treatment control. *, $p < 0.05$; ***, $p < 0.001$; ****, $p < 0.0001$.

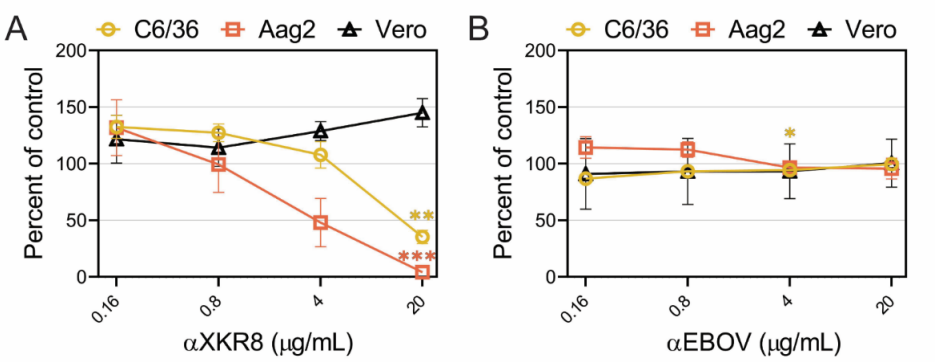

Figure 14. Sodium azide inhibits CHIKV infection in mosquito cell lines. CHIKV-Nluc stocks were used to assess the ability of **(A)** XKR8 or **(B)** EBOV antibodies to block infections into either C6/36, Aag2, or Vero cells at the indicated concentrations. Twenty-four hours following infection the cells were lysed with NanoGlo substrate and lysates were quantified with a GloMax Explorer. Data are presented as the mean ± SEM from at least three independent experiments performed in duplicate. Unpaired parametric Student's T-test with Welch's correction was performed to determine statistical significance compared to a no-treatment control.*, $p < 0.05$; ***, $p < 0.001$; ****, $p < 0.0001$.

Table 1. Percentage of sodium azide present in antibodies

Antibody	Catalog Number	Sodium Azide (%)
HSC70 monoclonal	Invitrogen, cat. MA3-014	0.05
Mouse IgG2a K Isotype control eBM2a	eBioscience Inc., cat. 14-472481	0.09
XKR8 antibody	ThermoFisher, cat. PA5-65799	0.02
ATP5B pAb	Abnova, cat. H00000506-D01P	0
human EBOV monoclonal KZ52	IBT, cat. 0260-001	0
ATP5B pAb (48)	Santa Cruz Biotech, cat. sc-16690	<0.1
CHIKV polyclonal	IBT, cat. 04-008	0

Vero and Aag2 cells display similar entry efficiency of CHIKV.

Finally, we directly compared the ability of CHIKV virions to enter and spread among all the cell lines evaluated. First, we added CHIKV-GFP to each cell line for two hours, removed the inoculum, and prevented subsequent rounds of infection by adding NH_4Cl to the media. After 18hrs, the number of virally infected cells was enumerated in the flow cytometer. Vero and Aag2 cells displayed the greatest number of CHIKV-infected cells, followed by C6/36 cells **(Figure 15A)**. In contrast, we observed significantly lower numbers of infected HAP1, VeroΔTIM/Axl, NIH3T3, and 293T cells **(Figure 15A)**. Next, we serially diluted the viral inoculum and added it to each cell type to determine the relative viral titer. CHIKV-GFP produced similar $TCID_{50}$ values in HAP, Vero, VeroΔTIM/Axl, C6/36, and Aag2 cell lines, while the same stock displayed a 10-fold lower $TCID_{50}$ value when added to NIH3T3 and 293T cells **(Figure 15B)**. This was a CHIKV specific phenotype, given that titers of VSV-G displayed distinct relative titers in 293T and mosquito cells **(Figure 15C)**.

We utilized recombinant VSV particles encoding its native glycoprotein or CHIKV glycoproteins from either the Asian 181/c25 or East-Central-South-African (ECSA) S27 strains to evaluate strain differences in CHIKV titers among cell lines **(Figure 16 A-B)**. We did not observe any major differences in titer trends between the two CHIKV glycoproteins. Interestingly, while the CHIKV-GFP viral titers were not significantly different when comparing Vero and VeroΔTIM/Axl, both rVSVΔG-181/c25 and rVSVΔG-S27 titers were 10-fold higher in Vero cells than VeroΔTIM/Axl. Further, C6/36 cells were not very permissive to rVSV particles containing its native glycoprotein or the strain-specific glycoprotein from CHIKV **(Figure 15C, Figure 16A-B)**.

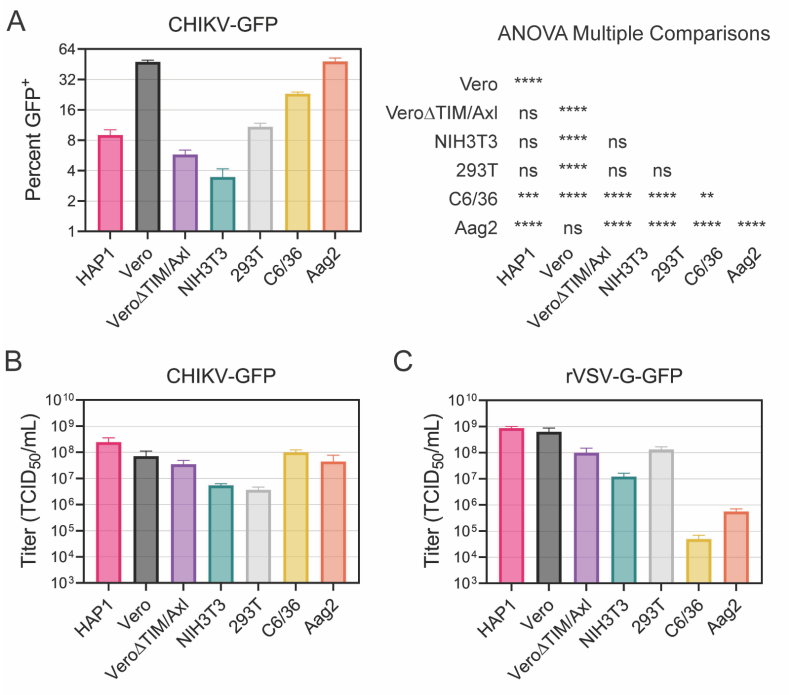

Figure 15. Vero and Aag2 cells display similar entry efficiency of CHIKV. (A) CHIKV-GFP entry among all mammalian and mosquito cell lines used was monitored after one round of replication. Percent of GFP$^+$ cells was determined through flow cytometry. Statistical significance corresponding to entry efficiency was calculated with a multiple comparison ANOVA analysis: *, $p < 0.05$; ***, $p < 0.001$; ****, $p < 0.0001$. Viral stocks of **(B)** CHIKV-GFP 181/c25, **(C)** rVSV-G-GFP were titrated in each mammalian and mosquito cells used. Data are presented as the mean ± SEM from three independent experiments. The results from the ANOVA with multiple comparisons can be found in **Table 2**.

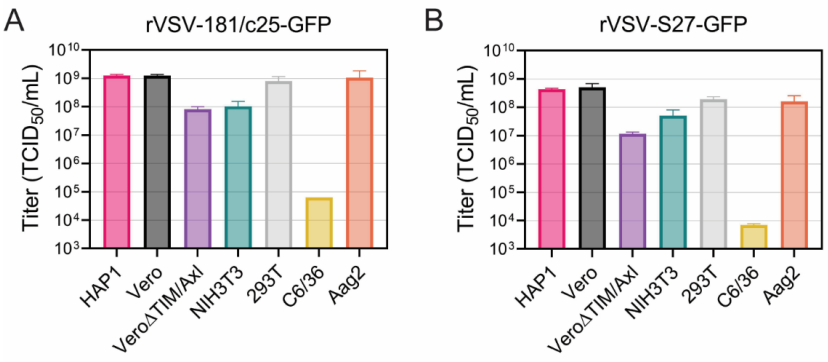

Figure 16. Titers of rVSV particles containing Asian and East-Central-South-African CHIKV envelopes are similar across cell lines. Viral stocks of **(A)** rVSV-181/c25-GFP, **(B)** rVSV-S27-GFP, were titrated in mammalian and mosquito cells used. Data are presented as the mean ± SEM from three independent experiments. The results from the ANOVA with multiple comparisons can be found in Table 2.

Table 2. ANOVA with multiple comparisons for Figure 14B-C and Figure 15

CHIKV-GFP titers				rVSV-G-GFP		
Tukey's multiple comparisons test	**Summary**	**Adjusted P Value**		**Tukey's multiple comparisons test**	**Summary**	**Adjusted P Value**
HAP1 vs. Vero	ns	0.5012		HAP1 vs. Vero	ns	0.9746
HAP1 vs. VeroΔPSR	ns	0.1948		HAP1 vs. VeroΔPSR	**	0.0039
HAP1 vs. NIH3T3	**	0.0021		HAP1 vs. NIH3T3	****	<0.0001
HAP1 vs. 293T	***	0.0006		HAP1 vs. 293T	*	0.0249
HAP1 vs. C6/36	ns	0.9531		HAP1 vs. C6/36	****	<0.0001
HAP1 vs. Aag2	ns	0.0976		HAP1 vs. Aag2	****	<0.0001
Vero vs. VeroΔPSR	ns	0.9966		Vero vs. VeroΔPSR	*	0.0249
Vero vs. NIH3T3	ns	0.0975		Vero vs. NIH3T3	****	<0.0001
Vero vs. 293T	*	0.0278		Vero vs. 293T	ns	0.1441
Vero vs. C6/36	ns	0.9768		Vero vs. C6/36	****	<0.0001
Vero vs. Aag2	ns	0.9523		Vero vs. Aag2	****	<0.0001
VeroΔPSR vs. NIH3T3	ns	0.294		VeroΔPSR vs. NIH3T3	*	0.017
VeroΔPSR vs. 293T	ns	0.0976		VeroΔPSR vs. 293T	ns	0.9746
VeroΔPSR vs. C6/36	ns	0.7359		VeroΔPSR vs. C6/36	****	<0.0001
VeroΔPSR vs. Aag2	ns	0.9999		VeroΔPSR vs. Aag2	****	<0.0001
NIH3T3 vs. 293T	ns	0.9967		NIH3T3 vs. 293T	**	0.0026
NIH3T3 vs. C6/36	*	0.0166		NIH3T3 vs. C6/36	****	<0.0001
NIH3T3 vs. Aag2	ns	0.5005		NIH3T3 vs. Aag2	***	0.0004
293T vs. C6/36	**	0.0045		293T vs. C6/36	****	<0.0001
293T vs. Aag2	ns	0.1947		293T vs. Aag2	****	<0.0001
C6/36 vs. Aag2	ns	0.499		C6/36 vs. Aag2	**	0.0018
rVSVΔG-181/c25-GFP				**rVSVΔG-S27-GFP**		
Tukey's multiple comparisons test	**Summary**	**Adjusted P Value**		**Tukey's multiple comparisons test**	**Summary**	**Adjusted P Value**
HAP1 vs. Vero	ns	>0.9999		HAP1 vs. Vero	ns	>0.9999
HAP1 vs. VeroΔPSR	**	0.0064		HAP1 vs. VeroΔPSR	****	<0.0001
HAP1 vs. NIH3T3	**	0.0064		HAP1 vs. NIH3T3	**	0.003
HAP1 vs. 293T	ns	0.9495		HAP1 vs. 293T	ns	0.6863
HAP1 vs. C6/36	****	<0.0001		HAP1 vs. C6/36	****	<0.0001
HAP1 vs. Aag2	ns	0.8428		HAP1 vs. Aag2	ns	0.2087
Vero vs. VeroΔPSR	**	0.0064		Vero vs. VeroΔPSR	****	<0.0001
Vero vs. NIH3T3	**	0.0064		Vero vs. NIH3T3	**	0.003
Vero vs. 293T	ns	0.95		Vero vs. 293T	ns	0.6856
Vero vs. C6/36	****	<0.0001		Vero vs. C6/36	****	<0.0001
Vero vs. Aag2	ns	0.8439		Vero vs. Aag2	ns	0.2083
VeroΔPSR vs. NIH3T3	ns	>0.9999		VeroΔPSR vs. NIH3T3	ns	0.3642
VeroΔPSR vs. 293T	ns	0.0523		VeroΔPSR vs. 293T	**	0.001
VeroΔPSR vs. C6/36	****	<0.0001		VeroΔPSR vs. C6/36	****	<0.0001
VeroΔPSR vs. Aag2	ns	0.0926		VeroΔPSR vs. Aag2	**	0.0063
NIH3T3 vs. 293T	ns	0.0526		NIH3T3 vs. 293T	ns	0.0791
NIH3T3 vs. C6/36	****	<0.0001		NIH3T3 vs. C6/36	****	<0.0001
NIH3T3 vs. Aag2	ns	0.093		NIH3T3 vs. Aag2	ns	0.3657
293T vs. C6/36	****	<0.0001		293T vs. C6/36	****	<0.0001
293T vs. Aag2	ns	>0.9999		293T vs. Aag2	ns	0.9761
C6/36 vs. Aag2	****	<0.0001		C6/36 vs. Aag2	****	<0.0001

Discussion

Efficient viral replication requires many cellular factors, some of which are involved in viral attachment and entry, and others are required for optimal replication to occur. CHIKV displays a wide cell and species tropism (15,16), suggesting it may utilize ubiquitous host factors that are conserved between the mosquito and mammalian hosts. Although several host factors facilitate CHIKV infection, none have been shown to be essential for productive infection. A ubiquitous attachment mechanism among all CHIKV susceptible cell lines may exist, but its identification has remained elusive. Alternatively, an array of studies on CHIKV entry suggests several disparate molecules, including proteins, carbohydrates, and lipids can mediate particle attachment at the virion-cell interface (17,21,25,27,33,46,47).

In this study, we compared the entry requirements for CHIKV in several mammalian and mosquito cell lines. Each mammalian cell line we examined varied in which attachment factor contributed more prominently to CHIKV infection. Overall, CHIKV infection proceeded most efficiently in the presence of either: HS in HAP1, PSRs in Vero cells, and Mxra8 in NIH3T3. While the majority of CHIKV entry occurred through different attachment factors, additional less efficient routes enabled entry in each cell line. In some cell lines, such as Vero cells, attachment appears highly efficient as additional factors did not further enhance infection. In contrast, CHIKV infection can be significantly enhanced in other cell lines such as HAP1 and 293T cells. Entry into mosquito cells appears to be independent of these mammalian attachment molecules. Additional proteins (*e.g.* C-type Lectins and Prohibitin-1) have been suggested to facilitate CHIKV infection (23,69), which were not examined in this study. Further, on

investigation of previously implicated mosquito cell attachment factors HSC70 and ATPSβ, we discovered that the sodium azide present in many commercial antibodies can block CHIKV infection in commonly used mosquito C6/36 and Aag2 cells.

Relative contribution of each attachment factor in mammalian cells

Mxra8 was found to mediate the entry of CHIKV into NIH3T3 cells by a CRISPR-Cas9 screen (17). While the presence of Mxra8 clearly enhances CHIKV infection in some cells, it is not required for infection in many cell types. CHIKV can infect Mxra8-deficient mice and mosquitoes lacking a Mxra8 orthologue, suggesting other pathways must also be used (17). NIH3T3 cells produce Mxra8 and high levels of HS on their cell surface, but do not produce TIM-1 (21,39,70). CHIKV infection was efficiently blocked with Mxra8 antibodies **(Figure 5D)**, whereas the addition of HS did not significantly alter infection **(Figure 5E)**. This suggests that, in NIH3T3 cells, Mxra8 is more important for entry than HS interactions. NIH3T3 cells were infected relatively poorly compared to the other cell lines **(Figure 15A and B)**. They also displayed lower VSV titers **(Figure 15C)**, suggesting they may be less permissive and prevent viral replication through an innate mechanism.

Like Mxra8, GAG production enhances CHIKV infection (21,33). While NIH3T3, Vero, and HAP1 cells endogenously produce GAGs (21), we found that heparan sulfate only competitively inhibited CHIKV infection in HAP1 cells. HAP1 cells also displayed the highest titers **(Figure 5A, Figure 15B)**, but when the virus was added for a short time period, infection was relatively low, similar to NIH3T3 and VeroΔTIM/Axl cells **(Figure 15A)**. CHIKV entry into HAP1 cells was enhanced with exogenous Mxra8, but not TIM-1 **(Figure 4A)**, suggesting Mxra8 can enhance entry during a short infection

time above the level provided by the naturally produced GAGs. These differences in infection suggest GAGs mediate CHIKV attachment but are inefficient and require additional time to capture viral particles effectively. Similar results are seen with other GAG-utilizing viruses. For example, herpes simplex virus 1 interacts with HS, mediating close contact with the cell and facilitating binding to additional receptors in the cell surface (71,72).

The attenuated CHIKV strain used in this study (181/c25) displays increased GAG dependence compared to circulating pathogenic strains based on interactions with residue 82 on E2 (20,21,33,73,74). The degree of GAG dependence appears to be strain specific (21). Given that we observed PS-dependent entry in Vero cells using a CHIKV strain with strong GAG affinity suggests that endemic strains may either (i) be more reliant on alternative attachment factors and/or (ii) be less infectious in the same context. A recent study found that exogenous production of TIM-1 in 293T increased CHIKV infection with East-Central-South-African (ECSA), West African (WA), and Asian (181/c25) strains (25). Similarly, we did not observe any major differences between the CHIKV 181/c25 and S27 envelopes when titrating the viral stocks in the different cell lines **(Figure 16 A-B)** suggesting that the efficiency of each entry pathway is more dependent on the host cell than the strain of CHIKV.

While Vero cells naturally produce PSRs (*i.e.*, TIM-1 and Axl) (41) and Mxra8, CHIKV entry is highly dependent on TIM-1 **(Figure 5F)** and was unaffected by the addition of Mxra8 antibody **(Figure 5D)**. CHIKV produced the highest level of GFP^+ cells when entering Vero cells and removal of the PSRs significantly decreased entry **(Figure 15A)**. Additionally, virion particle PS levels correlated with specific infectivity when

infecting Vero cells **(Figure 8, Figure 9)** and PS containing liposomes blocked infection. These data suggest TIM-1 and apoptotic mimicry are important for efficient entry into Vero cells. The addition of other attachment factors did not enhance entry in Vero cells **(Figure 4A)**, suggesting Vero cells are efficient at capturing PS-containing cargo. Removal of TIM-1 and Axl from Vero cells renders them less susceptible to CHIKV infection but given enough time, the virus can enter **(Figure 5B)**. Therefore, in the absence of PSRs, the molecular components facilitating virion attachment and entry in Vero cells are sufficient but inefficient.

Viral entry mechanisms into mosquito cells

Transmission of CHIKV to a mosquito vector can occur when a susceptible mosquito ingests blood from a viremic mammalian host. The literature exploring the host factors used by CHIKV to enter mosquito cells is limited. We evaluated the role of the previously identified binding partners during CHIKV infection of *Aedes* C6/36 and Aag2 cells. Neither GAGs nor PS inhibited CHIKV infection in mosquito cells and modulation of envelope PS did not affect the infectivity of the virus **(Figure 10)**. Given the cell line specific effects observed across mammalian cell lines, it should be noted that Aag2 cells are derived from larval homogenates and are not clonal cells.

Previous studies aiming to identify a receptor for CHIKV in mosquito cells suggest HSC70 (46) and ATPSβ (47) may be important entry factors. HSC70 is a chaperone protein that has been associated with many cellular processes including protein translocation, folding, and stabilization (75). ATPSβ is a mitochondrial protein that drives ATP synthesis (76). The proposed role of these proteins in CHIKV infection was previously demonstrated through antibody-mediated inhibition assays. We were

able to obtain the same HSC70 antibody employed in the prior study. Unfortunately, the ATPSβ antibody used previously was no longer available, therefore we purchased another polyclonal antibody that was made using a similar immunogen. While we observed dose-dependent inhibition of CHIKV infection in the presence of the HSC70 antibody, no effect was observed with the ATPSβ antibody **(Figure 13A, C)**. Several control antibodies also displayed inhibition of CHIKV infection **(Figure 13B and Figure 14A)**. Upon careful observation, we noted the inhibition correlated with the level of a commonly added antibody preservative, sodium azide. The ATPSβ antibody used in the previous paper contained NaN_3 as well, which may have produced the inhibitory results. NaN_3 is a highly toxic chemical that prevents proper phosphorylation and cytochrome oxidation. NaN_3 inhibits mitochondrial respiration in C6/36 cells at much lower concentrations than in mammalian cells (77) and efficiently blocked CHIKV replication in mosquito cells **(Figure 13)**. Future studies should carefully consider the composition of reagents when evaluating the role of proteins in mosquito cells. The previous work also used RNAi against ATPSβ or inhibitors against HSC70 which both reduced CHIKV levels (46,47). Reducing the levels/activities of either ATPSβ or HSC70 would be expected to decrease cellular metabolism or protein folding and inadvertently decrease CHIKV replication. Additional studies should follow up the roles of these proteins in CHIKV infection.

The entry factors responsible for CHIKV infection in mosquito cells remain unknown. However, many differences exist between mammalian and mosquito cells that could result in the expression of distinct cellular attachment factors important for CHIKV. For example, differences in protein post-translation modifications between

mammalian and invertebrate cells can contribute to differences in exposed cellular surface glycans (*e.g.,* N-glycosylation) available for attachment. Trimmed glycans produced in the endoplasmic reticulum of vertebrate cells travel to the Golgi where they encounter acetylglucosaminyl-, galactosyl-, and sialyl- transferases that mediate branching events to produce hybrid and complex glycans (78). Mosquito cells do not produce these transferases, creating mostly high-mannose or paucimannose glycans (79,80). We observed a slight increase in infection of C6/36 cells with PNGase-treated CHIKV virions **(Figure 12)**. This suggests that the removal of highly branched N-linked glycans derived from the mammalian host cells might enhance interactions with CHIKV mosquito receptors.

In addition, the plasma membrane of insect cells has a distinct lipid profile from that of mammalian cells (81). Vertebrate cells synthesize cholesterol, one of the main mediators of membrane fluidity (82). The inability of insect cells to *de novo* synthesize cholesterol leads to modulation of the production of other phospholipids (83,84). Insect cells display a two-fold increase in the production of phosphatidylethanolamine (PE) compared to mammalian cells (83). Not only is the amount of this aminophospholipid different, but its distribution in the plasma membrane of insect cells is also altered (81). The plasma membrane of mammalian cells exhibits a characteristic phospholipid asymmetry where PE and phosphatidylserine (PS) are maintained in the inner leaflet (85). These phospholipids are exposed after signaling events that trigger the activation of scramblases. Previous studies have shown that the constitutive activation of XKR scramblases exhibited by arthropod cells leads to a symmetrical distribution of phospholipids in the plasma membrane (81). Thereby increasing the amount of PE

consistently exposed in the exoplasmic leaflet, relative to mammalian cells. Studies evaluating the presence of phospholipid-binding receptors in mosquito cells are limited. Although we did not observe the role of PS-binding receptors in CHIKV entry into mosquito cells **(Figure 10)**, future studies should evaluate other lipid-binding proteins that may mediate CHIKV infection. TIM-1 orthologs have not been found in mosquito cells, but drosophila encodes PSR orthologs, and apoptotic cell clearance via phosphatidylserine exposure is conserved (86).

The potential role of apoptotic mimicry during natural infection

In humans, CHIKV infection is initiated by virion deposition into the skin dermis during the bite of an infectious female mosquito. Fibroblasts, keratinocytes, and resident macrophages support initial CHIKV infection (17,87). Fibroblasts are permissive for CHIKV and the infection appears to be predominately Mxra8-dependent (17). Keratinocytes present in the basal layer of the skin epidermis produce both TIM-1 and Axl (45,88) and are susceptible to CHIKV infection (17). A recent study demonstrated that the keratinocyte cell line, HaCat, produced low levels of Axl along with undetectable levels of TIM-1 and that the addition of TIM-1 increased CHIKV susceptibility and permissivity (25). Thus, keratinocytes may have a larger role in CHIKV infection establishment *in vivo* than previously thought. Macrophages also display PSRs, conferring phagocytic properties of apoptotic body clearance (89–91). PS-rich virions from either infected fibroblasts, keratinocytes, or mosquito inoculation may serve as an ideal target to attach to PSRs on resident macrophages. While macrophage infection via apoptotic mimicry could facilitate CHIKV dissemination *in vivo*, macrophages often are poor producers of CHIKV virus *in vitro* (92).

Understanding the entry requirements for attachment broadens our understanding of the molecular basis for the wide tissue tropism of CHIKV. Several entry pathways may exist through attachment factor binding in isolation or the involvement of cooperative interactions in a concerted binding-internalization process. However, the delineation of CHIKV virus-cell protein interactions leading to particle internalization across multiple cell lines is currently lacking. The complexity of CHIKV entry warrants future screens to adopt creative approaches to identify the host factors necessary for CHIKV infection among cell lines. Viral establishment, dissemination, and the cross-species transmission of CHIKV between mammalian and mosquito hosts are likely influenced by the assortment of cellular attachment factors across cells.

References

1. Powers AM, Brault AC, Tesh RB, Weaver SC. Re-emergence of Chikungunya and O'nyong-nyong viruses: evidence for distinct geographical lineages and distant evolutionary relationships. J Gen Virol. 2000 Feb;81(Pt 2):471–9.

2. Volk SM, Chen R, Tsetsarkin KA, Adams AP, Garcia TI, Sall AA, et al. Genome-scale phylogenetic analyses of chikungunya virus reveal independent emergences of recent epidemics and various evolutionary rates. J Virol. 2010 Jul;84(13):6497–504.

3. Angelini R, Finarelli AC, Angelini P, Po C, Petropulacos K, Silvi G, et al. Chikungunya in north-eastern Italy: a summing up of the outbreak. Euro Surveill. 2007 Nov 22;12(11):E071122 2.

4. Rezza G, Nicoletti L, Angelini R, Romi R, Finarelli AC, Panning M, et al. Infection with chikungunya virus in Italy: an outbreak in a temperate region. Lancet. 2007 Dec 1;370(9602):1840–6.

5. Vega-Rua A, Zouache K, Caro V, Diancourt L, Delaunay P, Grandadam M, et al. High efficiency of temperate Aedes albopictus to transmit chikungunya and dengue viruses in the Southeast of France. PLoS One. 2013;8(3):e59716.

6. Cassadou S, Boucau S, Petit-Sinturel M, Huc P, Leparc-Goffart I, Ledrans M. Emergence of chikungunya fever on the French side of Saint Martin island,

October to December 2013. Euro Surveill Bull Eur Sur Mal Transm Eur Commun Dis Bull. 2014 Apr 3;19(13):20752.

7. Romi R, Severini F, Toma L. Cold acclimation and overwintering of female Aedes albopictus in Roma. J Am Mosq Control Assoc. 2006 Mar;22(1):149–51.

8. Fischer D, Thomas SM, Suk JE, Sudre B, Hess A, Tjaden NB, et al. Climate change effects on Chikungunya transmission in Europe: geospatial analysis of vector's climatic suitability and virus' temperature requirements. Int J Health Geogr. 2013 Nov 12;12:51.

9. Ryan SJ, Carlson CJ, Mordecai EA, Johnson LR. Global expansion and redistribution of Aedes-borne virus transmission risk with climate change. PLoS Negl Trop Dis. 2019 Mar;13(3):e0007213.

10. Simizu B, Yamamoto K, Hashimoto K, Ogata T. Structural proteins of Chikungunya virus. J Virol. 1984 Jul;51(1):254–8.

11. Jose J, Snyder JE, Kuhn RJ. A structural and functional perspective of alphavirus replication and assembly. Future Microbiol. 2009 Sep;4(7):837–56.

12. Voss JE, Vaney MC, Duquerroy S, Vonrhein C, Girard-Blanc C, Crublet E, et al. Glycoprotein organization of Chikungunya virus particles revealed by X-ray crystallography. Nature. 2010 Dec 2;468(7324):709–12.

13. Sun S, Xiang Y, Akahata W, Holdaway H, Pal P, Zhang X, et al. Structural analyses at pseudo atomic resolution of Chikungunya virus and antibodies show mechanisms of neutralization. Elife. 2013 Apr 2;2:e00435.

14. Kielian M. Membrane fusion and the alphavirus life cycle. Adv Virus Res. 1995;45:113–51.

15. Matusali G, Colavita F, Bordi L, Lalle E, Ippolito G, Capobianchi MR, et al. Tropism of the Chikungunya Virus. Viruses. 2019 Feb 20;11(2):E175.

16. Salvador B, Zhou Y, Michault A, Muench MO, Simmons G. Characterization of Chikungunya pseudotyped viruses: Identification of refractory cell lines and demonstration of cellular tropism differences mediated by mutations in E1 glycoprotein. Virology. 2009 Oct;393(1):33–41.

17. Zhang R, Kim AS, Fox JM, Nair S, Basore K, Klimstra WB, et al. Mxra8 is a receptor for multiple arthritogenic alphaviruses. Nature. 2018 May;557(7706):570–4.

18. Tanaka A, Tumkosit U, Nakamura S, Motooka D, Kishishita N, Priengprom T, et al. Genome-Wide Screening Uncovers the Significance of N-Sulfation of Heparan Sulfate as a Host Cell Factor for Chikungunya Virus Infection. J Virol. 2017 Jul 1;91(13).

19. Weber C, Berberich E, von Rhein C, Henss L, Hildt E, Schnierle BS. Identification of Functional Determinants in the Chikungunya Virus E2 Protein. PLoS Negl Trop Dis. 2017 Jan;11(1):e0005318.

20. Sahoo B, Chowdary TK. Conformational changes in Chikungunya virus E2 protein upon heparan sulfate receptor binding explain mechanism of E2-E1 dissociation during viral entry. Biosci Rep. 2019 Jun 28;39(6).

21. McAllister N, Liu Y, Silva LM, Lentscher AJ, Chai W, Wu N, et al. Chikungunya Virus Strains from Each Genetic Clade Bind Sulfated Glycosaminoglycans as Attachment Factors. J Virol. 2020 Nov 23;94(24).

22. Prado Acosta M, Geoghegan EM, Lepenies B, Ruzal S, Kielian M, Martinez MG. Surface (S) Layer Proteins of Lactobacillus acidophilus Block Virus Infection via DC-SIGN Interaction. Front Microbiol. 2019;10:810.

23. Bucardo F, Reyes Y, Morales M, Briceno R, Gonzalez F, Lundkvist A, et al. Genetic polymorphisms in DC-SIGN, TLR3 and TNFa genes and the Lewis-negative phenotype are associated with Chikungunya infection and disease in Nicaragua. J Infect Dis. 2020 Jun 27;

24. Moller-Tank S, Kondratowicz AS, Davey RA, Rennert PD, Maury W. Role of the phosphatidylserine receptor TIM-1 in enveloped-virus entry. J Virol. 2013 Aug;87(15):8327–41.

25. Kirui J, Abidine Y, Lenman A, Islam K, Gwon YD, Lasswitz L, et al. The Phosphatidylserine Receptor TIM-1 Enhances Authentic Chikungunya Virus Cell Entry. Cells. 2021 Jul 20;10(7).

26. Carnec X, Meertens L, Dejarnac O, Perera-Lecoin M, Hafirassou ML, Kitaura J, et al. The Phosphatidylserine and Phosphatidylethanolamine Receptor CD300a Binds Dengue Virus and Enhances Infection. J Virol. 2016 Jan 1;90(1):92–102.

27. Zhang R, Earnest JT, Kim AS, Winkler ES, Desai P, Adams LJ, et al. Expression of the Mxra8 Receptor Promotes Alphavirus Infection and Pathogenesis in Mice and Drosophila. Cell Rep. 2019 Sep 3;28(10):2647-2658 e5.

28. Höök M, Kjellén L, Johansson S, Robinson J. CELL-SURFACE GLYCOSAMINOGLYCANS. Annu Rev Biochem. 1984 Jun;53(1):847–69.

29. Sarrazin S, Lamanna WC, Esko JD. Heparan sulfate proteoglycans. Cold Spring Harb Perspect Biol. 2011 Jul 1;3(7):a004952.

30. Byrnes AP, Griffin DE. Binding of Sindbis Virus to Cell Surface Heparan Sulfate. J Virol. 1998 Sep;72(9):7349–56.

31. Watterson D, Kobe B, Young PR. Residues in domain III of the dengue virus envelope glycoprotein involved in cell-surface glycosaminoglycan binding. J Gen Virol. 2012 Jan 1;93(1):72–82.

32. Shukla D, Liu J, Blaiklock P, Shworak NW, Bai X, Esko JD, et al. A Novel Role for 3-O-Sulfated Heparan Sulfate in Herpes Simplex Virus 1 Entry. Cell. 1999 Oct;99(1):13–22.

33. Silva LA, Khomandiak S, Ashbrook AW, Weller R, Heise MT, Morrison TE, et al. A single-amino-acid polymorphism in Chikungunya virus E2 glycoprotein influences glycosaminoglycan utilization. J Virol. 2014 Mar;88(5):2385–97.

34. Sinnis P, Coppi A, Toida T, Toyoda H, Kinoshita-Toyoda A, Xie J, et al. Mosquito Heparan Sulfate and Its Potential Role in Malaria Infection and Transmission. J Biol Chem. 2007 Aug;282(35):25376–84.

35. Cássaro CM, Dietrich CP. Distribution of sulfated mucopolysaccharides in invertebrates. J Biol Chem. 1977 Apr 10;252(7):2254–61.

36. Nakato H, Li JP. Functions of Heparan Sulfate Proteoglycans in Development: Insights From Drosophila Models. In: International Review of Cell and Molecular Biology [Internet]. Elsevier; 2016 [cited 2022 Oct 25]. p. 275–93. Available from: https://linkinghub.elsevier.com/retrieve/pii/S1937644816300193

37. Dinglasan RR, Alaganan A, Ghosh AK, Saito A, van Kuppevelt TH, Jacobs-Lorena M. *Plasmodium falciparum* ookinetes require mosquito midgut chondroitin sulfate proteoglycans for cell invasion. Proc Natl Acad Sci. 2007 Oct 2;104(40):15882–7.

38. Meertens L, Carnec X, Lecoin MP, Ramdasi R, Guivel-Benhassine F, Lew E, et al. The TIM and TAM families of phosphatidylserine receptors mediate dengue virus entry. Cell Host Microbe. 2012 Oct 18;12(4):544–57.

39. Jemielity S, Wang JJ, Chan YK, Ahmed AA, Li W, Monahan S, et al. TIM-family proteins promote infection of multiple enveloped viruses through virion-associated phosphatidylserine. PLoS Pathog. 2013 Mar;9(3):e1003232.

40. Richard AS, Zhang A, Park SJ, Farzan M, Zong M, Choe H. Virion-associated phosphatidylethanolamine promotes TIM1-mediated infection by Ebola, dengue, and West Nile viruses. Proc Natl Acad Sci U A. 2015 Nov 24;112(47):14682–7.

41. Brouillette RB, Phillips EK, Patel R, Mahauad-Fernandez W, Moller-Tank S, Rogers KJ, et al. TIM-1 Mediates Dystroglycan-Independent Entry of Lassa Virus. J Virol. 2018 Aug 15;92(16).

42. Zhang L, Richard AS, Jackson CB, Ojha A, Choe H. Phosphatidylethanolamine and Phosphatidylserine Synergize To Enhance GAS6/AXL-Mediated Virus Infection and Efferocytosis. J Virol. 2020 Dec 22;95(2).

43. Amara A, Mercer J. Viral apoptotic mimicry. Nat Rev Microbiol. 2015 Aug;13(8):461–9.

44. Shimojima M, Takada A, Ebihara H, Neumann G, Fujioka K, Irimura T, et al. Tyro3 family-mediated cell entry of Ebola and Marburg viruses. J Virol. 2006 Oct;80(20):10109–16.

45. Dejarnac O, Hafirassou ML, Chazal M, Versapuech M, Gaillard J, Perera-Lecoin M, et al. TIM-1 Ubiquitination Mediates Dengue Virus Entry. Cell Rep. 2018 May 8;23(6):1779–93.

46. Ghosh A, Desai A, Ravi V, Narayanappa G, Tyagi BK. Chikungunya Virus Interacts with Heat Shock Cognate 70 Protein to Facilitate Its Entry into Mosquito Cell Line. Intervirology. 2017;60(6):247–62.

47. Fongsaran C, Jirakanwisal K, Kuadkitkan A, Wikan N, Wintachai P, Thepparit C, et al. Involvement of ATP synthase β subunit in chikungunya virus entry into insect cells. Arch Virol. 2014 Dec;159(12):3353–64.

48. Ono N, Tatsuo H, Hidaka Y, Aoki T, Minagawa H, Yanagi Y. Measles Viruses on Throat Swabs from Measles Patients Use Signaling Lymphocytic Activation Molecule (CDw150) but Not CD46 as a Cellular Receptor. J Virol. 2001 May;75(9):4399–401.

49. Ran FA, Hsu PD, Wright J, Agarwala V, Scott DA, Zhang F. Genome engineering using the CRISPR-Cas9 system. Nat Protoc. 2013 Nov;8(11):2281–308.

50. Tsetsarkin K, Higgs S, McGee CE, De Lamballerie X, Charrel RN, Vanlandingham DL. Infectious clones of Chikungunya virus (La Réunion isolate) for vector competence studies. Vector Borne Zoonotic Dis Larchmt N. 2006;6(4):325–37.

51. Ramakrishnan MA. Determination of 50% endpoint titer using a simple formula. World J Virol. 2016 May 12;5(2):85–6.

52. Lay Mendoza MF, Acciani MD, Levit CN, Santa Maria C, Brindley MA. Monitoring Viral Entry in Real-Time Using a Luciferase Recombinant Vesicular Stomatitis Virus Producing SARS-CoV-2, EBOV, LASV, CHIKV, and VSV Glycoproteins. Viruses. 2020 Dec 17;12(12).

53. McCarthy MK, Davenport BJ, Reynoso GV, Lucas ED, May NA, Elmore SA, et al. Chikungunya virus impairs draining lymph node function by inhibiting HEV-mediated lymphocyte recruitment. JCI Insight. 2018 Jul 12;3(13).

54. Acciani MD, Lay Mendoza MF, Havranek KE, Duncan AM, Iyer H, Linn OL, et al. Ebola virus requires phosphatidylserine scrambling activity for efficient budding and optimal infectivity. J Virol. 2021 Jul 28;JVI0116521.

55. Nanbo A, Maruyama J, Imai M, Ujie M, Fujioka Y, Nishide S, et al. Ebola virus requires a host scramblase for externalization of phosphatidylserine on the surface of viral particles. PLoS Pathog. 2018 Jan;14(1):e1006848.

56. Graham FL, Smiley J, Russell WC, Nairn R. Characteristics of a human cell line transformed by DNA from human adenovirus type 5. J Gen Virol. 1977 Jul;36(1):59–74.

57. Roberts GC, Zothner C, Remenyi R, Merits A, Stonehouse NJ, Harris M. Evaluation of a range of mammalian and mosquito cell lines for use in Chikungunya virus research. Sci Rep. 2017 Dec;7(1):14641.

58. Kiesslich S, Kamen AA. Vero cell upstream bioprocess development for the production of viral vectors and vaccines. Biotechnol Adv. 2020 Nov 15;44:107608.

59. Kondratowicz AS, Lennemann NJ, Sinn PL, Davey RA, Hunt CL, Moller-Tank S, et al. T-cell immunoglobulin and mucin domain 1 (TIM-1) is a receptor for Zaire Ebolavirus and Lake Victoria Marburgvirus. Proc Natl Acad Sci U A. 2011 May 17;108(20):8426–31.

60. Lozach PY, Lortat-Jacob H, De Lacroix De Lavalette A, Staropoli I, Foung S, Amara A, et al. DC-SIGN and L-SIGN Are High Affinity Binding Receptors for Hepatitis C Virus Glycoprotein E2. J Biol Chem. 2003 May;278(22):20358–66.

61. Cao W, Henry MD, Borrow P, Yamada H, Elder JH, Ravkov EV, et al. Identification of alpha-dystroglycan as a receptor for lymphocytic choriomeningitis virus and Lassa fever virus. Science. 1998 Dec 11;282(5396):2079–81.

62. Jae LT, Raaben M, Riemersma M, van Beusekom E, Blomen VA, Velds A, et al. Deciphering the glycosylome of dystroglycanopathies using haploid screens for lassa virus entry. Science. 2013 Apr 26;340(6131):479–83.

63. Kunz S, Rojek JM, Kanagawa M, Spiropoulou CF, Barresi R, Campbell KP, et al. Posttranslational modification of alpha-dystroglycan, the cellular receptor for arenaviruses, by the glycosyltransferase LARGE is critical for virus binding. J Virol. 2005 Nov;79(22):14282–96.

64. Alvarez CP, Lasala F, Carrillo J, Muñiz O, Corbí AL, Delgado R. C-type lectins DC-SIGN and L-SIGN mediate cellular entry by Ebola virus in cis and in trans. J Virol. 2002 Jul;76(13):6841–4.

65. Takada A, Fujioka K, Tsuiji M, Morikawa A, Higashi N, Ebihara H, et al. Human macrophage C-type lectin specific for galactose and N-acetylgalactosamine promotes filovirus entry. J Virol. 2004 Mar;78(6):2943–7.

66. Bergelson JM, Cunningham JA, Droguett G, Kurt-Jones EA, Krithivas A, Hong JS, et al. Isolation of a Common Receptor for Coxsackie B Viruses and Adenoviruses 2 and 5. Science. 1997 Feb 28;275(5304):1320–3.

67. Acciani MD, Brindley MA. Scrambled or flipped: 5 facts about how cellular phosphatidylserine localization can mediate viral replication. PLoS Pathog. 2022 Mar;18(3):e1010352.

68. Segawa K, Kurata S, Yanagihashi Y, Brummelkamp TR, Matsuda F, Nagata S. Caspase-mediated cleavage of phospholipid flippase for apoptotic phosphatidylserine exposure. Science. 2014 Jun 6;344(6188):1164–8.

69. Wintachai P, Wikan N, Kuadkitkan A, Jaimipuk T, Ubol S, Pulmanausahakul R, et al. Identification of prohibitin as a Chikungunya virus receptor protein. J Med Virol. 2012 Nov;84(11):1757–70.

70. Kobayashi N, Karisola P, Peña-Cruz V, Dorfman DM, Jinushi M, Umetsu SE, et al. TIM-1 and TIM-4 glycoproteins bind phosphatidylserine and mediate uptake of apoptotic cells. Immunity. 2007 Dec;27(6):927–40.

71. Montgomery RI, Warner MS, Lum BJ, Spear PG. Herpes Simplex Virus-1 Entry into Cells Mediated by a Novel Member of the TNF/NGF Receptor Family. Cell. 1996 Nov;87(3):427–36.

72. Shieh MT, WuDunn D, Montgomery RI, Esko JD, Spear PG. Cell surface receptors for herpes simplex virus are heparan sulfate proteoglycans. J Cell Biol. 1992 Mar;116(5):1273–81.

73. Ashbrook AW, Burrack KS, Silva LA, Montgomery SA, Heise MT, Morrison TE, et al. Residue 82 of the Chikungunya virus E2 attachment protein modulates viral dissemination and arthritis in mice. J Virol. 2014 Nov;88(21):12180–92.

74. Hawman DW, Fox JM, Ashbrook AW, May NA, Schroeder KMS, Torres RM, et al. Pathogenic Chikungunya Virus Evades B Cell Responses to Establish Persistence. Cell Rep. 2016 Aug 2;16(5):1326–38.

75. Bukau B, Horwich AL. The Hsp70 and Hsp60 Chaperone Machines. Cell. 1998 Feb;92(3):351–66.

76. Leyva JA, Bianchet MA, Amzel LM. Understanding ATP synthesis: structure and mechanism of the F1-ATPase (Review). Mol Membr Biol. 2003 Jan;20(1):27–33.

77. Santana-Román ME, Maycotte P, Uribe-Carvajal S, Uribe-Alvarez C, Alvarado-Medina N, Khan M, et al. Monitoring Mitochondrial Function in Aedes albopictus C6/36 Cell Line during Dengue Virus Infection. Insects. 2021 Oct 14;12(10):934.

78. Turco SJ, Robbins PW. SYNTHESIS AND FUNCTION OF CARBOHYDRATE UNITS OF CELL SURFACE GLYCOPROTEINS. Ann N Y Acad Sci. 1978 Jun;312(1 Fibroblast Su):392–8.

79. Butters TD, Hughes RC, Vischer P. Steps in the biosynthesis of mosquito cell membrane glycoproteins and the effects of tunicamycin. Biochim Biophys Acta BBA - Biomembr. 1981 Feb;640(3):672–86.

80. Hsieh P, Robbins PW. Regulation of asparagine-linked oligosaccharide processing. Oligosaccharide processing in Aedes albopictus mosquito cells. J Biol Chem. 1984 Feb 25;259(4):2375–82.

81. Shiomi A, Nagao K, Yokota N, Tsuchiya M, Kato U, Juni N, et al. Extreme deformability of insect cell membranes is governed by phospholipid scrambling. Cell Rep. 2021 Jun 8;35(10):109219.

82. Yeagle PL. Cholesterol and the cell membrane. Biochim Biophys Acta BBA - Rev Biomembr. 1985 Dec;822(3–4):267–87.

83. Dawaliby R, Trubbia C, Delporte C, Noyon C, Ruysschaert JM, Van Antwerpen P, et al. Phosphatidylethanolamine Is a Key Regulator of Membrane Fluidity in Eukaryotic Cells. J Biol Chem. 2016 Feb 12;291(7):3658–67.

84. O'Neal AJ, Butler LR, Rolandelli A, Gilk SD, Pedra JH. Lipid hijacking: A unifying theme in vector-borne diseases. eLife. 2020 Oct 29;9:e61675.

85. Murate M, Abe M, Kasahara K, Iwabuchi K, Umeda M, Kobayashi T. Transbilayer lipid distribution in nano scale. J Cell Sci. 2015 Jan 1;jcs.163105.

86. van den Eijnde SM, Boshart L, Baehrecke EH, De Zeeuw CI, Reutelingsperger CP, Vermeij-Keers C. Cell surface exposure of phosphatidylserine during apoptosis is phylogenetically conserved. Apoptosis. 1998;3(1):9–16.

87. Bernard E, Hamel R, Neyret A, Ekchariyawat P, Moles JP, Simmons G, et al. Human keratinocytes restrict chikungunya virus replication at a post-fusion step. Virology. 2015 Feb;476:1–10.

88. Bauer T, Zagorska A, Jurkin J, Yasmin N, Koffel R, Richter S, et al. Identification of Axl as a downstream effector of TGF-beta1 during Langerhans cell differentiation and epidermal homeostasis. J Exp Med. 2012 Oct 22;209(11):2033–47.

89. Freeman GJ, Casasnovas JM, Umetsu DT, DeKruyff RH. TIM genes: a family of cell surface phosphatidylserine receptors that regulate innate and adaptive immunity. Immunol Rev. 2010 May;235(1):172–89.

90. Wang Q, Imamura R, Motani K, Kushiyama H, Nagata S, Suda T. Pyroptotic cells externalize eat-me and release find-me signals and are efficiently engulfed by macrophages. Int Immunol. 2013 Jun;25(6):363–72.

91. Pietkiewicz S, Schmidt JH, Lavrik IN. Quantification of apoptosis and necroptosis at the single cell level by a combination of Imaging Flow Cytometry with classical Annexin V/propidium iodide staining. J Immunol Methods. 2015 Aug;423:99–103.

92. Sourisseau M, Schilte C, Casartelli N, Trouillet C, Guivel-Benhassine F, Rudnicka D, et al. Characterization of reemerging chikungunya virus. PLoS Pathog. 2007 Jun;3(6):e89.

CHAPTER 4

CHIKUNGUNYA VIRUS RELEASE IS REDUCED BY TIM-1 RECEPTORS THROUGH BINDING OF ENVELOPE PHOSPHATIDYLSERINE[2]

[2] Reyes Ballista, J.M., Hoover, A.J., Noble, J.T., Acciani, M.D., Miazgowicz, K.L., Harrison, S.A., Tabscott, G.A.L., Duncan, A.M., Barnes, D.N., Jimenez, A.R. and Brindley, M.A., 2024. Chikungunya Virus Release is Reduced by TIM-1 Receptors Through Binding of Envelope Phosphatidylserine. Accepted by the Journal of Virology. Reprinted here with permission of publisher.

Abstract

T-cell immunoglobin and mucin domain protein-1 (TIM-1) mediates entry of chikungunya virus (CHIKV) into some mammalian cells through the interaction with envelope phospholipids. While this interaction enhances entry, TIM-1 has been shown to tether newly formed HIV and Ebola virus particles, limiting their efficient release. In this study, we investigate the ability of surface receptors such as TIM-1 to sequester newly budded virions on the surface of infected cells. We established a luminescence reporter system to produce chikungunya viral particles that integrate nano-luciferase and easily quantify viral particles. We found that TIM-1 on the surface of host cells significantly reduced CHIKV release efficiency in comparison to other entry factors. Removal of cell surface TIM-1 through direct cellular knock-out or altering the cellular lipid distribution enhanced CHIKV release. Over the course of infection, CHIKV was able to counteract the tethering effect by gradually decreasing the surface levels of TIM-1 in a process mediated by the nonstructural protein 2. This study highlights the importance of phosphatidylserine receptors in mediating not only the entry of CHIKV but also its release and could aid in developing cell lines capable of enhanced vaccine production.

Importance

Chikungunya virus (CHIKV) is an enveloped alphavirus transmitted by the bites of infectious mosquitoes. Infection with CHIKV results in the development of fever, joint pain, and arthralgia that can become chronic and last for months after infection. Prevention of this disease is still highly focused on vector control strategies. In

December 2023, a new live attenuated vaccine against CHIKV was approved by the FDA. We aimed to study the cellular factors involved in CHIKV release, to better understand CHIKV's ability to efficiently infect and spread among a wide variety of cell lines. We found that TIM-1 receptors can significantly abrogate CHIKV's ability to efficiently exit infected cells. This information can be beneficial for maximizing viral particle production in laboratory settings and during vaccine manufacturing.

Introduction

Chikungunya virus (CHIKV) is an enveloped positive-sense RNA virus from the *Togaviridae* family. Within the alphavirus genus, CHIKV causes the most human infections and is transmitted by the bites of infectious *Aedes aegypti* and *Aedes albopictus* mosquitoes (1). Chikungunya disease presents with fever, joint pain, stiffness, and arthralgia with some patients experiencing severe joint pain for months after infection. During outbreaks, efforts to slow transmission and spread focused on decreasing the mosquito vector populations. In December 2023, the FDA approved a new live attenuated vaccine for the prevention of CHIKV which will hopefully aid in slowing future outbreaks. We still lack antivirals to treat CHIKV infection, therefore, identifying important factors of CHIKV replication cycle may provide new targets for the development of new therapeutics.

Chikungunya virus encodes four non-structural proteins (nsP1-nsP4) and five structural and accessory proteins (C, E3, E2, 6k, TF, and E1). While the non-structural proteins are responsible for transcription and genome replication, the structural proteins assemble to form particles. CHIKV particles are composed of a nucleocapsid core

comprised of the RNA genome and capsid proteins, surrounded by a lipid envelope studded with glycoproteins (2). Structural studies observed the envelope E1-E2 spikes organized in a hexagonal lattice at the plasma membrane, the site of virus budding (3). As the nucleocapsid buds through the plasma membrane, both the capsid and glycoproteins are arranged in icosahedral shells (T=4) (3). Assembly of CHIKV is driven by the interaction of capsid protein and the cytoplasmic tail of the E2 protein (4–7). However, recent studies suggest that accessory proteins 6k and TF may also facilitate efficient exit of Sindbis virus, a closely related alphavirus (8).

While capsid and E2 interactions initiate CHIKV particle budding, subsequent events involving additional cellular proteins may be required for efficient release. Many enveloped viruses utilize the cellular endosomal sorting complexes required for transport (ESCRT) proteins to complete the final membrane scission (9). Once newly formed particles are separated from the plasma membrane, the particles need to escape from the infected cell to perpetuate infection. The interferon-induced transmembrane protein, tetherin/BST-2, is a cellular surface protein that can inhibit the release of enveloped viruses including human immunodeficiency virus (HIV), Ebola, and CHIKV (10–13). Although previous studies have shed light on the mechanisms of alphavirus budding, our knowledge of cellular factors that can alter particle release is limited.

Phosphatidylserine (PS) in the lipid envelope of viral particles influences multiple steps of the viral replication cycle (14). PS is an anionic phospholipid typically found on the inner leaflet of the plasma membrane (15). Apoptotic cells move PS to the outer leaflet which serves as a marker for cell clearance (16). This process is mediated by

flippases, which translocate PS from the outer leaflet to the inner leaflet of the plasma membrane, and scramblases which non-specifically shuffle PS between the leaflets. Viral envelopes rich in PS can enter cells via apoptotic mimicry, where outer leaflet PS in the viral envelope attaches to PS receptors on the surface of the host cells. Our group and others showed that CHIKV entry in certain cell lines (*i.e.,* Vero cells) is mainly mediated through attachment to PS receptors, such as T cell immunoglobulin mucin domain-1 (TIM-1) and receptor tyrosine kinase AXL (AXL) (17–19). Increased levels of PS in CHIKV's outer leaflet enhanced the specific infectivity of particles into Vero cells (17). While PS receptors can aid in virus entry, they can also modulate immune responses and reduce virion release. For example, PS receptors can prevent the efficient release of HIV and Japanese Encephalitis virus (JEV) by attaching to the viral envelope PS in newly budded particles (20, 21). To our knowledge, no previous studies have noted the role of PS receptors in the viral particle release of alphaviruses.

In this study, we aimed to understand the role of PS receptors in the release of CHIKV particles. To facilitate viral quantification, we utilized CHIKV tagged with a nano-luciferase directly integrated into viral particles. We found that cells lacking TIM-1 receptors released more CHIKV particles in comparison to their wildtype counterparts which sequestered particles through TIM-1 interaction. Likewise, cells producing exogenous TIM-1 released fewer particles. The change in particle release was directly attributed to the PS binding domain in TIM-1. Chikungunya infection counteracts this effect by reducing surface TIM-1 levels as infection proceeds. We demonstrate CHIKV nsP2-triggered shutoff of cellular transcription reduces TIM-1 protein levels, suggesting

it plays a role in counteracting TIM-1 in particle release. This study highlights an additional role of PS receptors in the CHIKV replication cycle.

Results

Chikungunya virus exhibits an increased release efficiency in Vero cells lacking PS receptors.

We previously demonstrated that CHIKV entry in Vero cells is facilitated by PS receptors (17). While entry into Vero cells lacking both TIM-1 and AXL (VeroΔTIM/AXL) was inefficient, the amount of virus produced from the cells was higher than expected. For example, when Vero and VeroΔTIM/AXL cells are infected with an equivalent amount of CHIKV particles, viral protein was poorly detected in VeroΔTIM/AXL cell lysates and more readily detected in the supernatant containing released viral particles. **(Figure 17A)**. If VeroΔTIM/AXL cells are infected with ten times more virions, Vero and VeroΔTIM/AXL cells display comparable levels of E1 protein **(Figure 17A)**. We observed more CHIKV E1 protein in the supernatant from VeroΔTIM/AXL than in parental cells and the release efficiency (ratio of protein levels in the supernatants over cell lysates) was increased 4-fold in ΔTIM/AXL cells **(Figure 17A)**. This data suggests that while PS receptors mediate CHIKV entry into Vero cells, they can also decrease particle release.

To more readily quantify CHIKV viral release efficiency, we cloned nano-luciferase (NLuc) to the N-terminus of the E2 glycoprotein as previously described **(Figure 17B)** (22). The recombinant virus contains NLuc in the virion, therefore viral particles can be readily quantified using a standard luminescence assay. Purified

CHIKV particles displayed three proteins (capsid, E1, and E2) and showed an increase of ~20kDa in the E2 protein, corresponding to the NLuc enzyme **(Figure 17C)**. Each particle theoretically incorporates 240 NLuc attached to each E2 molecule in the particle. Similar ratios of capsid:E1:E2 were observed in both the parental and tagged viruses suggesting NLuc incorporation did not impede or alter particle formation **(Figure 17C)**. While tagging the virus reduced CHIKV titers, it did not significantly alter the replication kinetics. Both tagged and untagged virus titers peaked around 48 hours after infection **(Figure 17D)**. When comparing the NLuc levels to infectious titers over time **(Figure 17E)**, we observed a consistent ratio of ~2700±280 RLU/TCID50 U once infection was established (36hpi onward), suggesting consistent luciferase activity is associated with infectious virions.

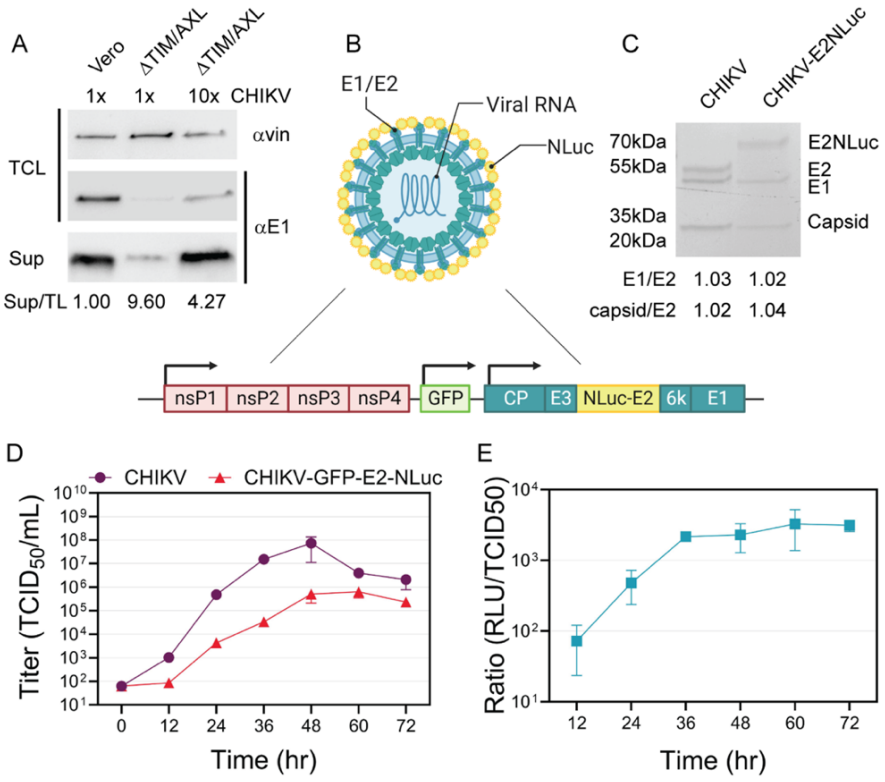

Figure 17. Nano luciferase tag serves as a measure for quantification of CHIKV viral particles. (A) Immunoblot analysis of total lysates and supernatants harvested

from CHIKV-infected Vero and VeroΔTIM/AXL cells at 18 hours post-infection. Cells were infected with CHIKV-GFP at an MOI of 0.5 (1x) or 5 (10x). Total cell lysates and purified supernatants were probed against CHIKV E1 or vinculin as a control. **(B)** Diagram of CHIKV-GFP-E2-NLuc virus genome used for release efficiency assays. Nano luciferase (NLuc) was inserted at the N-terminus of E2. Created in BioRender.com **(C)** Vero cells were infected with either CHIKV-GFP or CHIKV-GFP-E2-NLuc at an MOI of 0.5 and harvested at 18 hours post-infection. Supernatants were purified through ultracentrifugation and analyzed using a stain-free gel. **(D)** Multi-step replication curve of CHIKV and CHIKV-GFP-E2-NLuc in Vero cells (0.01 MOI). Supernatants of infected cells were harvested at each indicated time point. **(E)** Ratio between Relative Luminescence Units (RLU) and TCID50U/mL from supernatant samples harvested in the multi-step replication curve of cells infected with CHIKV-GFP-E2-NLuc. RLUs were calculated as fold over background luminescence levels at 0 hpi. Data represents the mean ±SEM from at least three independent trials.

To further investigate the role of PS receptors on CHIKV viral release, we infected Vero cells knocked out for TIM-1, AXL, or both TIM-1 and AXL with CHIKV-GFP-E2-NLuc. Release efficiency was calculated by determining the ratio between the luciferase activity present in the supernatant to the cell lysate levels relative to the parental Vero cells. We observed that CHIKV particles were 2-3 times more efficiently released in VeroΔTIM and VeroΔTIM/AXL cells than in the parental cell line, while CHIKV release in VeroΔAXL was not significantly different **(Figure 18A)**. Furthermore, CHIKV release efficiency in VeroΔTIM and the double knockout cell line VeroΔTIM/AXL were not significantly different, indicating that there is no synergistic role of TIM-1 and AXL in preventing particle release. We opted to continue further analyses with VeroΔTIM/AXL cells to evaluate the phenotypes in the absence of both PS receptors.

To ensure that the increase in release efficiency was not an artifact from the entry defect observed in cells lacking TIM-1 and AXL **(Figure 18B)**, we adjusted the input virus amount (10x) to ensure similar cell lysate luciferase levels **(Figure 18C-D)**. With similar entry levels, we observed that the ~300% increase in release efficiency was

maintained and variability among trials was reduced **(Figure 18C**). In contrast, the release efficiency of nano luciferase-tagged Vesicular Stomatitis virus, another enveloped virus, was not affected by the lack of PS receptors on the surface of the cells **(Figure 18E-F)**. We further confirmed the phenotype observed for CHIKV by bypassing the viral entry step *via* plasmid transfection of a nano-luciferase tagged structural cassette and assessing the release efficiency of produced virus-like particles (VLPs). CHIKV VLPs release efficiency similarly displayed a 3-fold increase in VeroΔTIM/AXL cells **(Figure 18G-H)**. Together these data indicate that cells lacking TIM release more CHIKV particles.

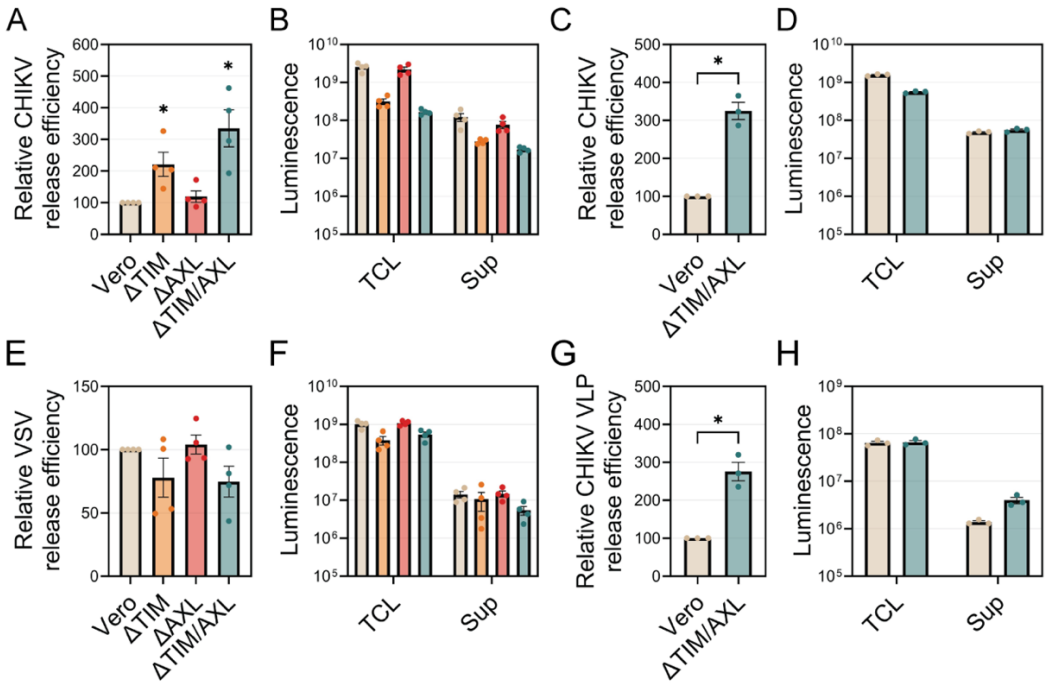

Figure 18. CHIKV particles are released more efficiently from Vero cells lacking TIM-1 receptors. Release efficiency assay of CHIKV-GFP-E2-NLuc in Vero, VeroΔTIM, VeroΔAXL, and VeroΔTIM/AXL cells (MOI 0.5, harvested at 18 hours) **(A)** and corresponding levels of luminescence present in the total cell lysates (TCL) and supernatants (sup) **(B)**. CHIKV release efficiency was calculated by determining the ratio between luminescence in the supernatant over luminescence in the cell lysates. Ratios were normalized to the release efficiency of wildtype counterparts (*i.e.,* Vero cells) to determine the relative release efficiency. Release efficiency assay with VeroΔTIM/AXL cells infected with ten times more CHIKV-GFP-E2-NLuc than Vero cells

(C) and corresponding luminescence levels **(D).** Release efficiency assay of VSV-GFP-M-NLuc in Vero, VeroΔTIM, VeroΔAXL, and VeroΔTIM/AXL cells (MOI of 1, harvested at 8hrs) **(E)** and corresponding luminescence levels **(F).** Release efficiency assay of CHIKV VLPs in Vero and VeroΔTIM/AXL cells transfected with a plasmid encoding CHIKV's structural cassette tagged with nano-luciferase (harvested at 24hrs post-transfection) **(G)** and corresponding luminescence levels **(H).** Data represent the mean ±SEM from at least three independent trials. Unpaired parametric Student's t-test with unequal variance (Welch's correction) was performed to determine statistical significance in comparison to the parental cell line. *, $p < .05$.

PS receptors increase levels of cell-associated virus through binding to envelope PS of budding virions.

Our data in Vero cells suggested that surface TIM-1 limited CHIKV particle release. TIM-1 is an integral membrane protein with a structure comprised of an N-terminal globular domain, a long highly glycosylated stem region, a transmembrane domain, and a cytoplasmic tail. The globular N-terminal domain contains the PS binding site (18, 23, 24). We hypothesized that TIM-1 binding to CHIKV envelope-PS decreases virion release from infected cells. Therefore, we asked if we could promote particle release by saturating TIM-1 with PS-containing liposomes post-virus entry. Fluorescently labeled PC:PE:PS liposomes were added to infected Vero or VeroΔTIM/AXL cells 6 hpi and release efficiency was calculated after 12 hours **(Figure 19A)**. The addition of liposomes was able to saturate the phospholipid-binding receptors in parental Vero cells, causing a dose-dependent increase in release efficiency **(Figure 19B)**. The addition of liposomes did not impact release in cells lacking PS receptors **(Figure 19B)**. Exogenous expression of hTIM-1 in parental Vero cells did not result in significant changes in the release efficiency of CHIKV **(Figure 19C)**. Vero cells naturally produce TIM-1 and transfection is unable to increase cell surface TIM-1 levels further

(17). In contrast, transfection of exogenous hTIM-1 in VeroΔTIM/AXL cells significantly decreased the release efficiency of CHIKV **(Figure 19D)**.

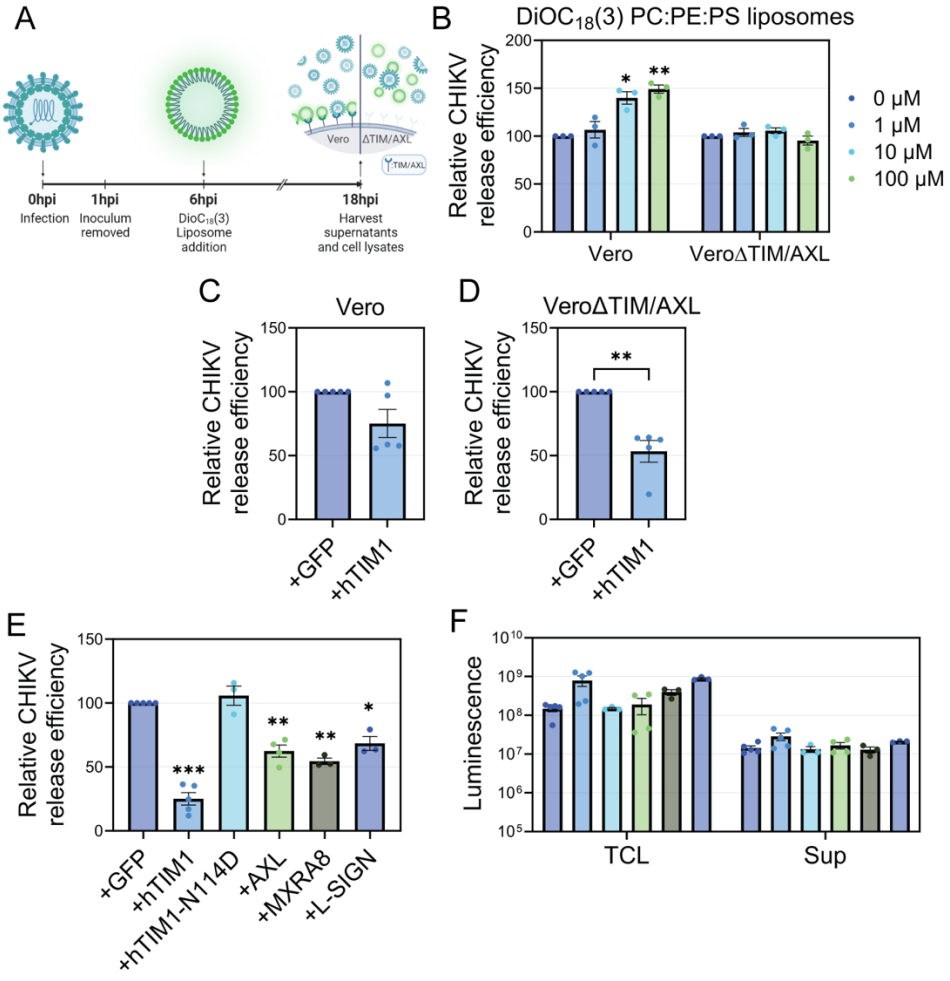

Figure 19. Chikungunya binds to the phospholipid binding domain of TIM-1, preventing its efficient release. (A) Experimental design for fluorescent liposome competition during release of CHIKV-infected Vero and VeroΔTIM/AXL cells. Created in BioRender.com **(B)** Increasing concentrations of fluorescent PC:PE:PS liposomes were added to CHIKV-E2-NLuc infected Vero (0.5 MOI) or VeroΔTIM/AXL (5 MOI) cells 6 hpi and release efficiency was calculated 18hrs post-infection. Data was normalized to the no-liposome control of each cell line to determine the relative release efficiency. Vero **(C)** and VeroΔTIM/AXL **(D)** cells were transfected with a plasmid encoding hTIM-1 and infected with CHIKV-E2-NLuc (0.5 MOI) 24 hours following transfection. Supernatants and cell lysates were harvested and release efficiency was calculated 18hrs post-infection. **(E)** 293T cells were transfected with plasmids encoding the indicated surface receptors and infected with CHIKV-E2-NLuc (0.5 MOI) 24 hours following transfection. Release efficiency was calculated 18hrs post-infection. Data was normalized to the GFP-transfected control to determine the relative release efficiency. **(F)** Corresponding levels of luminescence present in the total cell lysates (TCL) and supernatants (sup).

Data represents the mean ±SEM from at least three independent trials. Unpaired parametric Student's t-test with unequal variance (Welch's correction) was performed to determine statistical significance in comparison to the parental cell line or transfection control. *, $p < .05$; **, $p < .01$; ***, $p < .001$.

Next, we examined viral release in 293T cells producing different molecules known to mediate CHIKV entry into mammalian cells (17, 19, 25, 26). 293T cells do not produce TIM-1, AXL, MXRA8 nor L-SIGN receptors (17, 27). Therefore, cells were transfected with plasmid expression vectors and release efficiency was compared to transfection of a plasmid encoding GFP as a control **(Figure 19E)**. Similar to our previous data (17), production of TIM-1, MXRA8, and L-SIGN increased the entry efficiency of CHIKV as evidenced by the higher cell lysate luciferase activity **(Figure 19F)**. TIM-1 production decreased particle release by ~75%, while AXL, MXRA8, and L-SIGN decreased particle decrease by approximately 50% **(Figure 19E)**. Transfection of a TIM-1 mutant deficient in PS binding (N114D) (18) displayed similar release efficiency as GFP **(Figure 19E)**. These data suggest that CHIKV particle release can be suppressed by the overproduction of multiple entry factors, although TIM-1 was the most efficient.

Cellular knockout of CDC50a flippase subunit displays changes in chikungunya virus entry, replication, and release efficiency.

In our previous study, we produced PS-rich CHIKV particles by knocking out the flippase chaperone CDC50a, which increased outer leaflet PS in the plasma membrane of host cells (17). Unexpectedly, we observed phenotypic differences in CHIKV replication cycle in cells lacking CDC50a (ΔCDC50) that may also indicate enhanced particle release. In this study, we aimed to further investigate the relationship between outer leaflet PS and CHIKV using human haploid (HAP1) and vervet monkey kidney

(VeroS) cells knocked-out for CDC50a (ΔCDC50). CHIKV entered both HAP1 cell lines with similar efficiencies **(Figure 20A)**. Yet, supernatant titers were consistently higher from CHIKV-infected HAP1ΔCDC50 cells than parental HAP1 cells during a multi-step replication curve **(Figure 20B)**. CHIKV virions produced in HAP1ΔCDC50 cells contain higher levels of outer leaflet PS which results in higher particle specific infectivity when titrated on Vero cells (17). To determine if the higher titers observed in HAP1ΔCDC50 cells were all due to the enhanced particle infectivity, we examined the release efficiency from the cells. We observed a mild increase in CHIKV release in HAP1ΔCDC50 cells despite similar luminescence levels in the cell lysates **(Figure 20C)**. This suggests that HAP1ΔCDC50 cells release more particles which are also more infectious when compared to parental HAP1 cells. Next, we evaluated the levels of PS-binding receptors on the surface of HAP1ΔCDC50 cells with a surface biotinylation assay. Interestingly, we observed decreased levels of surface TYRO3 in uninfected HAP1ΔCDC50 cells, which may enhance CHIKV release **(Figure 20D)**. TYRO3 is the only known PS receptor produced in HAP1 cells. However, CHIKV does not rely solely on TYRO3 for entry in HAP1 cells (17), explaining why initial entry was not affected.

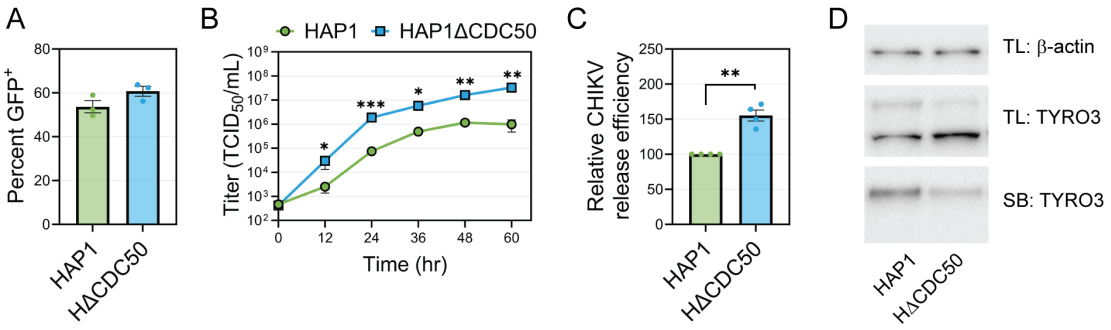

Figure 20. CHIKV displays an increase in release efficiency in HAP1ΔCDC50 cells and a decrease in surface receptor Tyro3. (A) Entry efficiency of CHIKV-GFP in

HAP1 and HAP1ΔCDC50 cells after a single round of infection (harvested at 12 hours). **(B)** Multi-cycle replication curve of CHIKV in HAP1 and HAP1ΔCDC50 cells (0.01 MOI). Supernatants of infected cells were collected at the indicated time points. Titers (TCID50 U/mL) were calculated through serial dilution using the Spearman-Kerber method. **(C)** Release efficiency of CHIKV-GFP-E2-NLuc (0.5 MOI, harvested at 18hrs) in HAP1 and HAP1ΔCDC50. Data was normalized to the release efficiency of the parental cell line to determine the relative release efficiency. **(D)** Surface biotinylation analysis of uninfected HAP1 and HAP1ΔCDC50 cells. Total lysates and surface proteins were probed using a Tyro3 antibody or Actin antibody as a loading control. Data represents the mean ±SEM from at least three independent trials. Unpaired parametric Student's t-test was performed to determine statistical significance in comparison to the parental cell line at each indicated timepoint. An unequal variance (Welch's correction) t-test was performed for normalized data. *, $p < .05$; **, $p < .01$; ***, $p < .001$.

Unlike in HAP1ΔCDC50 cells, CHIKV entry was dramatically decreased in VeroSΔCDC50 cells **(Figure 21A)**. While few CHIKV particles were able to initiate infection in the two-hour entry assay, we were able to detect infection and viral spread when the CHIKV inoculum was not removed **(Figure 21B)**. CHIK virions required an additional 24 hrs in VeroSΔCDC50 cells to obtain a similar number of GFP-positive cells **(Figure 21B)**. Supernatant titers from VeroS cells were higher during the early time points in a multi-cycle replication curve, but by 48 hr CHIKV-infected VeroSΔCDC50 cells produced higher titers than parental VeroS cells **(Figure 21C)**.

A stronger increase in release efficiency was observed in VeroSΔCDC50 cells in comparison to the HAP1ΔCDC50 cells **(Figure 21D-E)**. To overcome the entry defect observed in VeroSΔCDC50 cells, we evaluated the release efficiency after infecting VeroSΔCDC50 with five times more virus than parental cells **(Figure 21F)**. This led to similar levels of luminescence in the cell lysates of parental and VeroSΔCDC50 cells **(Figure 21G)**. VeroS cells lacking CDC50a activity produced 3-4 fold more CHIKV particles than parental VeroS cells **(Figure 21F)**. When bypassing the entry step

through transfection of a structural cassette, we also observed a 2-fold increase in VLP release efficiency **(Figure 21H-I)**. Transfection of a plasmid encoding CDC50a in VeroSΔCDC50 cells significantly decreased the release efficiency of CHIKV **(Figure 21J)**. These data suggest that while CDC50a is important for CHIKV entry into VeroS cells, it also plays a role in particle release.

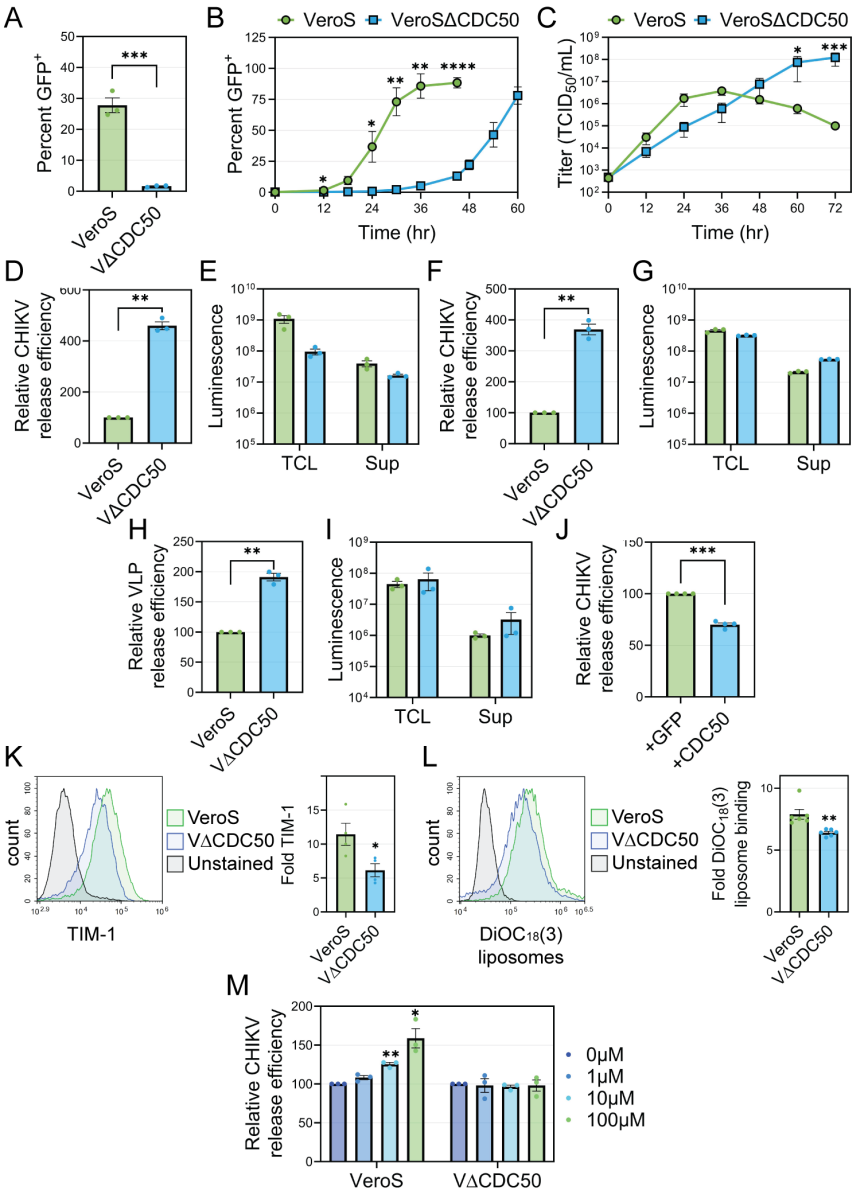

Figure 21. CHIKV entry is reduced, yet release is enhanced in VeroSΔCDC50 cells. **(A)** Entry efficiency of CHIKV-GFP in VeroS and VeroSΔCDC50 cells after one round of replication (harvested at 12hrs). **(B)** CHIKV-GFP viral spread in VeroS and

VeroSΔCDC50 cells. Cells were infected with CHIKV-GFP for one hour (0.1 MOI) and harvested at each indicated time point. Cells positive for infection were quantified using flow cytometry. **(C)** Multi-cycle replication curve CHIKV in VeroS and VeroSΔCDC50 cells (MOI 0.01). Supernatants of infected cells were harvested and titrated at the indicated time points. Release efficiency assay of CHIKV-GFP-E2-NLuc in VeroS and VeroSΔCDC50 cells (MOI 0.5, harvested at 18 hours) **(D)** and corresponding levels of luminescence present in the total cell lysates (TCL) and supernatants (sup) **(E).** Release efficiency was normalized to the parental cell line (*i.e.,* VeroS) to determine the relative release efficiency. Release efficiency assay of CHIKV-GFP-E2-NLuc when five times more virus as added to VeroSΔCDC50 than Vero cells to equalize cell lysate luminescence levels **(F)** and corresponding levels of luminescence present in the total cell lysates (TCL) and supernatants (sup) **(G)**. Release efficiency assay of CHIKV VLPs in VeroS and VeroSΔCDC50 cells transfected with a plasmid encoding CHIKV's structural cassette tagged with nano-luciferase (harvested at 24hrs post-transfection) **(H)** and corresponding luminescence levels **(I)**. **(J)** VeroSΔCDC50 cells were transfected with a plasmid encoding CDC50a and infected with CHIKV-E2-NLuc (0.5 MOI), release efficiency was assessed 18 hours post-infection. TIM-1 surface levels of uninfected VeroS and VeroSΔCDC50a were assessed via fluorescent staining using **(K)** a TIM-1 antibody or **(L)** binding of $DioC_{18}(3)$ fluorescent PC:PE:PS liposomes and analyzed through flow cytometry. Fold TIM-1 and liposome binding were determined by over the mean fluorescent intensity (MFI) of secondary-only or no-liposome control, respectively. **(M)** Increasing concentrations of fluorescent PC:PE:PS liposomes were added to CHIKV-E2-NLuc infected VeroS (0.5 MOI) or VeroSΔCDC50 (2.5 MOI) cells 6 hpi and release efficiency was calculated 18hrs post-infection. Data was normalized to the no-liposome control of each cell line to determine the relative release efficiency. Data represents the mean ±SEM from at least three independent trials. Unpaired parametric Student's t-test was performed to determine statistical significance in comparison to the parental cell line at each indicated timepoint. An unequal variance (Welch's correction) t-test was performed for normalized data. *, $p < .05$; **, $p < .01$; ***, $p < .001$; ****, $p < .0001$.

CHIKV entry into VeroS cells is dependent on TIM-1 (17). Because VeroSΔCDC50 cells display altered PS distribution, we hypothesized that the surface levels of TIM-1, a PS receptor, might be affected. When we examined surface TIM-1 production in uninfected VeroSΔCDC50 cells by surface staining **(Figure 21K)** and binding of fluorescently labeled PC:PE:PS liposomes **(Figure 21L)**, we noted a decrease that may explain both the decrease in CHIKV entry into VeroSΔCDC50 cells and the enhanced CHIKV release phenotype. Further, addition of PC:PE:PS liposomes

post-viral entry was able to saturate PS receptors on parental VeroS cells, leading to a dose-dependent increase in release efficiency **(Figure 21M)**. VeroSΔCDC50 cells did not display any differences in release efficiency with addition of PS-containing liposomes. These results suggest that a cellular lipid redistribution triggered by a knockout of CDC50a can decrease levels of PSRs on the surface of cells, causing an increase in CHIKV release.

CHIKV release efficiency correlates with the presence of phospholipid-binding receptors across cell lines.

To examine the correlation between cell surface PS receptors and release efficiency, we compared a panel of mammalian and mosquito cell lines. For evaluating the presence of phospholipid binding receptors across cell lines without species-specific antibodies, we quantified the cellular binding of fluorescently labeled PC:PE:PS liposomes in uninfected cells through flow cytometry **(Figure 22A-B, Table 3)**. Vero and VeroS cells displayed the highest levels of fluorescent liposome binding. Surprisingly, Aag2 cells displayed liposome binding levels two-fold above background strongly suggesting the presence of PC:PE:PS binding receptors in these cells.

We then assessed CHIKV particle release in each cell line by calculating the ratio between luminescence in the supernatant and the cell lysates of infected cells **(Figure 22C, Table 3)**. Surprisingly, CHIKV displayed the highest levels of release in a baby hamster kidney (BHK) derived cell line, BSR-T7/5. Similar findings were previously evidenced with BHK cells in Ramjag, et al., 2022 (22). We observed an inverse correlation between PC:PE:PS liposome binding and particle release in Vero, VeroS, VeroΔTIM/AXL, Aag2, and BSR-T7/5 cells **(Figure 22D)**. The release efficiency in

mosquito cell lines, C6/36 and Aag2, was similar to that of Vero cells despite not having any identified TIM or AXL homologs. This data further demonstrates the strong effect that levels of phospholipid binding receptors have on the efficient release of CHIKV virions.

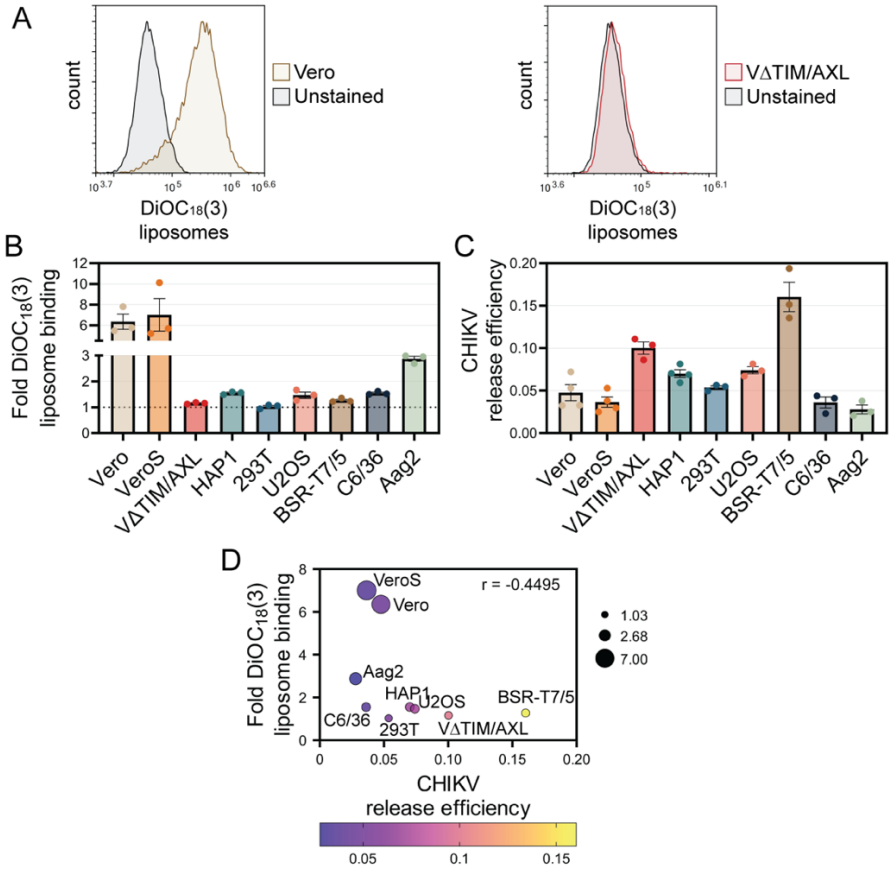

Figure 22. CHIKV release efficiency correlates with PC:PE:PS liposome binding in a panel of cell lines. (A) Representative histograms of binding of fluorescent liposomes in Vero and VeroΔTIM/AXL cells as a measure for phospholipid-binding receptors. **(B)** Fold binding of fluorescent PC:PE:PS liposomes in uninfected mammalian and mosquito cell lines. To remove differences in fluorescent background levels among cell lines, fold binding was determined by calculating the ratio of $DioC_{18}(3)$ mean fluorescent intensity (MFI) over no-liposome control for each cell line. The dotted line represents the threshold where $DioC_{18}(3)$ MFI was equivalent to no-liposome background levels indicating no binding occurred. **(C)** The release efficiency of CHIKV-GFP-E2-NLuc (0.5 MOI, harvested at 18hrs) in a panel of mammalian and mosquito cell lines. **(D)** Correlation analysis between liposome binding and CHIKV release efficiency. The size of circles represents the degree of liposome binding and colors indicate levels of release efficiency. Data represents the mean ±SEM from at least three independent trials.

Table 3. Statistical analysis of liposome binding and release efficiency in mammalian and mosquito cells. Significant differences were determined using an ordinary one-way ANOVA with Tukey's multiple comparisons test. Data represents the mean ±SEM from at least three independent trials. *, p < .05; **, p < .01; ***, p < .001****, p < .0001.

	Vero		VeroS		ΔTIM/AXL		HAP1		293T		C6/36		Aag2		U2OS	
	Fig 6B	Fig 6C	Fig 6B	Fig 6C	Fig 6B	Fig 6C	Fig 6B	Fig 6C	Fig 6B	Fig 6C	Fig 6B	Fig 6C	Fig 6B	Fig 6C	Fig 6B	Fig 6C
VeroS	ns	ns														
ΔTIM/AXL	**	***	***	****												
HAP1	ns	***	ns	****	ns	ns										
293T	ns	***	ns	****	*	ns	ns	ns								
C6/36	ns	***	ns	****	***	ns	ns	ns	ns	ns						
Aag2	ns	*	ns	**	***	ns	*	ns	ns	ns	ns	ns				
U2OS	ns	***	ns	****	ns	ns	ns	ns	ns	ns	ns	ns	*	ns		
BSR-T7/5	****	**	****	****	**	ns	****	ns	****	ns	****	ns	****	ns	****	ns

TIM-1 cell surface levels decrease gradually following CHIKV infection.

To enhance particle release and prevent superinfection, many viruses downregulate viral receptors (28–30). This downregulation can be through receptor saturation and subsequent endocytosis or direct receptor degradation (21, 31). For example, Japanese encephalitis virus (JEV) counteracts AXL's viral release inhibition by inducing AXL degradation through the ubiquitination pathway (21). In contrast, HIV encodes an accessory protein, Nef, which induces the engulfment of TIM-1, reducing TIM-1 protein from the cell surface (31). To examine if TIM-1 levels are changed by CHIKV infection, we infected VeroS cells and monitored TIM-1 levels on the plasma membrane. CHIKV infection significantly decreased TIM-1 levels **(Figure 23A)** and the

ability of cells to bind PC:PE:PS liposomes **(Figure 23B)**. To determine if this decrease was specific to TIM-1 and CHIKV infection, cells were mock infected, infected with CHIKV-GFP, or with Lymphocytic Choriomeningitis virus (LCMV-GFP). Cellular surface proteins were labeled with biotin when 90% of the infected cells were positive for GFP production **(Figure 23C)**. Total cell lysates and purified surface biotinylated proteins were separated on an SDS-PAGE gel and visualized on a BioRad stain-free gel **(Figure 23D)**. We found few differences between mock and infected cells, except for the production of the CHIKV envelope protein which was enriched in the surface fraction **(Figure 23D, Table 4)**. This suggests that CHIKV infection does not cause a global decrease in the production of surface proteins. Yet, immunoblot densitometry analysis displayed an 85% reduction of TIM-1 levels in purified surface proteins, while transferrin and AXL levels decreased by ~40% in CHIKV-infected cells **(Figure 23E)**. Infection with LCMV only decreased TIM-1 and AXL surface levels by ~15% and ~10%, respectively, and increased levels of transferrin by ~40% **(Figure 23E)**.

To further understand the mechanism of surface TIM-1 downregulation we evaluated the timing of this phenotype. Cells were infected with CHIKV at different time points to evaluate TIM-1 and liposome-binding levels throughout infection. No noticeable decreases were observed in cell viability levels of CHIKV-infected cells during the span of 18 hours **(Figure 23F)**. Cell surface TIM-1 levels were first reduced around 6-9hpi, concurring with E1 detection **(Figure 23G)**, and continued to decrease over time. After 12-15hr after infection, we observed a decrease of ~50% in the binding of fluorescently-labeled liposomes **(Figure 23H-I)**.

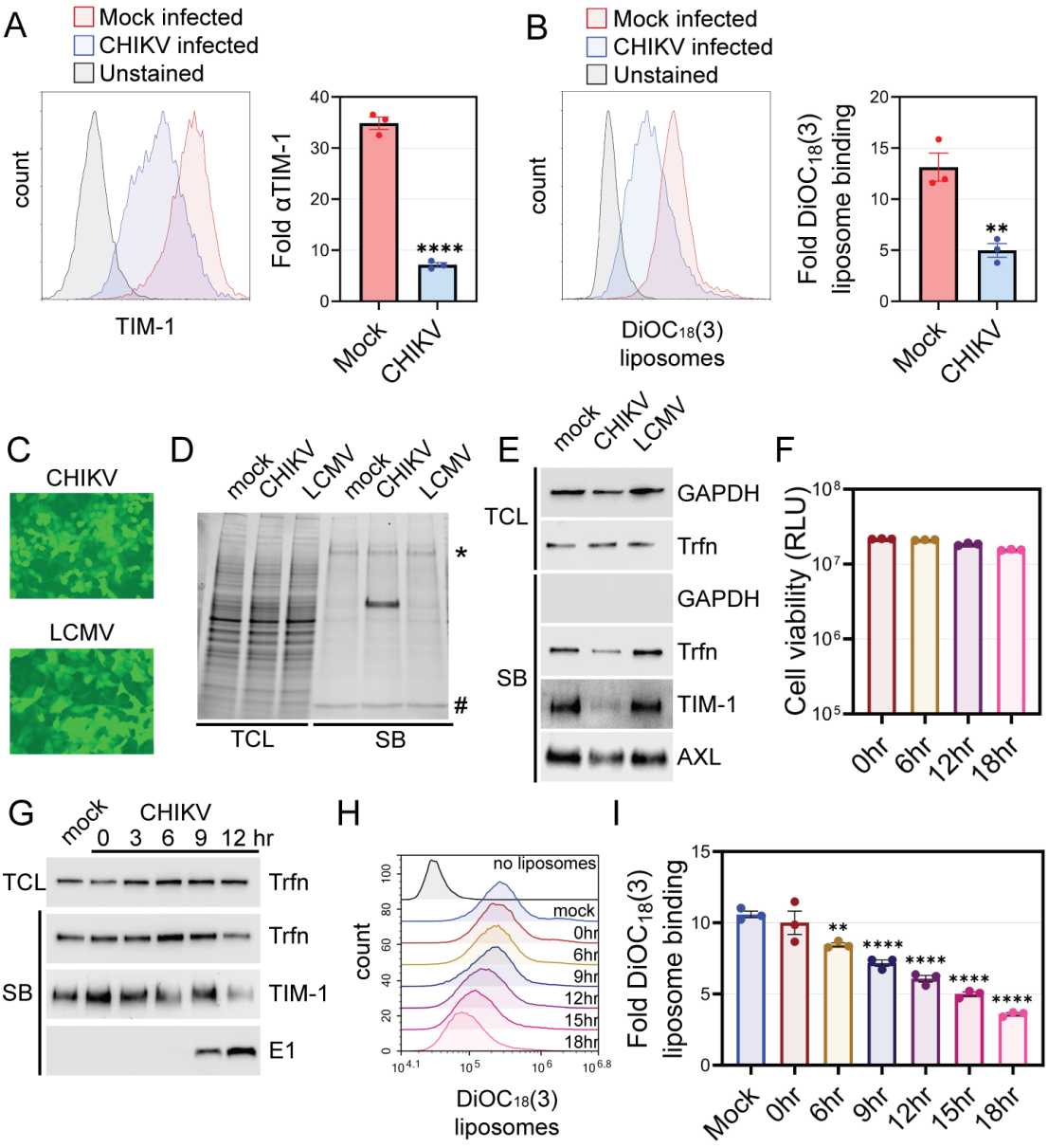

Figure 23. CHIKV infection gradually decreases surface levels of TIM-1. Levels of TIM-1 in the surface of mock-infected or CHIKV-infected VeroS cells (0.5 MOI) were assessed *via* receptor staining using a TIM-1 antibody **(A)** or binding of fluorescently labeled liposomes **(B)** and analyzed through flow cytometry. Fold TIM-1 and liposome binding were determined by over the mean fluorescent intensity (MFI) of secondary-only or no-liposome control, respectively. **(C)** VeroS cells were infected with either CHIKV-GFP (top, 0.5 MOI) or r3LCMV-GFP (bottom, 1 MOI) resulting in similar levels of infection. **(D)** The total protein present in total cell lysates (TCL) and biotinylated surface proteins (SB) of uninfected, CHIKV, and LCMV-infected VeroS cells were compared using a stain-free gel. The intensity of bands denoted with (*) or (#) were quantified using densitometry analysis. **(E)** Immunoblot analysis of samples shown in panel D. Samples were probed using GAPDH, transferrin (Trfn), TIM-1, or AXL antibodies. **(F)** Cell viability analysis of CHIKV-GFP infected cells throughout infection. VeroS cells

were infected with CHIKV-GFP (0.5 MOI) at different time points and harvested simultaneously for luminescent cell viability analysis. **(G)** CHIKV-GFP infected VeroS cells were infected at different time points, and harvested at the same time for surface biotinylation analysis. Infection was maintained for 0, 3, 6, 9 or 12 hours. Samples were probed using TIM-1, E1, or transferrin (Trfn) antibodies. **(H)** VeroS cells were infected with CHIKV at different time points, and subjected to fluorescent liposome binding simultaneously. Infection was maintained for 0, 3, 6, 9, 12, 15, or 18 hours and analyzed through flow cytometry. **(I)** Corresponding quantification of fluorescent PC:PE:PS liposome binding throughout the course of infection. Data represents the mean ±SEM from at least three independent trials. A student t-test (two groups) or an ordinary one-way ANOVA with multiple comparisons (more than two groups) was used to evaluate statistical differences in comparison to control. *, $p < .05$; **, $p < .01$; ****, $p < .0001$.

Table 4. Quantification of surface biotinylation samples of CHIKV-infected cells. Total cell lysate and surface biotinylated proteins of uninfected, CHIKV or LCMV-infected VeroS cells were quantified using densitometry analysis.

	Sample	Total Lane Volume (intensity)	Band (*) Adjusted Volume	Band (#) Adjusted Volume
TOTAL CELL LYSATES	Mock	2.15E+09		
	CHIKV	2.02E+09		
	LCMV	1.96E+09		
SURFACE BIOTINYLATION	Mock	9.88E+08	1.43E+07	2.02E+07
	CHIKV	1.09E+09	1.35E+07	2.19E+07
	LCMV	1.07E+09	1.52E+07	2.83E+07

TIM-1 downregulation is mediated by cellular transcriptional shutoff triggered by nsP2.

To determine if a specific viral protein triggers the decrease in surface TIM-1 levels, we transfected VeroS cells with plasmids encoding each of CHIKV's proteins. We quantified the levels of surface TIM-1 and fluorescent-liposome binding in comparison to the transfection of a control plasmid. CHIKV nsP2 alone triggered a

significant decrease in both surface TIM-1 levels and fluorescent-liposome binding **(Figure 24A-B)**. We did not observe any decreases in cell viability after overexpression of each viral protein **(Figure 24C)**. Although protein levels were variable, immunoblot analysis confirmed the production of each viral protein **(Figure 24D)**. This data suggests that the decrease of TIM-1 in CHIKV-infected cells might be mediated through the activity of the viral protein nsP2.

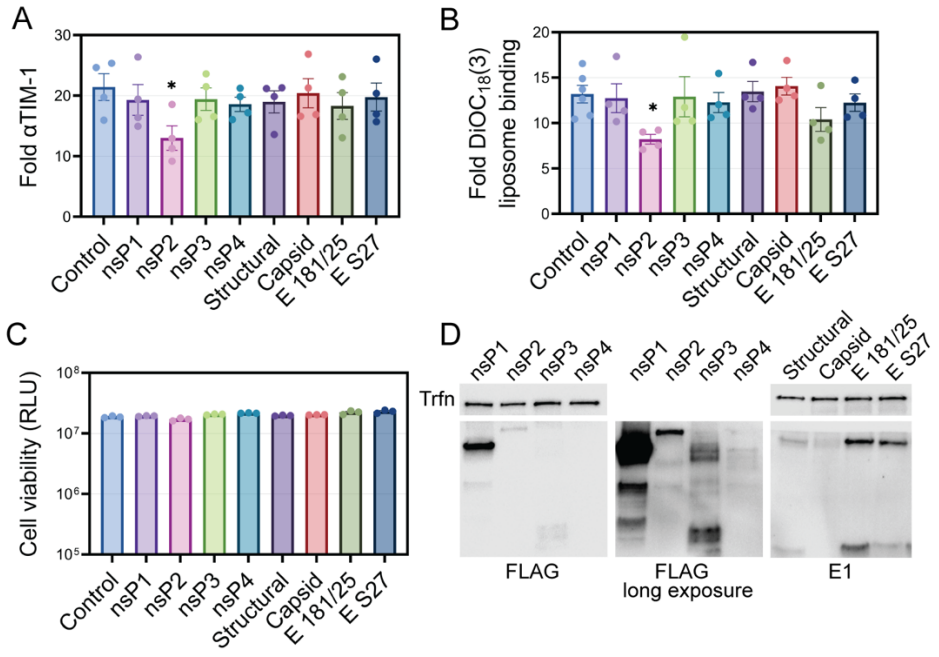

Figure 24. Levels of surface TIM-1 decrease after production of viral protein nsP2. Cells were transfected with expression plasmids encoding CHIKV nonstructural and structural proteins for 48 hours. Surface TIM-1 levels were determined through receptor staining using a TIM-1 antibody **(A)** or binding of fluorescently labeled liposomes **(B)** and analyzed through flow cytometry. Fold TIM-1 and liposome binding were determined over the mean fluorescent intensity (MFI) of secondary-only or no-liposome control, respectively. **(C)** Cell viability analysis was performed in cells transfected with CHIKV's protein-encoding plasmids after 48 hours. **(D)** Exogenous expression of CHIKV non-structural proteins tagged with FLAG tag was analyzed through SDS-PAGE using an antibody against FLAG or transferrin as loading control. nsP1 (~60kDa) was quickly detected in the cell lysates of transfection cells but longer exposure (right) was needed for detection of nsP2 (~90 kDa), nsP3 (~60 kDa), and nsP4 (~70 kDa). Exogenous expression of CHIKV structural proteins was analyzed using an antibody against CHIKV E1 or transferrin as a loading control. Data represents the mean ±SEM from at least three independent trials. An ordinary one-way ANOVA with multiple comparisons was used to evaluate statistical differences in comparison to control. *, $p < .05$.

During infection, nsP2 has been evidenced to translocate to the nucleus of host cells where it can trigger the shutoff of cellular transcription through the polyubiquitination of DNA-dependent RNA polymerase (32). This activity can be depleted by the substitution of amino acids alanine-threonine-leucine at position 674-676 of nsP2 (ATL674NGK) located in the methyltransferase-like domain of the viral protein (33). Additionally, nsP2 displays important protease activity that mediates the cleavage of CHIKV's nonstructural polyprotein allowing for proper replication. A mutation in the cysteine at position 478 to alanine has been evidenced to abolish the protease activity of nsP2 (34). To distinguish if the transcriptional shutoff or protease activity of nsP2 was responsible for the decrease in surface TIM-1 levels, we incorporated these two individual mutations (*i.e.,* ATL674NGK and C478A) in a plasmid encoding nsP2. Transfection of nsP2 bearing the ATL674NGK mutation displayed levels of TIM-1 **(Figure 25A)** and liposome binding **(Figure 25B)** similar to that of transfection of a control plasmid. In contrast, a mutation in the protease activity site (C478A) of nsP2 displayed a similar decrease of TIM-1 and liposome binding as wildtype nsP2. We observed no decrease in the cell viability of transfected cells **(Figure 25C)**. Production of each transfected nsP2-encoding plasmid was confirmed through immunoblot analysis **(Figure 25D)**. These results suggest that the ability of nsP2 to shut off cellular transcription triggers the downregulation of TIM-1 from the surface of cells.

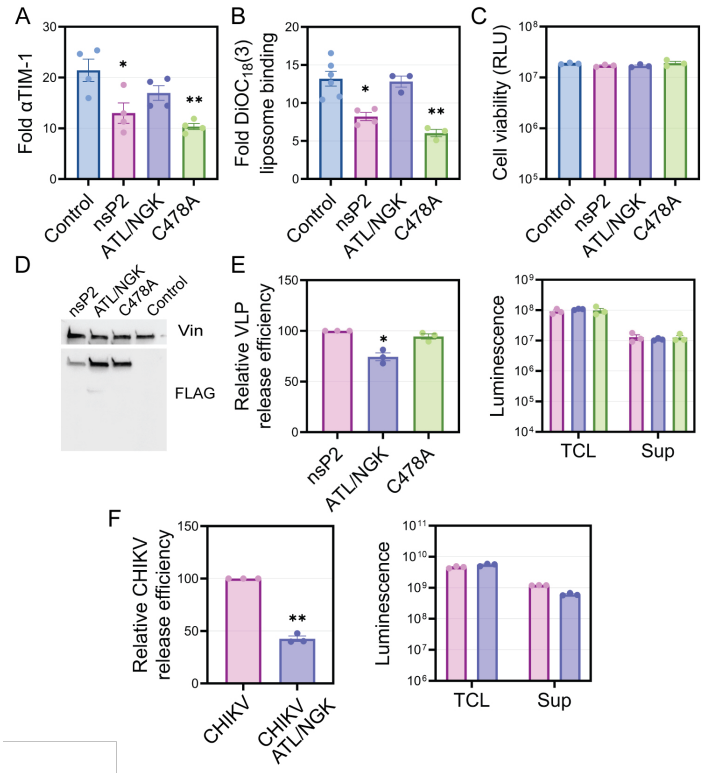

Figure 25. Cellular transcriptional shutoff triggered nsP2 causes a decrease in cell surface TIM-1 levels. Cells were transfected with expression plasmids encoding CHIKV's wildtype nsP2, nsP2 bearing a mutation in amino acid 674 (ATL674NGK) or protease inactive nsP2 with a mutation in amino acid 478 (C478A) for 48 hours. Surface TIM-1 levels were determined through receptor staining using a TIM-1 antibody **(A)** or binding of fluorescently labeled liposomes **(B)** and analyzed through flow cytometry. Fold TIM-1 and liposome binding were calculated over the mean fluorescent intensity (MFI) of secondary-only or no-liposome control, respectively. **(C)** Cell viability analysis was performed in transfected cells 48 hours post-transfection. **(D)** Exogenous expression levels of CHIKV nsP2 (wildtype and mutants ~90kDa) tagged with FLAG tag were analyzed through SDS-PAGE using an antibody against FLAG or vinculin as loading control. **(E)** Release efficiency assay of CHIKV VLPs coupled with exogenous expression of nsP2-encoding plasmids. VeroS cells were transfected with equal amounts of a plasmid encoding CHIKV's structural cassette tagged with nano-luciferase and a plasmid encoding either wildtype nsP2 or each mutant. Samples were harvested at 48hrs post-transfection and release efficiency was normalized relative to the wildtype nsP2 control. **(F)** Corresponding luminescence levels present in the total cell lysates (TCL) and supernatants (sup) are displayed. Release efficiency assay of VeroS cells infected with CHIKV-GFP-E2-NLuc (CHIKV) or CHIKV-GFP-E2-NLuc bearing the ATL674NGK mutation in nsP2 (CHIKV ATL/NGK) at an MOI of 0.5 (harvested 48 hours post-infection) **(G)** and corresponding luminescence levels **(D)**. Data represents the mean ±SEM from at least three independent trials. An ordinary one-way ANOVA with multiple comparisons was used to evaluate statistical differences in comparison to control. An unequal variance (Welch's correction) t-test was performed for normalized data. *, $p < .05$; **, $p < .01$.

Next, we evaluated if the ability of nsP2 ATL674NGK mutation to prevent a decrease in TIM-1 levels was reflected in the release efficiency of CHIKV particles. For this, we evaluated the VLP release efficiency by transfecting a plasmid encoding CHIKV structural cassette along with individual nsP2-encoding plasmids. We observed a significant decrease in the VLP release efficiency when co-transfected with nsP2 ATL674NGK in comparison to the wildtype nsP2 **(Figure 24E-F)**. Transfection of nsP2 C478A displayed similar levels of VLP release efficiency as the wild-type counterpart. We also observed a similar decrease in the release efficiency after infection of CHIKV bearing the nsP2 ATL674NGK **(Figure 24G-H)**. We were unable to evaluate the phenotype of infection with CHIKV bearing the C478A mutation since protease activity is required for virus replication. Overall, these results suggest that nsP2 downregulation of TIM-1 causes an increase in CHIKV release efficiency which can be hindered by an nsP2 ATL674NGK mutation.

Discussion

Our study provides evidence that surface receptors can prevent efficient CHIKV viral release. TIM-1 appeared to be more effective than TAM family receptors (*i.e.,* AXL) and other entry factors (*i.e.,* MXRA8 or L-SIGN) at preventing virions from completing their egress from infected cells. We propose that the release inhibition observed in Vero cells is mediated through the interaction between the PS-binding domain of TIM-1 and the lipid envelope surrounding CHIKV particles **(Figure 26)**. CHIKV entry is efficiently mediated by different molecules depending on the cell line (17). Presumably, these same factors that mediate entry can also capture newly formed particles, ultimately

reducing release. When various entry factors were transfected into 293T cells we observed they each reduced release, and TIM-1 was most effective. While most of the work presented here focused on Vero cells and TIM-1, the main entry receptor for CHIKV in these cells, we hypothesize removal of entry receptors important to other cell types would also enhance CHIKV release.

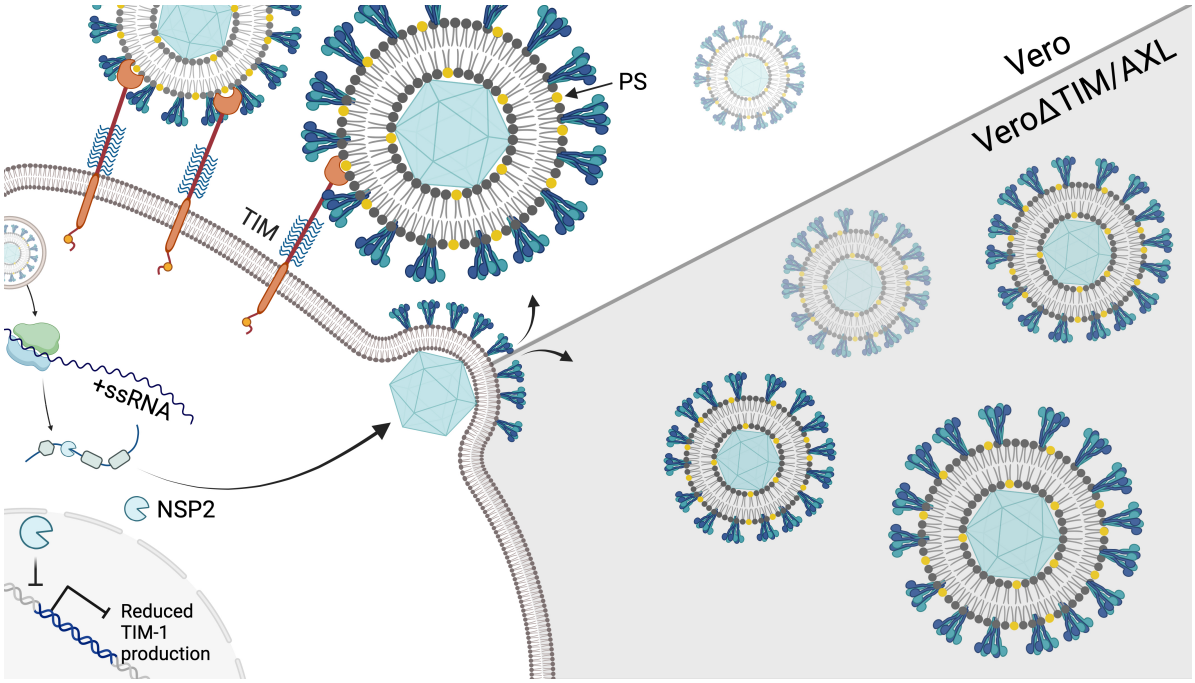

Figure 26. CHIKV release is decreased by TIM-1 binding to envelope PS but counteracted by nsP2-triggered cellular transcriptional shutoff. Diagram of mechanistic model displaying budding virions attached to TIM-1 in Vero cells and being released efficiently from VeroΔTIM/AXL cells. Nonstructural protein 2 (nsp2) decreases levels of TIM-1 over time by triggering the shutoff of cellular transcription. Created in BioRender.com

PS receptors from the TIM and TAM families interact with PS differently, which may contribute to phenotypic differences observed in viral release. Receptors from the TAM family, including TYRO3 and AXL, require a bridging ligand known as Gas6 (35). Previous studies demonstrate that this cofactor is present in the fetal bovine serum supplemented in the media of tissue culture cells at concentrations typically required to

bridge cell-PS binding (36). Although our infections took place in serum-containing media, AXL and/or Gas6 levels may not have been sufficient to link newly formed particles to the cell surface as well as TIM-1. CHIKV particles are made up of a highly organized lattice of glycoproteins with limited access to the lipid layer (2). Gas6 may not be able to access CHIKV PS as well as TIM-1, limiting the TAM family's ability to both mediate entry and reduce particle release. While we did not find a role for AXL in limiting CHIKV release in Vero cells, it is important to recognize that AXL can inhibit the release of other viral particles, as is the case for Japanese Encephalitis virus (JEV) (21).

HIV, JEV, and Ebola virus release is limited by PS receptors (20, 21). We found that particle retention by TIM and AXL could significantly reduce CHIKV release, but was not able to significantly reduce Vesicular Stomatitis virus (VSV) release. VSV infection consistently produces higher titers after a single round of infection compared to CHIKV, this may enable VSV to quickly saturate the PS binding sites and produce enough particles that limit the ability to observe a release defect. This phenotype could be general for a wider variety of enveloped viruses and may suggest that viruses that produce fewer virions per cell may be impacted more than viruses that produce larger quantities of particles.

We observed that increased release efficiency correlated with decreases in levels of surface receptors not only in VeroΔTIM/AXL but also in cells knocked out for the flippase subunit CDC50a. Cells knocked out for CDC50a lack flippase activity resulting in increased levels of outer leaflet PS, possibly leading to failure in efficient redistribution of their lipids to accommodate integral proteins. In general, transmembrane proteins (*e.g.,* TIM, AXL, TYRO3) can disrupt fluidity within the plasma

membrane which can trigger changes in the translocation of specific lipids (37). Additionally, the composition of the plasma membrane can prevent the insertion of receptors into the bilayer and induce changes in their topological orientation (37–39). TIM proteins have been shown to preferentially enter the lipid bilayer among unsaturated phospholipids rather than saturated ones (38). Consequently, we hypothesize that ΔCDC50 cells might undergo a redistribution of membrane proteins and a decrease in the proper insertion of these membrane receptors (*i.e.,* TIM-1 and TYRO3), resulting in increased CHIKV release.

CHIKV release efficiency among cell lines is inversely correlated with the presence of phospholipid-binding receptors. We found that the release efficiency of mosquito cells C6/36 and Aag2 was similar to that of Vero cells, which express TIM-1 and AXL receptors. Aag2 cells were able to significantly bind PS-containing liposomes, although previous studies have failed to identify homologs for PS receptors in mosquito cells. Future studies should further explore cellular receptors that might be playing a role in preventing the efficient exit of viral particles in these cells. Mosquito cells display potential budding of alphaviruses from internal membranes such as cytopathic vacuoles (40). It would be interesting if PS receptors or other cellular proteins present in these vacuoles could attach to new virions before they reach the cell surface. This mechanism would not be surprising as viruses such as JEV that bud from the endoplasmic reticulum have been shown to bind to AXL (21).

CHIKV infection decreased cell surface TIM-1 in a mechanism mediated by nsP2. While infection also reduced surface proteins AXL and transferrin, surface TIM-1 levels were more significantly depleted. The CHIKV-induced receptor decrease may not

be specific, but might disproportionally affect surface proteins with shorter half-lives such as TIM-1 (half-life <2hrs) (31). Alphavirus' nsP2 plays many roles in the evasion of the immune system including shutoff of cellular transcription, disrupting IFN responses, and mediating superinfection exclusion in alphaviruses by interfering with the formation of replication complexes of incoming viruses (33, 41–43). Previous studies have provided evidence for a decrease in levels of MHC class 1 molecules from the surface of infected joint fibroblasts triggered by the nsP2 (44). Ware *et al.* (2024), demonstrated that the activity of the methyltransferase-like domain of nsP2 (*i.e.,* amino acids ATL position 674) was responsible for this decrease resulting in the escape of CD8+ T cell immune response. Coupled with our study, this supports the importance of nsP2 activity in mediating the downregulation of surface receptors and its importance in disease pathogenesis.

This study provides evidence for the importance of PS receptors during the egress of CHIKV. The ability of CHIKV to counteract this inhibition through the activity of the methyltransferase domain of nsP2 could result in more efficient disease spread and immune evasion inside the host. Viruses that employ PS receptors during viral entry are primarily transmitted through fluids that lack extracellular vesicles (*e.g.,* blood-ingesting insects) which can compete for binding to these receptors (45). However, viruses like CHIKV might display an advantage in the presence of extracellular vesicles post-entry for enhancing its release efficiency during transmission.

The increase in the production of viral particles from cells lacking TIM-1, increased infectivity of virions previously observed in ΔCDC50 cells (17), and the correlation observed between the presence of PS binding receptors and release

efficiency could be employed to maximize particle production during vaccine development. Vero cells are often used for the production of viral vaccines given their ability to yield high viral titers and susceptibility to a wide variety of viruses (46–49). Employing cellular characteristics that can maximize the release of viral particles should be taken into consideration when developing new designer cell lines for this purpose (46). Further studies should also characterize the extent to which phospholipid-binding receptors could inhibit the efficient egress of other highly pathogenic enveloped viruses.

Materials and Methods

Cells. All mammalian cell lines were maintained at 37˚C and 5% CO_2. Parental monkey Vero cells and Vero cells knocked out for TIM (VeroΔTIM), AXL (VeroΔAXL), and both (VeroΔTIM/AXL) were a gift from Dr. Wendy Maury from the University of Iowa (50). All Vero cells, including Vero-humanSLAM (VeroS) (51), VeroS knocked out for CDC50a chaperone (VeroSΔCDC50) (17), and baby hamster kidney cells (BHK) stably expressing T7 RNA polymerase (BSR-T7/5) (52) cells were maintained in DMEM supplemented with 5% FBS. Parental human haploid cells (HAP1) and HAP1 knocked out for CDC50a (HAP1ΔCDC50) cells were purchased from Horizon Discovery and maintained in Iscoves' modified Dulbecco's Medium (DMEM) supplemented with 8% fetal bovine serum (FBS). Human osteosarcoma U2OS cells were a gift from Dr. Neale Ridgway from Dalhousie University (53). Human 293T and U2OS cells were maintained with DMEM media supplemented with 10% FBS. Mosquito cell lines were kept at 28˚C and maintained in Leibovitz's L-15 media supplemented with 10% FBS (C6/36 – *Aedes albopictus*) or HyClone SFX-Insect media supplemented with 2% FBS (Aag2 - *Aedes aegypti*).

Viruses. All chikungunya infections were performed using the attenuated vaccine strain 181 clone 25 (181/c25). Full-length CHIKV genome was untagged (CHIKV), encoded *gfp* as an additional transcription unit between the non-structural and structural gene (CHIKV-GFP) (54), contained NLuc inserted at the N-terminus of E2 (CHIKV-E2-NLuc, CHIKV-GFP-E2-NLuc) or contained a mutation in nsP2 substituting amino acids A-T-L in position 674 for N-G-K (CHIKV-E2-Nluc-nsP2-ATL674NGK). The described changes were introduced into the molecular clone pSinRep5-181/25c (Addgene cat. 60078), a gift from Dr. Terrance Dermody. To recover the virus, plasmids were linearized and *in vitro* transcribed with the mMessage mMachine SP6 transcription kit (Invitrogen, cat. AM1340) per the manufacturer's protocol to produce the full-length positive-sense mRNA which was transfected into VeroS cells using Lipofectamine MessengerMax Transfection Reagent (Invitrogen, cat. LMRNA001) following the manufacturer's instructions. Vesicular Stomatitis virus (VSV) used to perform release efficiency assays was tagged with nano-luciferase in the coding region of the matrix protein (M) following residue 37 and encodes GFP as an additional transcriptional unit at a post-G site (VSV - M-NLuc-GFP) as described in (55, 56). Tri-segmented attenuated lymphocytic choriomeningitis virus encoding GFP (LCMV-GFP) was a gift from Dr. Luis Martínez-Sobrido (57). CHIKV and VSV stocks were propagated using Vero cells and LCMV stocks were propagated in BSR-T7/5 cells. All stocks were titrated on Vero cells using serial dilutions to determine the tissue culture infection dose 50 (TCID50) according to the Spearman-Karber method.

Virus Release Assays: Immunoblots. Vero or VeroΔTIM/AXL cells were plated in 10 cm^2 dishes at a density of $2.5x10^6$ per plate, one day before infection. Cells were

infected with CHIKV-GFP at an MOI of 0.5 (Vero, ΔTIM/AXL 1x) or 5 (ΔTIM/AXL 10x). After one hour of infection, the inoculum was removed and replaced with fresh DMEM 5% FBS, and cells were incubated at 37˚C. Eighteen hours following infection, supernatants were collected, and cells were lysed in M2 lysis buffer (50 mM Tris [pH 7.4], 150 mM NaCl, 1 mM EDTA, 1% Triton X-100) for 5 minutes and collected. Cell lysate samples were cleared by centrifuging at 6,000xg for 25 minutes. Supernatant samples were cleared twice at 6,000xg for five minutes and concentrated with ultracentrifugation over a 20% sucrose cushion for 3 hours at 28,000 rpm at 4°C. Purified pellets were resuspended in 200μl of 1x PBS. Cell lysates and purified supernatants were separated on an SDS-PAGE and analyzed through immunoblotting against vinculin as a loading control (1:2,000, MGA465GA, BioRad) or CHIKV E1 glycoprotein (1:1,000, MAB97792, R&D systems). Protein levels were quantified through Image Lab 6.1 densitometry analysis.

Viral Protein Composition Analysis of Purified Viral Particles. Vero cells were plated in 10 cm^2 dishes at a density of $5x10^6$ per plate. The following day, each plate was infected with either CHIKV-GFP or CHIKV-GFP-E2-NLuc at an MOI of 0.5. After one hour of infection, the inoculum was removed and replaced with fresh DMEM. The supernatant of infected cells was harvested 18 hours post-infection and cleared twice at 6,000xg for five minutes. Viral particles were purified and concentrated by ultracentrifugation over a 20% sucrose cushion for 3 hours at 28,000 rpm at 4°C. Purified pellets were resuspended in PBS and analyzed on a stain-free gel.

Multi-step Replication Curves. Vero, VeroS, and VeroSΔCDC50 cells were plated at $2.5x10^5$ cells/well in a 12-well plate while HAP1 and HAP1ΔCDC50 cells were plated at

a density of $3.0x10^5$ cells/well. Cells were infected with untagged CHIKV or CHIKV-GFP-E2-NLuc at an MOI of 0.01. One hour after infection, the inoculum was removed and replaced with complete media. At each indicated time point, supernatants were collected and replaced with corresponding media containing FBS. Samples were titrated by calculating the tissue culture infection dose 50 (TCID50) on Vero cells using the Spearman-Karber method. Luminescence of each supernatant sample was quantified using the Nano-Glo Substrate (Promega) and measured in a GloMax Explorer (Promega) luminometer.

Virus Release Assays: Infection. Cells were plated in 24-well plates at a density of $2.5x10^5$ cells/well, one day before infection. CHIKV particles were added for one hour at an MOI of 0.5 unless stated otherwise. After one hour, inoculum was removed, and replaced with media containing FBS, and cells were incubated at 37˚C. Eighteen hours following infection, supernatants were collected, and cells were lysed in M2 lysis buffer for 5 minutes. Vesicular Stomatitis virus infections were performed at an MOI of 1 for one hour and samples were harvested 8 hours post-infection as described. Release efficiency analysis between CHIKV and CHIKV bearing nsP2 ATL674NGK mutation was harvested 48 hours after infection.

Samples were cleared by centrifuging at 17,000xg for either 5 minutes (supernatants) or 25 minutes (cell lysates). Luminescence in supernatants and cell lysates was determined using the Nano-Glo Substrate (Promega) and measured in a GloMax Explorer (Promega) luminometer. Release efficiency was calculated as the ratio of luminescence in the supernatant divided by the luminescence in the cell lysates. When comparing phenotypes with a common parental cell line, release efficiency was

normalized and displayed as relative release efficiency, in comparison to the wildtype counterpart.

Virus Release Assays: Transfections and Plasmids. To assess the release efficiency of CHIKV viral-like particles (VLP), Vero and VeroΔTIM/AXL cells were plated in a 24-well plate at a density of $5x10^4$ cells/well. The following day, cells were transfected with a plasmid encoding CHIKV's structural cassette (C, E3, E2, 6K, E1) with NLuc inserted at the N-terminus of E2 to produce luminescent VLPs (Addgene cat. 215699). Vero and VeroΔTIM/AXL transfections were performed using Jet Optimus (Polyplus, #101000025) following the manufacturer's protocol. Supernatants and cell lysates were collected 24 hours post-transfection and release assays were performed as described previously.

Vero and VeroΔTIM/AXL cells were also transfected with plasmids encoding hTIM-1-GFP or GFP using Jet Optimus. 24 hours following transfection, CHIKV inoculum was added at an MOI of 0.5 for one hour and subsequently replaced with complete media. Supernatants and cell lysates were harvested 18 hours post-infection. Release assay was performed as described above.

293T cells were plated in a 24-well plate at a density of $1.5x10^5$ cells/well one day before transfections. The following day, cells were transfected with plasmids encoding hTIM-1-GFP, TIM-1-N114D, AXL, MXRA8, or L-SIGN using Jet Prime (Polyplus, #101000027) following the manufacturer's protocol. TIM plasmids were a gift from Dr. Wendy Maury (18). AXL (BC032229), MXRA8 (BC006213) (17), and L-SIGN (BC038851) plasmids were purchased from Transomic and cloned into expression

vectors. The following day after transfection, cells were infected, and release assays were performed at 18hpi as described above.

VeroS and VeroSΔCDC50 cells were plated in a 24-well plate at a density of $1x10^5$ cells/well. The following day, cells were transfected with a plasmid encoding CHIKV structural cassette tagged with nano-luciferase or with plasmids encoding CDC50a or GFP as control. To obtain similar levels of transfection efficiency in VeroS and VeroSΔCDC50 cells, transfections were performed using ViaFect transfection reagent (Promega, cat. E4981) at a ratio of reagent to DNA of 6:1, following manufacturer's protocol. Supernatants and cell lysates of VLP release assays were collected 24 hours post-transfection and analyzed as described previously. VeroSΔCDC50 cells transfected with CDC50-encoding plasmid (Addgene cat. 215702) were infected the following day with CHIKV-E2-NLuc at an MOI of 0.5. Viral inoculum was replaced with complete media after one hour and supernatants and cell lysates were harvested for analysis after 18 hours of infection.

To analyze the VLP release efficiency in the presence of nsP2 mutants, VeroS cells were plated at a density of $1x10^5$ cells/well in a 24-well plate. The following day, cells were transfected with equal amounts of a plasmid encoding CHIVK structural cassette tagged with nano-luciferase and each nsP2 [nsP2 (Addgene cat. 215695), nsP2 ATL674NGK, and nsP2 C478A]. After 48 hours post-transfection, supernatants and cell lysates were harvested, and release efficiency was analyzed as described above.

Virus Release Assays: $DioC_{18}(3)$ PC:PE:PS liposomes. PC:PE:PS liposomes (75% PC: 20% PE: 5% PS) were prepared as described in (58) with the addition of $DiOC_{18}(3)$

(3,3'-Dioctadecyloxacarbocyanine Perchlorate) (Invitrogen, D275) for fluorescence, following manufacturer's indications. Vero and VeroΔTIM/AXL cells were plated at a density of $2.5x10^5$ cells/well in a 24-well plate. VeroS and VeroSΔCDC50 cells were plated in a 24-well plate at a density of $1x10^5$ cells/well. The next day, cells were infected at an MOI of 0.5 for one hour and the inoculum was replaced with complete media. Six hours post-infection, $DioC_{18}$(3) PC:PE:PS liposomes were sonicated for 1 hour and added to the cells at the indicated concentrations. Supernatants and cell lysates were collected 18 hours post-infection and release assays were performed as described above.

Entry Assays. Cells were plated in a 48-well plate at a density of $1x10^5$ cells/well (HAP1, HAP1ΔCDC50) or in a 24-well plate at $1.25x10^5$ cells/well (VeroS, VeroSΔCDC50). The next day, cells were infected with enough CHIKV-GFP infectious viral particles to obtain approximately 50% of infected cells after 12 hours. Inoculum was removed from the cells after one hour and treated with 30 mM ammonium chloride (NH_4Cl) after 2 hours to prevent subsequent rounds of infection. Infected cells were resuspended in PBS, fixed using 4% formaldehyde, and the percentage of GFP+ cells was quantified using a NovoCyte Quanteon cytometer (Agilent).

Surface Biotinylation. HAP1, HAP1ΔCDC50, and VeroS cells were plated in a 6-well plate at a density of $1x10^6$ cells/well. For analysis of levels of surface receptor TYRO3 in HAP1 cell lines, uninfected cells were harvested the following day. For analysis of surface receptors after viral infection through immunoblots, VeroS cells were either mock infected or infected one day after plating with CHIKV-GFP (MOI 0.5) or LCMV-GFP (MOI 1) and harvested at the indicated time points. Cells were washed with cold

PBS, and surface proteins were biotinylated with 0.5 mg/mL sulfosuccinimidyl-2-(biotinamido) ethyl-1,3-dithiopropionate (ThermoFisher) on ice for 45 minutes with gentle shaking. The reaction was quenched using Tris-HCl and cells were lysed with M2 lysis buffer at 4˚C. Samples were centrifuged at 17,000xg for 10 minutes. A fraction of the lysate was saved (total cell lysate, TCL), and the surface proteins were bound to streptavidin Sepharose beads overnight at 4°C (GE Healthcare). Beads were then washed with buffer containing 100 mM Tris, 500 mM lithium chloride, 0.1% Triton X-100 followed by a buffer containing 20 mM HEPES [pH 7.2], 2 mM EGTA, 10 mM magnesium chloride, 0.1% Triton X-100. Samples were then analyzed through immunoblotting probing against TYRO3 (1:1000, R&D Systems, MAB859100), TIM (TIM (1:500, AF1750, R&D Systems), AXL (1:100, AF154, R&D Systems), GAPDH (1:2000, Santa Cruz Biotech, #sc-47724), Transferrin (1:1,000, PA5-27739, ThermoFisher), or CHIKV E1 (1:1,000, MAB97792, R&D systems).

Viral Spread Kinetics Assay. VeroS and VeroSΔCDC50 were plated in a 24-well plate at a density of $1.25x10^5$ cells/well. One day after plating, cells were infected with CHIKV-GFP at an MOI of 0.1 for one hour. At the indicated time points, cells were lifted using trypsin, resuspended in PBS, and fixed in 4% formaldehyde. A NovoCyte Quanteon cytometer (Agilent) was used to analyze 10,000 live cells and quantify the percentage of GFP+ cells over time.

Flow Cytometry TIM-1 Surface Staining. Cells were plated at a density of $1.0x10^6$ cells/well in a 6-well plate one day prior to staining. For analysis of baseline levels of TIM-1 in the surface of VeroS and VeroSΔCDC50 cells, samples were harvested from uninfected cells one day after plating. For analysis of TIM-1 surface levels following

infection, VeroS cells were infected with CHIKV-GFP at an MOI of 0.5 and harvested 18 hours post-infection. To determine the effect of viral protein expression on the surface levels of TIM-1, VeroS cells were transfected with expression plasmids encoding CHIKV's non-structural proteins bearing a FLAG tag [nsP1 (Addgene cat. 215694), nsP2 (Addgene cat. 215695), nsP2 ATL674NGK, nsP2 C478A, nsP3 (Addgene cat. 215696), and nsP4 (Addgene cat. 215697)], a structural cassette (C, E3, E2, 6K, E1) (Addgene cat. 215698), capsid (Addgene cat. 215701), E 181/25 (Southeast Asian strain) (Addgene cat. 215700) or E S27 (African strain). Plasmid encoding E S27 was a gift from Dr. Graham Simmons (59). Transfections were performed using Jet Optimus (Polyplus, #101000025) following the manufacturer's protocol. Two days following transfection, samples were harvested for surface staining.

Monolayers were cooled, washed, and treated with a blocking solution (dPBS +Ca2 +Mg2 with 2% (v/v) FBS) containing an anti-hTIM1(1:50-1:100, AF1750, R&D Systems) antibody. Samples were incubated at 4˚C with gentle shaking for one hour and washed three times with ice-cold PBS. A blocking solution containing the corresponding secondary antibody, donkey anti-goat Alexa Fluor 594 (1:2500, A32758, Invitrogen), was added. Samples were incubated at 4˚C in the dark with gentle shaking for 30 minutes. Samples were washed three additional times with PBS, lifted via scraping, and analyzed using a NovoCyte Quanteon cytometer (Agilent). Populations of live, single cells were gated using FSC/SSC and SSC-A/SSC-H, respectively. The AF594 gate was set with a secondary-only control. The AF594 MFI of 10,000 live, single cells was quantified. AF594 fluorescence was measured with a 561-nm laser with a 615/20 "PE-Texas Red" bandpass filter; all filter sets had default gain. Fold TIM-1 levels

were calculated over the mean fluorescence intensity (MFI) of a secondary-only control to eliminate background levels.

Liposome Binding Assay. For comparison of liposome binding among different cell lines, cells were plated in a 12-well plate at a density of $5x10^5$ cells/well, and binding was assessed from uninfected cells the following day. For assessing liposome binding following infection, VeroS cells were plated at a density of $2.5x10^5$ cells/well in a 12-well plate. CHIKV inoculum was added at an MOI of 0.5 for 1hr and binding was assessed after 18hrs. To evaluate the effect of CHIKV's proteins on liposome binding, VeroS cells were plated in a 24-well plate at a density of $1x10^5$ cells/well. The following day, cells were transfected with plasmids encoding for CHIKV's non-structural proteins with a FLAG tag, a structural cassette, capsid, E 181/25 (Southeast Asian strain), or E S27 (African strain). Transfections were performed using Jet Optimus (Polyplus, #101000025) following the manufacturer's protocol. Two days following transfection, binding was assessed.

To measure liposome binding, cells were placed on ice for 30 minutes. $DioC_{18}(3)$ PC:PE:PS liposomes were sonicated for 1 hour and added to the cells at a final concentration of 10μM. Liposomes were bound to cells for 1 hour on ice, removed, and washed with FBS-free media. Cells were lifted in FBS-free media and fixed in equal volume of 4% formaldehyde.

Samples were analyzed using a NovoCyte Quanteon cytometer (Agilent). Populations were gated using SSC-H/FSC-H and SSC-A/SSC-H to identify live and single cells, respectively. A 488-nm laser with a 530/30 "FITC" bandpass filter was used to assess $DiOC_{18}(3)$ fluorescence. A $DiOC_{18}(3)$+ gate was set using non-liposome-

treated cells as a $DiOC_{18}(3)$- control. The $DiOC_{18}(3)$ MFI of 10,000 live, single events was quantified. Fold liposome binding was calculated over the MFI of non-liposome-treated cells to eliminate non-specific background levels.

Cell Viability Assay. For cell viability analysis following infection, VeroS cells were plated in a 48-well plate at a density of $1.5x10^5$ cells/well. The following day, cells were infected with CHIKV-GFP at an MOI of 0.5 at different time points. At the final timepoint infected cells were harvested for analysis of ATP levels using Cell Titer Glo luminescent cell viability assay (Promega, cat. G7570) following manufacturers' indications. Relative luminescence units (RLU) were measured using a GloMax Explorer (Promega) luminometer

For determining cell viability following viral protein expression, cells were plated in a 48-well plate at a density of $9.0x10^4$ cells/well. The following day, cells were transfected with expression plasmids encoding the indicated viral proteins using Jet Optimus transfection reagent. Two days after transfections, cell viability was quantified as described previously.

Statistical Analysis. All graphs were made and analyzed using GraphPad Prism (v10.1.1, macOS). An unpaired parametric student's T-test was performed to determine the significance between two groups. For data determining statistical significance among two groups where data was normalized, a Welch's correction was used. For logarithmic data, values were first natural log (ln) transformed and then analyzed with T-tests using a Welch's correction. An ordinary one-way ANOVA with multiple comparisons was used to evaluate statistical differences among more than two groups with non-normalized data.

References

1. Caglioti C, Lalle E, Castilletti C, Carletti F, Capobianchi MR, Bordi L. 2013. Chikungunya virus infection: an overview. New Microbiol 36:211–227.

2. Yap ML, Klose T, Urakami A, Hasan SS, Akahata W, Rossmann MG. 2017. Structural studies of Chikungunya virus maturation. Proc Natl Acad Sci 114:13703–13707.

3. Chmielewski D, Schmid MF, Simmons G, Jin J, Chiu W. 2022. Chikungunya virus assembly and budding visualized in situ using cryogenic electron tomography. Nat Microbiol 7:1270–1279.

4. Brown R, Wan J, Kielian M. 2018. The Alphavirus Exit Pathway: What We Know and What We Wish We Knew. Viruses 10:89.

5. Suomalainen M, Liljeström P, Garoff H. 1992. Spike protein-nucleocapsid interactions drive the budding of alphaviruses. J Virol 66:4737–4747.

6. Owen KE, Kuhn RJ. 1997. Alphavirus Budding Is Dependent on the Interaction between the Nucleocapsid and Hydrophobic Amino Acids on the Cytoplasmic Domain of the E2 Envelope Glycoprotein. Virology 230:187–196.

7. Ivanova L, Schlesinger MJ. 1993. Site-directed mutations in the Sindbis virus E2 glycoprotein identify palmitoylation sites and affect virus budding. J Virol 67:2546–2551.

8. Elmasri Z, Negi V, Kuhn RJ, Jose J. 2022. Requirement of a functional ion channel for Sindbis virus glycoprotein transport, CPV-II formation, and efficient virus budding. PLOS Pathog 18:e1010892.

9. Votteler J, Sundquist WI. 2013. Virus Budding and the ESCRT Pathway. Cell Host Microbe 14:232–241.

10. Jones PH, Maric M, Madison MN, Maury W, Roller RJ, Okeoma CM. 2013. BST-2/tetherin-mediated restriction of chikungunya (CHIKV) VLP budding is counteracted by CHIKV non-structural protein 1 (nsP1). Virology 438:37–49.

11. Ooi Y, Dubé M, Kielian M. 2015. BST2/Tetherin Inhibition of Alphavirus Exit. Viruses 7:2147–2167.

12. Kaletsky RL, Francica JR, Agrawal-Gamse C, Bates P. 2009. Tetherin-mediated restriction of filovirus budding is antagonized by the Ebola glycoprotein. Proc Natl Acad Sci 106:2886–2891.

13. Perez-Caballero D, Zang T, Ebrahimi A, McNatt MW, Gregory DA, Johnson MC, Bieniasz PD. 2009. Tetherin Inhibits HIV-1 Release by Directly Tethering Virions to Cells. Cell 139:499–511.

14. Acciani MD, Brindley MA. 2022. Scrambled or flipped: 5 facts about how cellular phosphatidylserine localization can mediate viral replication. PLoS Pathog 18:e1010352.

15. Leventis PA, Grinstein S. 2010. The Distribution and Function of Phosphatidylserine in Cellular Membranes. Annu Rev Biophys 39:407–427.

16. Segawa K, Nagata S. 2015. An Apoptotic ‘Eat Me’ Signal: Phosphatidylserine Exposure. Trends Cell Biol 25:639–650.

17. Reyes Ballista JM, Miazgowicz KL, Acciani MD, Jimenez AR, Belloli RS, Havranek KE, Brindley MA. 2023. Chikungunya virus entry and infectivity is primarily facilitated through cell line dependent attachment factors in mammalian and mosquito cells. Front Cell Dev Biol 11:1085913.

18. Moller-Tank S, Kondratowicz AS, Davey RA, Rennert PD, Maury W. 2013. Role of the phosphatidylserine receptor TIM-1 in enveloped-virus entry. J Virol 87:8327–41.

19. Kirui J, Abidine Y, Lenman A, Islam K, Gwon YD, Lasswitz L, Evander M, Bally M, Gerold G. 2021. The Phosphatidylserine Receptor TIM-1 Enhances Authentic Chikungunya Virus Cell Entry. Cells 10.

20. Li M, Ablan SD, Miao C, Zheng Y-M, Fuller MS, Rennert PD, Maury W, Johnson MC, Freed EO, Liu S-L. 2014. TIM-family proteins inhibit HIV-1 release. Proc Natl Acad Sci 111.

21. Xie S, Liang Z, Yang X, Pan J, Yu D, Li T, Cao R. 2021. Japanese Encephalitis Virus NS2B-3 Protein Complex Promotes Cell Apoptosis and Viral Particle Release by Down-Regulating the Expression of AXL. Virol Sin 36:1503–1519.

22. Ramjag A, Cutrone S, Lu K, Crasto C, Jin J, Bakkour S, Carrington CVF, Simmons G. 2022. A high-throughput screening assay to identify inhibitory antibodies targeting alphavirus release. Virol J 19:170.

23. McIntire JJ, Umetsu DT, DeKruyff RH. 2004. TIM-1, a novel allergy and asthma susceptibility gene. Springer Semin Immunopathol 25:335–348.

24. Moller-Tank S, Maury W. 2014. Phosphatidylserine receptors: Enhancers of enveloped virus entry and infection. Virology 468–470:565–580.

25. Zhang R, Kim AS, Fox JM, Nair S, Basore K, Klimstra WB, Rimkunas R, Fong RH, Lin H, Poddar S, Crowe JE, Doranz BJ, Fremont DH, Diamond MS. 2018. Mxra8 is a receptor for multiple arthritogenic alphaviruses. Nature 557:570–574.

26. Klimstra WB, Nangle EM, Smith MS, Yurochko AD, Ryman KD. 2003. DC-SIGN and L-SIGN Can Act as Attachment Receptors for Alphaviruses and Distinguish between Mosquito Cell- and Mammalian Cell-Derived Viruses. J Virol 77:12022–12032.

27. Shimojima M, Takada A, Ebihara H, Neumann G, Fujioka K, Irimura T, Jones S, Feldmann H, Kawaoka Y. 2006. Tyro3 family-mediated cell entry of Ebola and Marburg viruses. J Virol 80:10109–16.

28. Landi A, Iannucci V, Nuffel AV, Meuwissen P, Verhasselt B. 2011. One protein to rule them all: modulation of cell surface receptors and molecules by HIV Nef. Curr HIV Res 9:496–504.

29. Schneider-Schaulies J, Schnorr JJ, Brinckmann U, Dunster LM, Baczko K, Liebert UG, Schneider-Schaulies S, ter Meulen V. 1995. Receptor usage and differential downregulation of CD46 by measles virus wild-type and vaccine strains. Proc Natl Acad Sci U S A 92:3943–3947.

30. Breiner KM, Urban S, Glass B, Schaller H. 2001. Envelope protein-mediated down-regulation of hepatitis B virus receptor in infected hepatocytes. J Virol 75:143–150.

31. Li M, Waheed AA, Yu J, Zeng C, Chen H-Y, Zheng Y-M, Feizpour A, Reinhard BM, Gummuluru S, Lin S, Freed EO, Liu S-L. 2019. TIM-mediated inhibition of HIV-1 release is antagonized by Nef but potentiated by SERINC proteins. Proc Natl Acad Sci 116:5705–5714.

32. Akhrymuk I, Kulemzin SV, Frolova EI. 2012. Evasion of the innate immune response: the Old World alphavirus nsP2 protein induces rapid degradation of Rpb1, a catalytic subunit of RNA polymerase II. J Virol 86:7180–7191.

33. Akhrymuk I, Lukash T, Frolov I, Frolova EI. 2019. Novel Mutations in nsP2 Abolish Chikungunya Virus-Induced Transcriptional Shutoff and Make the Virus Less Cytopathic without Affecting Its Replication Rates. J Virol 93:e02062-18.

34. Rausalu K, Utt A, Quirin T, Varghese FS, Žusinaite E, Das PK, Ahola T, Merits A. 2016. Chikungunya virus infectivity, RNA replication and non-structural polyprotein processing depend on the nsP2 protease's active site cysteine residue. Sci Rep 6:37124.

35. Stitt TN, Conn G, Gore M, Lai C, Bruno J, Radziejewski C, Mattsson K, Fisher J, Gies DR, Jones PF. 1995. The anticoagulation factor protein S and its relative, Gas6, are ligands for the Tyro 3/Axl family of receptor tyrosine kinases. Cell 80:661–670.

36. Morizono K, Xie Y, Olafsen T, Lee B, Dasgupta A, Wu AM, Chen ISY. 2011. The Soluble Serum Protein Gas6 Bridges Virion Envelope Phosphatidylserine to the TAM Receptor Tyrosine Kinase Axl to Mediate Viral Entry. Cell Host Microbe 9:286–298.

37. Bevers EM, Williamson PL. 2016. Getting to the Outer Leaflet: Physiology of Phosphatidylserine Exposure at the Plasma Membrane. Physiol Rev 96:605–645.

38. Kerr D, Gong Z, Suwatthee T, Luoma A, Roy S, Scarpaci R, Hwang HL, Henderson JM, Cao KD, Bu W, Lin B, Tietjen GT, Steck TL, Adams EJ, Lee KYC. 2021. How Tim proteins differentially exploit membrane features to attain robust target sensitivity. Biophys J 120:4891–4902.

39. Scott HL, Heberle FA, Katsaras J, Barrera FN. 2019. Phosphatidylserine Asymmetry Promotes the Membrane Insertion of a Transmembrane Helix. Biophys J 116:1495–1506.

40. Jose J, Taylor AB, Kuhn RJ. 2017. Spatial and Temporal Analysis of Alphavirus Replication and Assembly in Mammalian and Mosquito Cells. mBio 8:e02294-16.

41. Reitmayer CM, Levitt E, Basu S, Atkinson B, Fragkoudis R, Merits A, Lumley S, Larner W, Diaz AV, Rooney S, Thomas CJE, Von Wyschetzki K, Rausalu K,

Alphey L. 2023. Mimicking superinfection exclusion disrupts alphavirus infection and transmission in the yellow fever mosquito *Aedes aegypti*. Proc Natl Acad Sci 120:e2303080120.

42. Göertz GP, McNally KL, Robertson SJ, Best SM, Pijlman GP, Fros JJ. 2018. The Methyltransferase-Like Domain of Chikungunya Virus nsP2 Inhibits the Interferon Response by Promoting the Nuclear Export of STAT1. J Virol 92:e01008-18.

43. Cherkashchenko L, Rausalu K, Basu S, Alphey L, Merits A. 2022. Expression of Alphavirus Nonstructural Protein 2 (nsP2) in Mosquito Cells Inhibits Viral RNA Replication in Both a Protease Activity-Dependent and -Independent Manner. Viruses 14:1327.

44. Ware BC, Parks MG, Da Silva MOL, Morrison TE. 2024. Chikungunya virus infection disrupts MHC-I antigen presentation via nonstructural protein 2. PLOS Pathog 20:e1011794.

45. Groß R, Reßin H, Von Maltitz P, Albers D, Schneider L, Bley H, Hoffmann M, Cortese M, Gupta D, Deniz M, Choi J-Y, Jansen J, Preußer C, Seehafer K, Pöhlmann S, Voelker DR, Goffinet C, Pogge-von Strandmann E, Bunz U, Bartenschlager R, El Andaloussi S, Sparrer KMJ, Herker E, Becker S, Kirchhoff F, Münch J, Müller JA. 2024. Phosphatidylserine-exposing extracellular vesicles in body fluids are an innate defence against apoptotic mimicry viral pathogens. Nat Microbiol 9:905–921.

46. Genzel Y. 2015. Designing cell lines for viral vaccine production: Where do we stand? Biotechnol J 10:728–740.

47. Konishi K, Yamaji T, Sakuma C, Kasai F, Endo T, Kohara A, Hanada K, Osada N. 2022. Whole-Genome Sequencing of Vero E6 (VERO C1008) and Comparative Analysis of Four Vero Cell Sublines. Front Genet 13:801382.

48. Demirden SF, Kimiz-Gebologlu I, Oncel SS. 2024. Animal Cell Lines as Expression Platforms in Viral Vaccine Production: A Post Covid-19 Perspective. ACS Omega 9:16904–16926.

49. Barrett PN, Mundt W, Kistner O, Howard MK. 2009. Vero cell platform in vaccine production: moving towards cell culture-based viral vaccines. Expert Rev Vaccines 8:607–618.

50. Brouillette RB, Phillips EK, Patel R, Mahauad-Fernandez W, Moller-Tank S, Rogers KJ, Dillard JA, Cooney AL, Martinez-Sobrido L, Okeoma C, Maury W. 2018. TIM-1 Mediates Dystroglycan-Independent Entry of Lassa Virus. J Virol 92.

51. Ono N, Tatsuo H, Hidaka Y, Aoki T, Minagawa H, Yanagi Y. 2001. Measles Viruses on Throat Swabs from Measles Patients Use Signaling Lymphocytic Activation Molecule (CDw150) but Not CD46 as a Cellular Receptor. J Virol 75:4399–4401.

52. Buchholz UJ, Finke S, Conzelmann K-K. 1999. Generation of Bovine Respiratory Syncytial Virus (BRSV) from cDNA: BRSV NS2 Is Not Essential for Virus Replication in Tissue Culture, and the Human RSV Leader Region Acts as a Functional BRSV Genome Promoter. J Virol 73:251–259.

53. Dorighello G, McPhee M, Halliday K, Dellaire G, Ridgway ND. 2023. Differential contributions of phosphotransferases CEPT1 and CHPT1 to phosphatidylcholine homeostasis and lipid droplet biogenesis. J Biol Chem 299:104578.

54. Lay Mendoza MF, Acciani MD, Levit CN, Santa Maria C, Brindley MA. 2020. Monitoring Viral Entry in Real-Time Using a Luciferase Recombinant Vesicular Stomatitis Virus Producing SARS-CoV-2, EBOV, LASV, CHIKV, and VSV Glycoproteins. Viruses 12.

55. Acciani MD, Lay Mendoza MF, Havranek KE, Duncan AM, Iyer H, Linn OL, Brindley MA. 2021. Ebola virus requires phosphatidylserine scrambling activity for efficient budding and optimal infectivity. J Virol JVI0116521.

56. Soh TK, Whelan SPJ. 2015. Tracking the Fate of Genetically Distinct Vesicular Stomatitis Virus Matrix Proteins Highlights the Role for Late Domains in Assembly. J Virol 89:11750–11760.

57. Cheng BYH, Ortiz-Riaño E, de la Torre JC, Martínez-Sobrido L. 2015. Arenavirus Genome Rearrangement for the Development of Live Attenuated Vaccines. J Virol 89:7373–7384.

58. Zhang L, Richard AS, Jackson CB, Ojha A, Choe H. 2020. Phosphatidylethanolamine and Phosphatidylserine Synergize To Enhance GAS6/AXL-Mediated Virus Infection and Efferocytosis. J Virol 95.

59. Salvador B, Zhou Y, Michault A, Muench MO, Simmons G. 2009. Characterization of Chikungunya pseudotyped viruses: Identification of refractory cell lines and

demonstration of cellular tropism differences mediated by mutations in E1 glycoprotein. Virology 393:33–41.

CHAPTER 5

CONCLUSIONS

The arthritogenic alphavirus chikungunya (CHIKV), has affected more than 15 countries in the Americas in the last five years (1). Infectious *Aedes* mosquitoes transmit CHIKV during bloodmeal acquisition, causing several debilitating symptoms including fever, joint pain, and long-lasting arthralgia (2). In November 2023, a live-attenuated vaccine for CHIKV was approved for the first time by the U.S. Food and Drug Administration (FDA) (3). However, efforts should continue to broaden the availability of targets for vaccines and antiviral therapeutics.

CHIKV displays a broad cell tropism and an ability to disseminate through a complex array of tissues in both the mammalian host and mosquito vector (4). Despite efforts to understand the intricacies of CHIK viral replication cycle, many mechanisms remain to be elucidated. During entry, CHIKV can attach to proteinaceous receptors like the Matrix Remodeling Associated 8 protein (MXRA8), complex carbohydrates like glycosaminoglycans (GAGs), and phosphatidylserine receptors (PSR) like the T cell immunoglobulin and mucin domain-1 (TIM-1), among many others (5–9).

Despite an effort to characterize CHIKV's cellular binding partners, no attachment factor is classified as indispensable for mediating entry into host cells. Furthermore, the identification and characterization of CHIKV entry factors has often been restricted to specific cell lines. For example, CHIKV use of MXRA8 has been well characterized in murine cell lines including mouse fibroblast (NIH3T3) cells and a few

human cell lines (5). However, few studies have characterized and preferential use of these entry factors by comparing multiple cell lines. In Chapter 3, we evaluated the relevance of multiple binding partners during CHIKV entry into a panel of mammalian and mosquito cells. We underline the importance of each entry factor and demonstrate that CHIKV's entry pathway is highly dependent on the cell line and the availability of molecules at the surface of these cells.

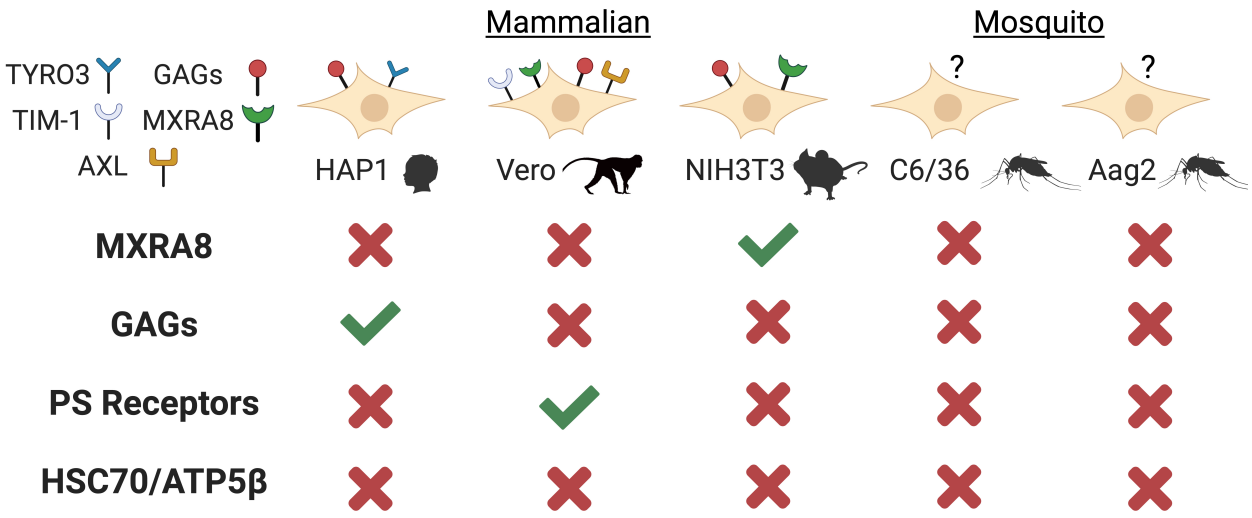

Figure 27. Summary of cellular receptors displayed and CHIKV's primary entry mechanism in each cell line. Molecules evidenced to mediate attachment of CHIKV into each cell line are indicated with (✓), where an (X) indicates that the molecule does not appear to mediate CHIKV entry. Diagram was created with Biorender.com

CHIKV entry was mainly mediated by TIM-1 in Vero cells, heparan sulfate in HAP1 cells, and MXRA8 in NIH3T3 cells. Despite being good modulators of entry into Vero cells, CHIKV was able to attach and enter Vero cells lacking PSR when added at high concentrations. Although infection in these cells was inefficient, the data suggested that CHIKV can utilize an alternate less effective pathway in these cells. Additionally, entry of CHIKV in mosquito cell lines was independent of all three of these molecules

implying that additional factors could mediate this process. We evaluated attachment molecules like heat shock cognate 70 protein (HSC70) and ATP synthase β (ATPSβ) previously implicated in mediating CHIKV entry in mosquito cells (10, 11). Our results did not support these molecules as mediators of entry and suggested that the presence of an antibody preservative alone, sodium azide, triggered the inhibition of CHIKV entry in mosquito cells. The lack of orthologs of proteinaceous receptors like MXRA8 or PSR in mosquito cells further underlines the mystery of CHIKV receptors in these cells.

Only a few cellular factors, including tetherin/BST-2, have been recognized for hindering CHIKV release (12, 13). Besides mediating entry, phosphatidylserine receptors can also play a role in other steps of the viral replication cycle. For instance, receptors like TIM-1 and AXL can prevent the release of human immunodeficiency virus (HIV) and Japanese encephalitis virus (JEV) viral particles from the surface of infected cells (14, 15). To evaluate PSR and other attachment molecules as release inhibitory molecules, in Chapter 4, we assessed CHIKV release efficiency in the presence or absence of multiple binding partners. TIM-1 had the greatest ability to prevent the release of CHIK virions by attaching to envelope phospholipids.

It was particularly surprising to observe that Aag2 mosquito cells displayed significant levels of liposome-binding receptors and CHIKV release efficiency comparable to that displayed in Vero cells. These results were intriguing taking into consideration that PC:PE:PS liposomes were unable to inhibit CHIKV infection in Aag2 mosquito cells, as seen in Chapter 3. It is possible that these cells produce aminophospholipid-binding receptors but that the mechanism of CHIK viral entry is independent of the interaction between envelope phospholipids and surface receptors.

Knockout of a required flippase subunit, CDC50a, inhibits the normal transmembrane location of phospholipids causing an increase in PS in the plasma membrane's outer leaflet. In addition to this phenotype, we observed that Vero cells knocked out for CDC50a (ΔCDC50) displayed lower surface levels of TIM-1 resulting in an overall increase in CHIKV release efficiency. We consistently observed a correlation between the levels of PS-binding receptors at the cell surface and the efficiency of CHIKV release in multiple mammalian and mosquito cell lines. However, it is important to underline that altering the normal lipid distribution mechanisms within the plasma membrane could also play a role in the fluidity, formation of membrane curvatures, and proper recruitment to host factors, which could contribute to an increase in CHIKV particle release. Other enveloped viruses, like Ebola virus, require the activity of phospholipid translocators (i.e. scramblase XKR8) for efficient assembly and viral egress. Future studies should further discern between the effect of high levels of outer leaflet PS and decreased levels of TIM-1 displayed by VeroΔCDC50 cells on CHIKV release.

CHIKV counteracted the tethering inhibition of TIM-1 through a cellular transcriptional shutoff triggered by the viral protein nsP2. As discussed in Chapter 2, alphavirus nsP2 plays many roles in mediating the evasion of the immune system during infection. The ability of CHIKV's nsP2 to decrease the levels of surface receptors like TIM-1, consequently resulting in increased viral particle production, provides a substantial advantage during transmission and spread within its hosts. Transcriptional shutoff by CHIKV's nsP2 can also trigger a decrease in levels of major histocompatibility complex class 1 (MHC-1) from the surface of joint tissue fibroblasts, leading to

persistent infections (16). These results not only highlight the key roles of nsP2 in virus infection but also provide an insight into the ability of PS-receptors to modulate CHIKV transmission at larger scales, beyond *in vitro* studies.

Understanding the function of phosphatidylserine and phospholipid-binding receptors during viral infection is essential due to its great influence in many steps of the replication cycle (17). There is a connection between the viral mode of transmission and the use of apoptotic mimicry as a mechanism of entry. Viruses that utilize apoptotic mimicry are more likely to be transmitted through the bloodmeal intake by arthropods, given that the blood is deficient in extracellular vesicles that could otherwise compete for cellular attachment (18). We observed similar inhibition of CHIKV entry into Vero cells with the addition of PC:PE:PS liposomes, showing the ability of *in vitro* studies to provide insight into mechanisms arising during authentic viral transmission.

Final Remarks

The work presented in this dissertation highlights the importance of phospholipids and phospholipid-binding receptors in two key steps of the viral replication cycle: entry and release. We can expand our knowledge of the use of apoptotic mimicry in the context of cell-line dependency and aid in the broad viral tropism displayed by CHIKV. During egress, we contribute to the characterization of a less-known role of PS receptors in inhibiting the release of enveloped viruses.

We hope that these studies serve as a building point for future studies to expand on how phospholipids could play a role in the infection of other alphaviruses. Future studies should more thoroughly assess the possible production of phospholipid-binding receptors in mosquito cells, particularly Aag2, and characterize possible alternate entry

mechanisms. This investigation should lead the path to understanding the role of lipids in other stages of CHIK viral cycle not evaluated in this dissertation, particularly replication. Finally, these findings could be translated into the identification of possible antiviral or therapeutic targets by assessing the phenotypes of viral clinical isolates and comparing multiple CHIKV lineages.

References

1. Areas at Risk for Chikungunya. Center for Disease Control and Prevention - Chikungunya virus. https://www.cdc.gov/chikungunya/geo/index.html.

2. Caglioti C, Lalle E, Castilletti C, Carletti F, Capobianchi MR, Bordi L. 2013. Chikungunya virus infection: an overview. New Microbiol 36:211–227.

3. 2023. FDA Approves First Vaccine to Prevent Disease Caused by Chikungunya Virus. FDA US Food and Drug Administration. https://www.fda.gov/news-events/press-announcements/fda-approves-first-vaccine-prevent-disease-caused-chikungunya-virus.

4. Matusali G, Colavita F, Bordi L, Lalle E, Ippolito G, Capobianchi MR, Castilletti C. 2019. Tropism of the Chikungunya Virus. Viruses 11:E175.

5. Zhang R, Kim AS, Fox JM, Nair S, Basore K, Klimstra WB, Rimkunas R, Fong RH, Lin H, Poddar S, Crowe JE, Doranz BJ, Fremont DH, Diamond MS. 2018. Mxra8 is a receptor for multiple arthritogenic alphaviruses. Nature 557:570–574.

6. Song H, Zhao Z, Chai Y, Jin X, Li C, Yuan F, Liu S, Gao Z, Wang H, Song J, Vazquez L, Zhang Y, Tan S, Morel CM, Yan J, Shi Y, Qi J, Gao F, Gao GF. 2019. Molecular Basis of Arthritogenic Alphavirus Receptor MXRA8 Binding to Chikungunya Virus Envelope Protein. Cell 177:1714-1724 e12.

7. McAllister N, Liu Y, Silva LM, Lentscher AJ, Chai W, Wu N, Griswold KA, Raghunathan K, Vang L, Alexander J, Warfield KL, Diamond MS, Feizi T, Silva LA, Dermody TS. 2020. Chikungunya Virus Strains from Each Genetic Clade Bind Sulfated Glycosaminoglycans as Attachment Factors. J Virol 94.

8. Kirui J, Abidine Y, Lenman A, Islam K, Gwon YD, Lasswitz L, Evander M, Bally M, Gerold G. 2021. The Phosphatidylserine Receptor TIM-1 Enhances Authentic Chikungunya Virus Cell Entry. Cells 10.

9. Carnec X, Meertens L, Dejarnac O, Perera-Lecoin M, Hafirassou ML, Kitaura J, Ramdasi R, Schwartz O, Amara A. 2016. The Phosphatidylserine and Phosphatidylethanolamine Receptor CD300a Binds Dengue Virus and Enhances Infection. J Virol 90:92–102.

10. Ghosh A, Desai A, Ravi V, Narayanappa G, Tyagi BK. 2017. Chikungunya Virus Interacts with Heat Shock Cognate 70 Protein to Facilitate Its Entry into Mosquito Cell Line. Intervirology 60:247–262.

11. Fongsaran C, Jirakanwisal K, Kuadkitkan A, Wikan N, Wintachai P, Thepparit C, Ubol S, Phaonakrop N, Roytrakul S, Smith DR. 2014. Involvement of ATP synthase β subunit in chikungunya virus entry into insect cells. Arch Virol 159:3353–3364.

12. Ooi Y, Dubé M, Kielian M. 2015. BST2/Tetherin Inhibition of Alphavirus Exit. Viruses 7:2147–2167.

13. Jones PH, Maric M, Madison MN, Maury W, Roller RJ, Okeoma CM. 2013. BST-2/tetherin-mediated restriction of chikungunya (CHIKV) VLP budding is counteracted by CHIKV non-structural protein 1 (nsP1). Virology 438:37–49.

14. Li M, Ablan SD, Miao C, Zheng Y-M, Fuller MS, Rennert PD, Maury W, Johnson MC, Freed EO, Liu S-L. 2014. TIM-family proteins inhibit HIV-1 release. Proc Natl Acad Sci USA 111.

15. Xie S, Liang Z, Yang X, Pan J, Yu D, Li T, Cao R. 2021. Japanese Encephalitis Virus NS2B-3 Protein Complex Promotes Cell Apoptosis and Viral Particle Release by Down-Regulating the Expression of AXL. Virol Sin 36:1503–1519.

16. Ware BC, Parks MG, Da Silva MOL, Morrison TE. 2024. Chikungunya virus infection disrupts MHC-I antigen presentation via nonstructural protein 2. PLoS Pathog 20:e1011794.

17. Acciani MD, Brindley MA. 2022. Scrambled or flipped: 5 facts about how cellular phosphatidylserine localization can mediate viral replication. PLoS Pathog 18:e1010352.

18. Groß R, Reßin H, Von Maltitz P, Albers D, Schneider L, Bley H, Hoffmann M, Cortese M, Gupta D, Deniz M, Choi J-Y, Jansen J, Preußer C, Seehafer K, Pöhlmann S, Voelker DR, Goffinet C, Pogge-von Strandmann E, Bunz U, Bartenschlager R, El Andaloussi S, Sparrer KMJ, Herker E, Becker S, Kirchhoff F, Münch J, Müller JA. 2024. Phosphatidylserine-exposing extracellular vesicles in

body fluids are an innate defence against apoptotic mimicry viral pathogens. Nat Microbiol 9:905–921.